



Fate of nanoparticles in the aquatic environment

Removal of engineered nanomaterials from the
water phase under environmental conditions

Joris T.K. Quik

Fate of nanoparticles in the aquatic environment

Removal of engineered nanomaterials from the water phase under environmental conditions

Joris T.K. Quik

Quik JTK (2013) Fate of nanoparticles in the aquatic environment. Removal of engineered nanomaterials from the water phase under environmental conditions. PhD thesis, Radboud University Nijmegen, The Netherlands

© 2013 Joris Quik, all rights reserved.

ISBN: 978-90-6464-692-8

Fate of nanoparticles in the aquatic environment

Removal of engineered nanomaterials from the water phase under environmental conditions

Proefschrift

ter verkrijging van de graad van doctor
aan de Radboud Universiteit Nijmegen
op gezag van de rector magnificus prof. mr. S.C.J.J. Kortmann,
volgens besluit van het college van decanen
in het openbaar te verdedigen op maandag 23 september 2013
om 12.30 uur precies

door

Joris Theodoor Kamal Quik

geboren op 22 juli 1982
te Knokke-Heist, België

Promotoren:

Prof. dr. ir. D. van de Meent

Prof. dr. ir. A.J. Hendriks

Manuscriptcommissie:

Prof. dr. A.M.J. Ragas (voorzitter)

Prof. dr. M. Cohen Stuart (Wageningen Universiteit)

Prof. dr. ir. W.J.G.M. Peijnenburg (Universiteit Leiden)

This research was financially supported by the National Institute for Public Health and the Environment (RIVM, SOR-S340030), and by the EU FP6 project NanoInteract (NMP4-CT-2006-033231).

“The earth is but one country and mankind its citizens.”

— Bahá'u'lláh

Contents:

Abbreviations		1
Chapter 1	General Introduction	3
Chapter 2	How to assess exposure of aquatic organisms to engineered nanomaterials?	9
Chapter 3	Effect of dissolved organic matter on cerium dioxide nanoparticles settling in model fresh water	35
Chapter 4	Natural colloids are the dominant factor in the sedimentation of nanoparticles	47
Chapter 5	Nanomaterials in natural waters: sedimentation rates and attachment efficiencies for heteroaggregation	57
Chapter 6	Rapid settling of nanoparticles due to heteroaggregation with suspended sediment	77
Chapter 7	Empirical versus mechanistic modeling of engineered nanomaterial aggregation and sedimentation in water	91
Chapter 8	Synthesis	103
Appendices		107
	A: Supporting information to chapter 2	108
	B: Supporting information to chapter 3	110
	C: Supporting information to chapter 4	117
	D: Supporting information to chapter 5	121
	E: Estimating the attachment efficiency for heteroaggregation of nanoparticles and natural colloids from sedimentation experiments	127
	F: Supporting information to chapter 6	136
Literature		143
Summary		157
Samenvatting		161
Dankwoord		165
Curriculum vitae and list of publications		169

Abbreviations

List of most common abbreviations used in this thesis.

AA	Brabantse Aa (small stream)
B-DOM	Bihain Dissolved Organic Matter
CNT	Carbon Nanotubes
DLS	Dynamic Light Scattering
DLVO	Derjaguin-Landau-Verwey-Overbeek
DOC	Dissolved Organic Carbon
DOM	Dissolved Organic Matter
EC	Electric Conductivity
ENM	Engineered Nanomaterials
ICP-MS	Inductively Coupled Plasma Mass Spectroscopy
IJ	IJsselmeer (lake)
KG	Karregat (small pond)
MS	Nieuwe Waterweg near Maassluis (brackish)
MWCNT	Multiwalled Carbon Nanotubes
NC	Natural Colloid
nC ₆₀	Fullerene Nanoparticles
nm	Nanometer (10 ⁻⁹ meter)
NP	Nanoparticle
NTA	Nanoparticle Tracking Analysis
NZ	Noordzee (North Sea)
PEC	Predicted Environmental Concentration
PNEC	Predicted No-Effect Concentration
PSD	Particle Size Distribution
PVP	Polyvinylpyrrolidone
RL	Rhine (river)
SR-DOM	Suwannee River Dissolved Organic Matter
SS	Suspended Sediment
TEM	Transmission Electron Microscopy

Chapter 1

General introduction

1.1 Engineered nanomaterials and nanotechnology

Nanotechnology refers to the manipulation of materials at the nanoscale. The possibilities of this research field were envisioned by Richard Feynman in a famous talk in 1959.¹ Later, between 1981 and 1992 the term nanotechnology was popularized and the scanning tunneling microscope and the atomic force microscope became well established leading to the research field we know today.² Yet the field of nanotechnology continues to grow with increased application of nanomaterials in consumer products.^{3,4} The main reason that materials at the nano-scale are of specific interest are the changes in physico-chemical properties which are different at the nano-scale compared to the bulk material. These changes are mostly related to the increase in surface area to volume ratio, resulting in changes in physico-chemical properties related to color,⁵ solubility,⁶ conductivity⁷ and catalytic activity⁸ of engineered nanomaterials (ENMs).

Increasing quantities of materials at this small size are being produced.⁹ Although nanomaterials have many benefits¹⁰ the implications of large quantities of these types of materials entering the environment has not been fully understood.¹¹⁻¹⁶ While this is generally the case when novel chemicals are developed, the question remains whether current guidelines for risk assessment of novel chemicals, such as implemented in the Registration, Evaluation, Authorisation and Restriction of Chemical substances (REACH),¹⁷ are adequate for ENMs. Risk assessment of chemicals is based on both exposure and effect assessment.¹⁸ The exposure assessment is based on a good understanding of the environmental behavior of chemicals combined with quantification of the fate processes using modeling tools. Using such tools, the predicted exposure concentrations are estimated from the physico-chemical characteristics of the aquatic system and chemical in question. The current methods used for exposure assessment are based on the physico-chemical behavior of the dissolved form of a chemical. For this reason we need to investigate the applicability of these methods for ENMs because it is likely that the inherent particulate nature of ENMs demands a novel approach to exposure assessment of these materials.¹⁹ In order to adapt or develop new exposure assessment methods we need to fully understand the fate of ENMs in the natural environment and we should be able to derive quantitative descriptions of the relevant fate processes.

There have been several definitions of nanomaterials with the most discussed being the recent recommendation by the EU.²⁰ This recommendation classified nanomaterials as a new chemical group, defined by its external dimensions between 1

and 100 nm.²¹ This was done in order to help regulators in creating legislation for the safe use of ENMs. However, it is argued that this arbitrary definition is not related to the specific size dependent physico-chemical properties for which ENMs are designed.^{20, 22} In this work the term ENM is used to indicate intentionally manufactured materials with external dimensions up to 100 nm.

1.2 Colloid science and the behavior of nanomaterials in water

Understanding the behavior of ENMs is part of colloid science which began in the middle of the nineteenth century. Colloid science studies systems in the colloidal domain, defined by the size of particles at which the inherent kinetic or thermal energy is similar or larger than that provided by external forces, such as gravity. This is generally the case for particles up to a few micrometers in diameter. Colloid science has developed the theoretical background for particle – particle interactions and on the stability of these systems in suspension.^{23, 24} Important processes for the fate of ENMs in water are particle transport following Stokes' law,²⁵ Brownian motion as described by Einstein²⁶ and aggregation first described by Von Smullochowski.²⁷ These processes can be combined into a quantitative description of particle transport in water, which takes into account the aggregation of particles to larger aggregates combined with sedimentation.²⁴ Aggregation of particles is dependent on (a) attachment efficiency and (b) the collision frequency. The attachment efficiency depicts the chance that upon collision of two particles they will stick together and form an aggregate. This is dependent on the interaction forces such as electrostatic repulsion and van der Waals attraction as described by the Derjaguin-Landau-Verwey-Overbeek (DLVO) theory.^{28, 29} Additionally other non-DLVO interactions can also influence the attachment efficiency, such as steric hindering, magnetic forces and hydration forces.^{30, 31} Although there are quantitative descriptions for these particle interactions,³¹ the calculation of the attachment efficiency in complex media is only possible using semi-empirical models.^{32, 33} The collision frequency depicts the amount of collisions between particles that could potentially result in the formation of an aggregate. This frequency is dependent on Brownian motion, fluid motion and differential settling which can be calculated using particle and suspending medium properties.³⁴ These theories allow for modeling of aggregation. Together with sedimentation this forms the basis for modeling transport of ENMs in aquatic systems.^{24, 35}

The natural environment is however much more complex than the relatively simple experimental systems used, up to now, to investigate these colloidal processes.^{16, 31} Particularly quantifying the relevant parameters in natural aquatic systems is problematic.³⁶⁻³⁸ In natural aquatic systems a large range of naturally occurring colloids (NCs) are present comprising of inorganic colloids and natural organic matter.^{39, 40} The behavior of such natural colloids has been studied widely as these play an important role in the fate of trace metals and organic compounds.⁴¹⁻⁴⁵ As ENMs are yet another type of colloid in this system, the interaction between NCs and ENMs needs to be understood.^{16, 46}

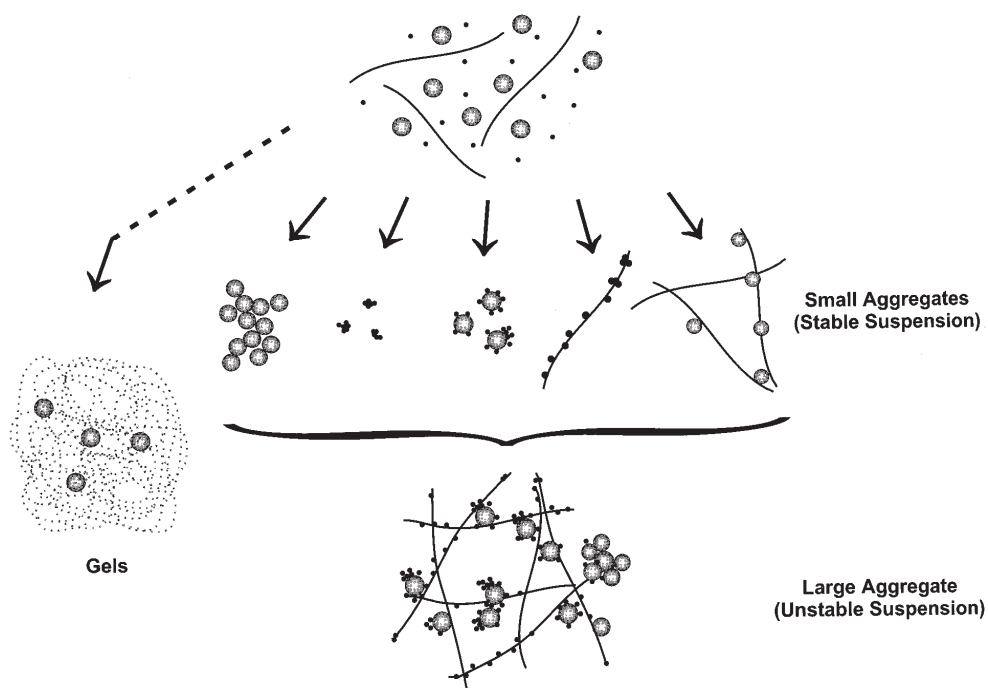


Figure 1.1. Major types of aggregates formed from natural colloids in the three-colloidal component system: FC (or AROM) = small points; IC = circles; RB = lines. Both FC and polysaccharides can also form gels, which are represented here as grey areas into which IC can be embedded. Reprinted with permission from Buffle et al.⁴¹. Copyright 1998 American Chemical Society.

Buffle et al.⁴¹ has given a description of the behavior of the whole range of natural colloids based on the different possible interactions between the different fractions of NCs. In the so called three component approach⁴¹ the main components are (i) fulvic

compounds (FC) or aquagenic refractory organic matter (AROM), (ii) rigid biopolymers (RB), all comprising natural organic matter (NOM). And the third component consists of (iii) inorganic colloids (IC) which mainly comprise of aluminosilicates (clays), silica, and iron oxyhydroxyde particles. From these three compounds it is thought that there are two major but opposite effects: the stabilization against aggregation by FC and the destabilization by RB (Figure 1.1). This stabilizing effect on inorganic colloids was shown for a range of organic macro molecules present in natural organic matter.^{42, 47-56} This stabilizing fraction of NOM is further referred to as dissolved organic matter (DOM), because it is generally fractionated from NOM by filtration (<0.2 μm). Recently similar research has also shown the stabilizing effect of DOM on different types of carbon, metal and metal oxide ENMs, such as C_{60} ,⁵⁷ carbon nanotubes,^{58, 59} Au,⁶⁰ Al_2O_3 ⁶¹ and TiO_2 ⁶² nanoparticles (NPs). It indeed seems as the stabilizing effect previously observed for natural IC is similar for ENMs. However, the interaction of ENMs with the whole scale of NCs present in natural waters is not studied as only the smaller NOM fraction, DOM, was taken into account in these studies.

1.3 Aim and outline of this thesis

The fate of ENMs in aquatic systems needs to be understood. Although for ENMs, aggregation and sedimentation are known to affect the fate of ENMs in the aquatic environment, the quantification of all fate processes that affect the fate of ENMs in aquatic systems is still unknown. In particular the effect of NCs on the fate of ENMs has not yet been investigated experimentally. It is however thought that NCs are important in the further fate of ENMs in the environment.

The main aim of this thesis is to further the understanding of the fate processes affecting ENMs in the aquatic environment. This is done with the purpose of better estimating the exposure concentrations of ENMs. This has three different aspects, (i) identify the most relevant fate processes, (ii) provide quantitative data of these processes for ENMs in order to (iii) develop a modeling approach for these fate processes to calculate concentrations of ENMs. Part of this is to develop methods for further estimating the key parameters needed for environmental exposure modeling.

This is done by first identifying the differences in fate processes affecting conventional chemicals and ENMs (**Chapter 2**). This includes a brief literature review of dissolution and sedimentation processes as ENM specific fate processes and the proposal of a modeling approach for these two processes that can be easily applied in current exposure modeling methods. Then the effect of DOM on the stability of CeO_2

NPs is investigated, focusing on sedimentation as fate process for ENMs (**Chapter 3**). This is followed by two studies focusing on the effect NCs, as a whole, have on the sedimentation of ENMs. The sedimentation rates are quantified using an empirical model (**Chapter 4 and 5**). This is followed by the quantification of the interaction between ENMs and NCs by introducing a new method for measurement of the attachment efficiency for heteroaggregation between ENMs and NCs (**Chapter 5**). In addition to NCs the effect of suspended sediment (SS) on the removal of ENMs from water phase has been studied by quantifying sedimentation rates for SS assisted removal from the water phase as well as aged SS-ENM agglomerates (**Chapter 6**). The attachment efficiency for heteroaggregation between SS and ENMs is estimated with the previously developed method (**Chapter 6**). This is concluded by the development of a mechanistic model to simulate the aggregation and sedimentation of ENMs and NCs in order to further discuss and explain the observed sedimentation and aggregation data from the previous chapters (**Chapter 7**). This is followed by the synthesis (**Chapter 8**).

Chapter 2

How to assess exposure of aquatic organisms to engineered nanomaterials?

JORIS T.K. QUIK, J. ARIE VONK, STEFFEN FOSS HANSEN, ANDERS
BAUN AND DIK VAN DE MEENT

Published as "How to assess exposure of aquatic organisms to manufactured nanomaterials" in Environment International 37: 1068-1077 (2011)

Abstract

Ecological risk of chemicals is measured by the quotient of predicted exposure concentrations and predicted no effect concentrations, which are hard to assess for engineered nanomaterials (ENMs). This paper proposes modifications to currently used models, in order to make them suitable for estimating exposure concentrations of ENMs in the aquatic environment. We have evaluated the adequacy of the current guidance documents for use with ENMs and conclude that nano-specific fate processes, such as sedimentation and dissolution need to be incorporated. We have reviewed the literature on sedimentation and dissolution of ENMs in environmentally relevant systems. We deduce that the overall kinetics of water-sediment transport of ENMs should be close to first-order. The lack of data on dissolution of ENMs under environmentally realistic conditions calls for a pragmatic decision on which rates to be used in modeling. We find that first-order removal kinetics for dissolution seems adequate. Based on limited data from literature, probable removal rates range from $0\text{--}10^{-4}\text{ s}^{-1}$ for sedimentation, and from $0\text{--}10^{-5}\text{ s}^{-1}$ for dissolution. Further experimental data at environmentally relevant conditions for sedimentation and dissolution of ENMs are needed.

2.1 Introduction

The recent large increase in production, species, and utilization of ENMs has raised concerns that the release of these materials into the environment may pose a serious threat, and consequently calls for environmental risk assessment of ENMs.^{12, 15, 16, 63} The current approach to environmental risk characterization for chemicals in the EU is based on the quotient of a predicted environmental concentration (PEC) and a predicted no-effect concentration (PNEC), and is elaborated into the guidance on information requirements and chemical safety assessment¹⁷ and formalized in the European Union System for the Evaluation of Substances (EUSES).⁶⁴ In principle, the PEC/PNEC ratio should characterize the environmental risk of nanomaterials just as well as it does for conventional chemicals. However, assessment of PEC and PNEC for nanomaterials is not straightforward. As ENMs tend to aggregate, ENMs are often present in a range of sizes. So the assessment of the PNEC in terms of concentration of nanoparticles is not trivial. Experimental measurement of exposure concentrations (PEC) – in the laboratory, let alone in the field – is challenging, to say the least. When measurement is no option, prediction of exposure concentrations, based on a known

emission, is often the only alternative, but suffers from even greater difficulty. Question is how to account for ENM-specific environmental behavior in assessing PEC, which is not addressed nor worked out in the European Chemicals Agency guidance¹⁷ and EUSES.^{65, 66}

In this chapter, we address this question. We discuss the adequacy of the currently used exposure assessment modeling framework for use with ENMs and identify its weakness in describing colloidal processes. We have reviewed the literature to gather quantitative information supporting the exposure assessment modeling of ENMs focusing on two main nano-specific removal processes, sedimentation and dissolution. In the last part of this paper, we provide a brief overview of the different approaches already used to model exposure concentrations of ENMs including the physical and chemical laws which form the basis for an exposure assessment model of ENMs. Finally we propose a possible way forward in further adaptation of current models to make them fit for use with ENMs. We indicate both the feasibility of using first order removal rates for this purpose and the limitation of currently available experimental data.

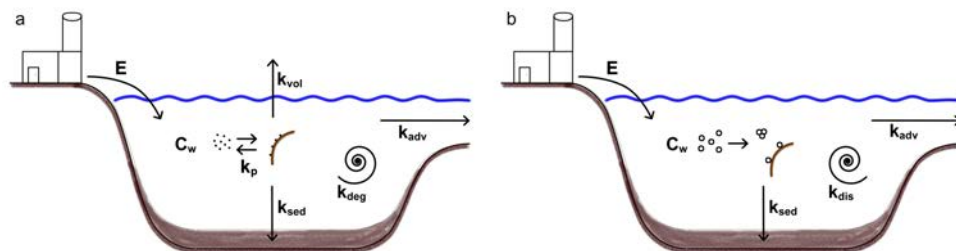


Figure 2.1. Schematic indication of the environmental fate processes for conventional chemicals (a) and nanomaterials (b).

2.1.1 Current guidance on exposure assessment and engineered nanomaterials

Under EU regulation, exposure estimation for the purpose of environmental risk assessment of nanomaterials is considered to be covered satisfactorily by guidance on Registration, Evaluation, Authorization and Restriction of Chemicals (REACH). REACH guidance R.16 prescribes model algorithms to estimate concentrations of chemical substances in water, starting from known or estimated emission rates.¹⁷

The concentration of a chemical substance in water is thought to represent the balance of an emission E (kg s^{-1}) into a water body of volume V (m^3) and a number of

removal processes, each characterized by first-order removal rate constants k_i (s^{-1}). The fate process accounted for in the REACH guidance (Figure 2.1a), are (i) advection out of the system (k_{adv}), (ii) volatilization to air (k_{vol}), (iii) degradation (i.e. transformation into other chemicals or complete mineralization, k_{deg}), and (iv) sorption to suspended particles according to an equilibrium constant K_p ($L\ kg^{-1}$), and subsequent deposition to sediment (k_{sed}). From these processes, of which the rate constants must be measured or estimated via established theoretical or empirical relationships, the model algorithms deduce a steady-state concentration C_w ($kg\ m^{-3}$) of the substance dissolved in water, see equation 2.1.

$$C_w = \frac{E}{(k_{adv} + k_{vol} + k_{deg} + k_{sed}) \cdot V} \quad (\text{Eq. 2.1})$$

We can ask ourselves several questions regarding the exposure assessment of ENMs: Do ENMs behave in the same way as conventional chemical substances? Can the concentration of nanoparticles, suspended in water, be derived from the emission to water the same way as for conventional chemical substances? Do we have measured rate constants for removal of nanoparticles from water? Can we estimate removal rate constants for nanoparticles from theory? Are there nano-specific processes that cannot be accommodated in the current guidance?

First, there are processes in the guidance that are irrelevant for nanoparticles. For example, volatilization from water is an important process for many conventional chemicals, but is likely negligible for ENMs. This can be dealt with easily by assigning the value of zero to the volatilization rate constant. Then a major question is whether/how removal of nanoparticles from water by deposition to sediment can be described using the current guidance, which assumes equilibrium partitioning between dissolved and sorbed chemical, followed by (partial) sedimentation of the suspended matter. It is well known from colloid science that, small particles in water tend to progressively form aggregates and agglomerates that, when grown big enough, deposit, eventually leading to near-complete removal of the aggregated material to the sediment (Figure 2.1b). Another issue is dissolution. REACH regulation focuses on (bioavailable) chemical substances in the dissolved state; it is assumed that, immediately upon release to water, chemicals are entirely in the dissolved state. This is obviously different for nanoparticles, where (i) focus is on the presence of solid particles, suspended in water, and (ii) it could be assumed that, immediately following release to water, the material is entirely in the suspended state. In order to estimate the concentration of nanoparticles in water, it is essential that the process of dissolution is taken into account (Figure 2.1b). Based on these differences between

conventional chemicals and ENMs it is thought that at least some amendments to the current guidance are necessary in order to make the current REACH guidance suitable for predicting concentrations of nanoparticles in water.

2.1.2 Background on sedimentation and dissolution

The commonly used two-stage description of water-sediment transport of chemical substances (i.e. rapid equilibrium partitioning of dissolved chemical onto suspended particulate matter, followed by transport with settling suspended particles to sediment) is clearly not suitable to model the behavior of ENMs. In a recent review, Petosa et al.³¹ showed that the aggregation and deposition behavior under laboratory conditions can generally be semi-quantitatively described via the Derjaguin and Landau, Verwey and Overbeek (DLVO) theory, which describes the forces between charged surfaces interacting through a liquid medium. However, Petosa et al.³¹ also indicates the non-DLVO behavior that is generally found in the more complex natural systems where surface coatings result in steric hindering or where unusual shapes of nanoparticles give rise to unpredicted behavior. Aggregation is dependent on the collision frequency and the attachment efficiency of the particles. It has been shown that the attachment efficiency is largely affected by the ionic strength and dissolved organic matter (DOM) content of natural waters.^{38, 67} The ultimate consequence of aggregation is sedimentation of these nanoparticle aggregates to the sediment. In addition to aggregation, nanoparticles will deposit on other surfaces, like natural colloids.^{31, 38, 68} This tendency of ENMs to attach to other solids has been poorly studied although there have been some studies of interactions with wastewater treatment solids.^{68, 69} Most studies look at the underlying processes of aggregation, studying the effect of the physicochemical properties of the aquatic matrix and ENM themselves. The link between aggregation and sedimentation seems clear, but a quantitative description is far from trivial.³⁸ However, recently several studies have described the sedimentation behavior of ENMs in increasingly complex environmental matrices, ranging from artificial media with added DOM to natural river water and sea water.^{67, 70, 71}

Dissolution of ENMs is in essence the transformation of the solid form of a chemical compound to the dissolved ionic form or other species of a compound depending on environmental conditions. According to the ECHA Guidance document on Environmental Risk Assessment for metals and metal compounds, the prediction of the environmental exposure concentration should be based on the relevant soluble metal ion or other metal species that is bioavailable or may become available through

transformation processes.¹⁷ However, the extent or rate of dissolution of chemicals, in this case ENMs, is not taken into account by the current EUSES models. The dissolution kinetics for ENMs have been described in several studies, but these are often determined under extreme oxidative, acidic, or alkaline conditions.⁷²⁻⁷⁷ On the other hand, several biologically relevant studies on particle dissolution were done as part of assessing the biological effect of airborne exposure to particles.⁷⁸⁻⁸⁰ Additionally, a few studies have looked at the dissolution of mineral particles, e.g. clays.^{81, 82} Only recently is the dissolution of ENMs considered in studies on environmental fate and effects of ENMs.⁸³⁻⁸⁸ A few studies have specifically measured Ag nanoparticle dissolution under environmentally and biologically relevant conditions.^{77, 89-91}

2.2. Sedimentation

The relationship between sedimentation of ENMs and different environmental conditions is discussed. In paragraphs 2.2.1, we focus on the chemical composition of the aquatic matrix, looking at parameters like pH, ionic strength and DOM content and in paragraph 2.2.2 we focus on the effect of natural colloids and organisms on the fate of ENMs in surface waters. The complexity of the studies discussed ranges from defined salt solutions to complex natural water samples. An elaborate overview of the studies on sedimentation of metals (Ag, Au, and Fe), metal oxides (CeO₂, Fe₂O₃, TiO₂, and ZnO), and carbon ENMs (carbon nano-tubes (CNT) and nC₆₀) is presented in Table 2.1.

2.2.1 *Composition of aquatic matrix*

DOM is found to have a stabilizing effect on various types of ENMs in aqueous suspension, thus counteracting sedimentation.^{58, 70, 71, 92} Several factors seem to influence sedimentation of CNT, such as addition of DOM, prolonged stirring, and functionalized CNT, which all show less sedimentation than pristine CNT added to synthetic freshwater, see Figure 2.2.^{58, 92} Hyung et al.⁵⁸ showed that upon addition of relatively high concentrations of CNT to DOM rich water, up to 3.5% remained in suspension after 4 days of settling. Kennedy et al.⁹² tested the sedimentation behavior of CNT in time. Within 40 minutes, the concentration stabilized and only a slow sedimentation rate was observed afterwards. The sedimentation behavior of CeO₂ nanoparticles in artificial fresh water also showed fast sedimentation during the first day.⁷⁰ After 12 days of sedimentation without addition of DOM almost no CeO₂ nanoparticles remained suspended, but with addition of 0.5–40 mg L⁻¹ DOM, 5–40% of

the initially added nanoparticles remained suspended. In an elaborate multi-dimensional parameter testing study by Von der Kammer et al.⁷¹, about 70–90% of initially added TiO₂ nanoparticles remained suspended after 15 hours of settling in presence of DOM. In the same study increasing concentrations of NaCl, CaCl₂, and Na₂SO₄ resulted in a significant increase in sedimentation compared to the addition of DOM. However, the degree of sedimentation showed large variability depending on pH and salt concentration.

In addition to DOM, different kinds of polymers and other stabilizing agents are often added to stabilize ENMs against aggregation and this logically also decreases sedimentation rates. This was seen in a study by Limbach et al.⁶⁹, who tested the stability of CeO₂ nanoparticles at different NaCl concentrations. CeO₂ nanoparticles dispersed with acryl polymer and benzyl sulfonic acid did not show significant sedimentation up to 0.1 M and 0.01 M NaCl, respectively, after 4 days of settling. Bare CeO₂ nanoparticles only remained relatively stable at 0.001 M NaCl. Similarly Phenrat et al.⁹³ concluded that the sedimentation rate is lower for Fe⁰ nanoparticles whose surface has been modified by polymers. During the 24 hour sedimentation study of Fe⁰ nanoparticles, about 60% of the surface modified particles and 10% of nanoparticles aged for 11 months remained suspended compared to less than 1% for fresh or bare Fe⁰ nanoparticles.

Almost all of the above mentioned studies use artificial suspension media and only a few studies have used natural aquatic matrices to test the behavior of ENMs. Lin et al.⁹⁴ studied the stability of CNT in surface water samples. CNT only remained suspended in freshwater containing anionic and nonionic surfactants or at the highest DOM concentration (28 mg L⁻¹). Keller et al.⁶⁷ studied the aggregation and sedimentation in time of TiO₂, ZnO, and CeO₂ nanoparticles in 10 different types of environmental water matrices, ranging from freshwater to seawater. Between 10–90% of nanoparticles remained suspended after 6 hours of sedimentation, with DOM content and ionic strength explaining most of the variation. DOM generally stabilized against aggregation and consequently sedimentation, whereas water samples with high ionic strength showed faster sedimentation due to increased aggregation. Keller et al.⁶⁷ reported initial sedimentation rates for 10 mg L⁻¹ particle suspensions ranging from 10⁻⁷ to 10⁻⁴ s⁻¹ depending on DOM content and ionic strength.

2.2.2 Natural colloids and organisms

Natural aquatic matrices consist of more than just DOM and salts, E.g. natural colloids (NCs) and a range of organisms are usually also present. These can also affect

the fate of ENMs. However, no studies present data on the effects of natural colloids on sedimentation of ENMs. From theory we can derive that an increase in particle concentration increases the collision frequency and thus aggregation and consequently sedimentation rates.^{67, 95} The presence of natural colloids is likely to also be present as a surface area for potential deposition of ENMs.

Although this interaction with natural colloids has not been studied experimentally, the effect of bacteria on the removal of ENMs from the water phase has been studied as interaction with suspended biomass and biofilm. Kiser et al.⁶⁸ found that the presence of wastewater biomass resulted in a greatly increased settling of C₆₀ and Ag nanoparticles. The presence of biofilms also affects the depletion of ENMs from free suspension in the aquatic environment. Battin et al.⁹⁶ used a unique flow through flume system to measure the transport of TiO₂ nanoparticles in the aquatic environment. They found increased removal of nanoparticles from the water with a microbial biofilm present. Without biofilm about 90% of the initially added nanoparticles are removed after 6.5 hours, compared to nearly 99% after only 3 hours with biofilm present. Additionally in a different study by Ferry et al.⁹⁷ the partitioning of Au nano-rods was studied in a estuarine mesocosm study containing biofilms, sediments, plants, animals and sea water. The largest fraction of Au was found in the biofilm (61.0%), followed by the sediment (24.5%), sea water (8.61%), and animals (6.18%). In addition to partitioning of nanoparticles to the biofilm or wastewater biomass, there are other organisms to which nanoparticles can adsorb. In co-authorship with Van Hoecke et al.⁹⁸ we reported that CeO₂ nanoparticles cluster together with algal cells to form clumps exceeding 1 mm. And that CeO₂ nanoparticles adhere to *Danio rerio* fish embryos (Figure A.1 in Appendix A).

Some aquatic organisms, like filter feeders can possibly have an effect on particle coating and aggregation. Filella et al.⁹⁹ showed that in presence of *Daphnia hyaline*, which feed on particles of about 600 nm, the particle size distribution showed more particles with a diameter below 500 nm present. A change towards smaller particle aggregates upon excretion from *Daphnia magna* has also been described for C₆₀¹⁰⁰. In another study with CNT and *D. magna*, Roberts et al.¹⁰¹ showed a biological modification of a water-soluble, lysophosphatidylcholine-coated single walled CNT upon ingestion by *D. magna*. The organisms decreased the concentration of single walled CNT remaining in suspension after 48 hours by 50% by stripping of the lysophosphatidylcholine from the particle surface.

Sedimentation seems to be largely dependent on environmental characteristics, such as the presence of DOM or other stabilizing agents and the ionic strength or presence

of different electrolytes. Additionally sedimentation is affected by the chemical composition of ENMs, but more importantly the presence of surface functionalization. The presence of DOM, or surface modifications by functionalization, or capping by a stabilizing agent decreases the sedimentation rate, indicated by the solid symbols in Figure 2.2. Non-functionalized carbon ENMs show the fastest sedimentation followed by metal and metal oxide nanoparticles, indicated by open symbols in Figure 2.2. This figure shows a selection of sedimentation data of several types of ENMs where the fraction remaining in suspension (C_w/C_0) is given as function of sedimentation time. Figure 2.2, as well as Figure 2.3, were constructed by obtaining data from the respective publication or directly from the author. These data and their respective sources are given in Table A.1 and Table A.2 in Appendix A, respectively.

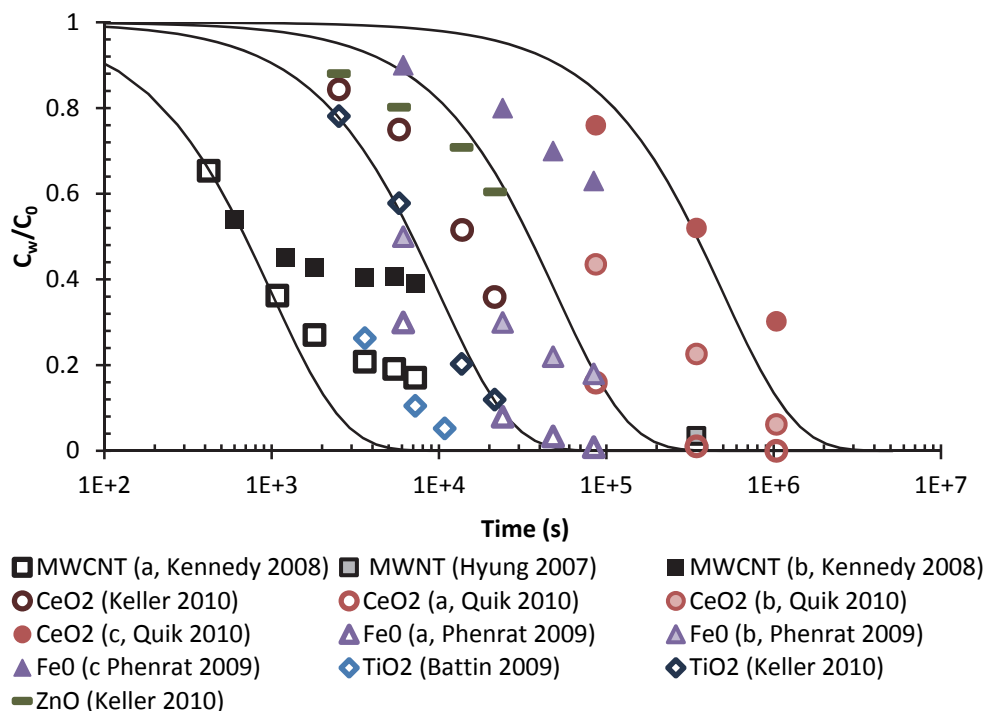


Figure 2.2. Fraction of nanomaterial, C_w/C_0 , remaining in suspension as a function of sedimentation time taken from literature.^{58, 67, 70, 92, 93, 96} A distinction is made between nanomaterials with (filled symbol) and without (open symbol) DOM or surface modification. The lines present a first order removal model ($C_w/C_0 = \exp(-k_{sed} t)$) with k_{sed} values ranging from 2×10^{-6} to 10^{-3} s^{-1} .

Table 2.1. Overview of nanomaterial sedimentation studies

Nano-material Size (method)	Method for measuring the nanomaterial concentration	Suspension matrix	Result or main conclusion	Ref.
Au 15 x 62 nm (TEM)	Au concentration during 250 hour mesocosm experiment in water, sediment, biofilm and organisms by ICP-MS.	Estuarine mesocosm experiment with sea water, sediment, sea grass, microbes, snails, clams, shrimp and fish.	Equilibrium within 5 hours in sea water at 0.4 $\mu\text{g L}^{-1}$ Au. Fraction of 8.61% in sea water, 24.5% in sediment, and 61.0% in biofilm.	⁹⁷
CeO ₂ 24.5 nm (BET) 60 nm (DLS)	Ce concentration in the supernatant after 4 days settling by ICP-OES.	Deionized water with 0.0001–0.46 M NaCl and pH 3–12. With and without acryl polymer or benzyl sulfonic acid.	At low ionic strength around pH 8 about 7% remained suspended which goes up to 75% as pH goes up or down. With increasing ionic strength 3% remains suspended. Less sedimentation is observed in presence of acryl polymer or benzyl sulfonic acid.	⁶⁹
CeO ₂ 20 nm (BET) 169 nm (NTA)	Ce concentration in the supernatant during 12 days of settling with ICP-MS.	Deionized water and OECD algae medium with 0–40 mg C L ⁻¹ SR-DOM and Bihain DOM.	Sedimentation rate decreases significantly after 1 day. Increasing DOM content resulted in an increasing fraction, 5–40% of CeO ₂ nanoparticles remaining suspended.	⁷⁰
TiO ₂ 27 nm (TEM) 194 nm (DLS) ZnO 24 nm (TEM) 205 nm (DLS) CeO ₂ 67 x 8 nm (TEM) 231 nm (DLS)	Removal of nanoparticles (10 to 200 mg L ⁻¹ initial) from suspension during 6 hours with UV _{vis} spectrophotometry.	10 different water types, ranging from natural and artificial freshwater to seawater.	The initial sedimentation rate ranged from around 10 ⁻⁷ to 10 ⁻⁴ s ⁻¹ for the three particle types. These are based on the first few to 60 minutes of sedimentation. DOM content and ionic strength explain the range in sedimentation rates found.	⁶⁷
TiO ₂ 21 nm (-) 293 nm (DLS) TiO ₂ 10 nm (-) 302 nm (DLS)	Removal of nanoparticles (10 mg L ⁻¹ initial) from the supernatant after 15 hours of sedimentation by nephelometric turbidity measurement.	Deionized water with various concentrations of NaCl, CaCl ₂ , Na ₂ SO ₄ , and DOM at pH between 3.5 and 7.5.	60–90% remains suspended at near neutral pH upon addition of DOM and diphosphate. 0–20% remains suspended with increasing NaCl or Na ₂ SO ₄ concentration. 0–80% remains suspended at various CaCl ₂ concentrations.	⁷¹

Nano-material Size (method)	Method for measuring the nanomaterial concentration	Suspension matrix	Result or main conclusion	Ref.
TiO ₂ 40 nm (-) 200 nm (DLS) ZnO 50–70 nm (-) 320 nm (DLS) Fe ₂ O ₃ 5–25 nm (-) 200 nm (DLS) NiO 10–20 nm (-) 750 nm (DLS) SiO ₂ 10 nm (-) 740 nm (DLS)	Measures metal concentration (10 mg L ⁻¹ initial) in the supernatant after 1 hour sedimentation by GFAA.	Deionized water with 0.01 M NaHCO ₃ (pH 8.2) w/o 0.1 M MgCl ₂ or 20–60 mg L ⁻¹ KAl(SO ₄) ₂ .	60-90% nanoparticles remained suspended. 20-80% nanoparticles remained suspended upon addition of MgCl ₂ or KAl(SO ₄) ₂ . With TiO ₂ and NiO nanoparticles showing the highest and lowest remaining fraction of particles, respectively.	102
TiO ₂ 21 nm (-) 1283 nm (DLS) TiO ₂ 10 nm (-) 1085 nm (DLS)	Removal of nanoparticles from a stream microcosm by online nephelometric turbidity measurements during 6.5 hours circulation.	Flow through system with and without biofilm with natural lake water.	80-90% removal after 6.5 hours without biofilm. 95-99% removal after 3 hours with biofilm. First order removal kinetics fitted the data correctly with exception of the first hour for several scenarios.	96
TiO ₂ 35 nm (-) 350–7100 nm (DLS)	Measures Ti concentration (2 g L ⁻¹ initial) in the supernatant during 10 days settling with ICP-OES	12 different soil suspensions with pH ranging from 6.2 to 8.6, DOC from 51 to 158 mg L ⁻¹ , and ionic strength from 0.2 to 8.6 mM.	1.17–2.83% remained suspended after 10 days of settling. Two sedimentation regimes were observed were 98% was removed after 1 day versus 90% after 2 days.	103
Fe ₃ O ₄ 20–30 nm (-) Fe ⁰ 28 nm (-)	Removal of nanoparticles (5 mg L ⁻¹ initial) from suspension during 1500 min. with UV _{vis} spectrophotometry.	Hanks basic salt solution (HBSS), Dulbecco's Modified Eagle's Medium (DMEM), and RPMI-1640 growth medium.	Unmodified materials, Fe ⁰ and Fe ₃ O ₄ show rapid aggregation and sedimentation whereas the sodium polyaspartate coated and aged particles show much slower sedimentation.	93
Fe ₃ O ₄ 27.5 nm (-) Fe ⁰ 40 nm (-)	Removal of nanoparticles (2 - 1320 mg L ⁻¹ initial) from suspension during 20 min with UV _{vis} spectrophotometry.	Deionized water with 0.001 M NaHCO ₃	A strong increase in sedimentation was observed with increasing particle concentration resulting in increasing removal due to sedimentation from 2-99%.	95

Chapter 2

Nano-material Size (method)	Method for measuring the nanomaterial concentration	Suspension matrix	Result or main conclusion	Ref.
MWCNT 10–30 nm x 10–30 μm (-) 209–223 nm (DLS)	Removal of CNT (100 mg L^{-1} initial) from suspension during 120 min. with UV_{vis} spectrophotometry.	Deionized water, moderately hard-reconstituted freshwater with and without 100 mg L^{-1} SR-DOM, and 20‰ seawater.	Within 40 minutes only a slow decrease in concentration of MWCNT is seen. Addition of DOM increased the fraction suspended after 40 minutes from about 20–40%.	92
MWCNT 140 nm x 7 μm (-)	Black carbon concentration in the supernatant after 4 days settling by thermal optical transmission.	Deionized water with 0–100 mg L^{-1} SR-DOM, and Suwannee River water	Between 1.4–2.8% of 50 mg L^{-1} MWCNT remained suspended in deionized water with 10–100 mg L^{-1} DOM present. Up to 3.5% MWCNT remained suspended in Suwannee River water.	58
MWCNT 28 nm x 1–2 μm (TEM)	Removal of MWCNT (100 mg L^{-1} initial) from suspension after 48 hours with UV_{vis} spectrophotometry.	Eight types of natural fresh water with added anionic, cationic and nonionic surfactants.	DOM and anionic and nonionic surfactants decreased sedimentation of MWCNT.	94
nC ₆₀ 88 nm (PALS)	Removal of nanoparticles in the supernatant after 30 min. settling by UV_{vis} or metal concentration by ICP-OES.	Deionized water with 1 or 2 mM NaHCO ₃ buffer at pH 7, with and without DOM and suspended solids	Sedimentation increases in presence of biosolids for nC ₆₀ and Ag nanoparticles. This is not found for nC ₆₀ (OH) _x , TiO ₂ or f-Ag nanoparticles.	68
nC ₆₀ (OH) _x 48 nm (PALS)				
TiO ₂ 40 nm (PALS)				
Ag 13 nm (PALS)				
f-Ag 3 nm (PALS)				

2.3. Dissolution

An elaborate overview of studies on dissolution of ENMs is provided in Table 2.2 and based on this the following discussion is focused at (i) particle properties like chemical composition and size, and on (ii) the effect of the suspension matrix, like pH and DOM content.

2.3.1 Particle properties

The chemical composition of ENMs, specifically at the interface between the solid and liquid phase, is the basis for dissolution behavior. Carbon ENMs are generally considered to be insoluble in water. However, in some cases the individual carbon particles in the water phase can be considered as dissolved, e.g. derivatized C₆₀ or nano-crystals of C₆₀ in water (termed nC₆₀). On the other hand, metal oxide ENMs show a great range in degree of solubility; metal oxide nanoparticles like TiO₂^{72, 104} and CeO₂⁹⁸ are found to be practically insoluble, whereas ZnO,^{76, 83-85, 87} CuO,⁸⁷ and Al₂O₃^{73, 74, 82, 104} can dissolve under natural conditions. Although not much is known about the dissolution kinetics of metal nanoparticles, several metals are known to dissolve to some extent, e.g. Ag nanoparticles.^{77, 89-91}

One of the reasons for focusing on ENM dissolution is the assumption that the greater surface to volume ratio would lead to increased dissolution. For several types of ENMs increased dissolution of the nanoparticulate form has been reported. Nanoparticulate CuO showed a higher availability of Cu ions than bulk CuO particles, but lower availability than CuSO₄ salt, as measured by recombinant *Escherichia coli* Cu-sensor.⁸⁷ Elzey et al.⁷⁷ measured less dissolution of bulk Ag particles (10 µm) compared to Ag nanoparticles (10 nm) under the same solution conditions. Ho et al.⁹⁰ measured a size dependent decrease in dissolution rate with increasing particle diameter for Ag nanoparticles ranging from 5 to 20 nm. The dissolution rate of PbS nanoparticles varied by at least 1 order of magnitude as function of particles size, and also due to the aggregation state of the particles.⁸⁸ The increased dissolution for ENMs is not always clear, in a study by Franklin et al.⁸⁴, no difference was found between dissolution of the bulk and nano form of ZnO. Additionally nanoparticulate ZnO showed similar bioavailability of Zn ions as bulk and ZnSO₄ salts in 6 types of river water, as reported by Blinova et al.⁸⁷ who measured the bioavailability of Zn ions by recombinant *Escherichia coli* Zn-sensor. However, in another study with 26 nm and 216 nm sized ZnO particles, Wong et al.⁸⁵ found that the ZnO nanoparticles showed greater dissolution in seawater than the larger ZnO particles, reaching equilibrium

concentrations of 3.7 mg L^{-1} and 1.6 mg L^{-1} Zn respectively, within 72 hours. Although this is what would be expected because of the higher surface area of ENMs, there is a possibility that the higher dissolution found by Wong et al.⁸⁵ is due to fractionation error between the particulate and dissolved fraction by $0.1 \mu\text{m}$ filtration, leaving the possibility of 26 nm particles to pass the filter. Although the effect of increased dissolution of ENMs compared to their counterpart is not found for ZnO, other ENMs, like CuO, Ag and PbS did show this effect, making it likely that indeed the large surface area of ENMs compared to that of bulk materials causes an increase in dissolution rates.

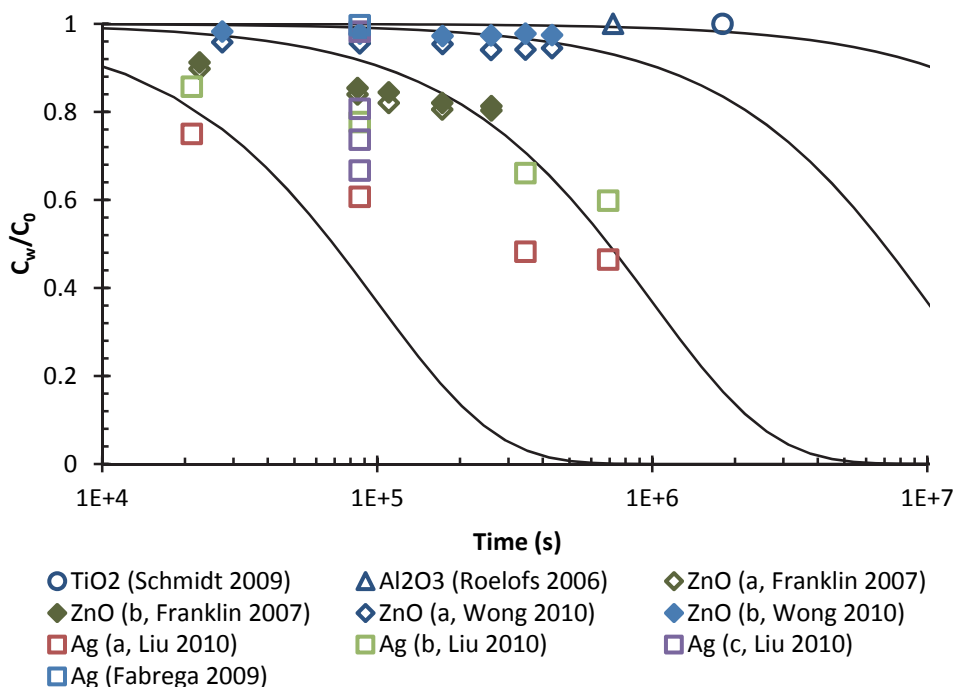


Figure 2.3. Fraction of nanomaterial (open symbol) and bulk material (filled symbol), C_w/C_0 , remaining in suspension as a function of dissolution time. taken from literature.^{72, 74, 84-86, 91} The lines present a first order removal model ($C_w/C_0 = \exp(-k_{\text{dis}} t)$) with k_{dis} values ranging from 10^{-5} to 10^{-8} s^{-1} .

2.3.2 Aquatic matrix

Most metal and metal oxide ENMs (Ag, TiO₂, and ZnO) show increased dissolution at extreme pH values.^{72, 76, 77, 90} Dissolution of Ag ENMs is primarily due to oxidation of surface Ag⁰ to ionic Ag⁺.^{90, 91} Liu and Hurt⁹¹ found that in 2 mg L⁻¹ Ag at pH 4 less than 0.05 mg L⁻¹ Ag dissolved under anoxic conditions compared to 0.6 mg L⁻¹ Ag in an air saturated solution. With increasing pH from 4 to 9, the dissolution of Ag-nanoparticles decreased in deionized water, as measured after 1 day equilibrating. Elzey et al.⁷⁷ measured a similar decrease in Ag dissolution with increasing pH from 0.5 to 6.5. Ho et al.⁹⁰ found a strong relationship between the concentration of H₂O₂ with the dissolution rate of Ag nanoparticles. In presence of H₂O₂, an increase in dissolution rate with increasing pH from pH 6 to 8.5 is seen.⁹⁰ This is likely due to the fact that the higher H⁺ concentration at lower pH counteracts the oxidizing effect of H₂O₂. On the other hand, Fabrega et al.⁸⁶ also found an increase in dissolved Ag with increasing pH from 6 to 9 in bacteria growth medium, in absence of H₂O₂.

Several studies have shown the importance of DOM in particle dissolution.^{82, 87, 90, 91} For Ag nanoparticles, the addition of Poly-vinylpyrrolidone (PVP) or DOM decreased the dissolution of Ag nanoparticles.^{87, 90, 91, 105} Also for Al₂O₃ particles suspensions at pH 3, the addition of fulvic acid as a type of DOM decreased dissolution.⁸² Most likely this decrease is due to ions adsorbed to DOM not passing the ultrafiltration membranes used. Metal ions form complexes with DOM which reduces their bioavailability, as shown for Cu and Zn ions.⁸⁷ Furthermore, the presence of Halide ions Cl⁻ and Br⁻ caused a large decrease in oxidative dissolution of Ag nanoparticles.⁹⁰ The formation of AgCl or AgBr on the surface of the Ag particles or the precipitation of AgCl or AgBr could explain the lower dissolved Ag measured. The difference in methods used to distinguish between dissolved and particulate chemicals can be seen in Table 2.2. Unfortunately most studies do not test the purity of used ENMs for presence of precursor materials containing the dissolved metals. Moreover the exclusion of particulate ENMs from solution needs to be tested to validate the measurement method. This beckons the development of standard measurement methods for dissolved particulate matter.

Although the dissolution behavior of ENMs is not fully understood and needs further investigation, it is clear that environmental conditions, like pH, presence of oxidizing agents or certain electrolytes as well as particle properties like size and surface chemistry can change the degree of dissolution. A selection of dissolution data for several types of ENMs is presented in Figure 2.3 (see Table A.2 in Appendix A for data and sources). A long term study monitoring the dissolution of clay minerals,

zeolites, and quartz in seawater indicated that the dissolution can be described by a first order reaction.⁸¹ Characteristic rate constants were found to be in the order of 10^{-7} s^{-1} . The data presented in Figure 2.3 suggest that first order removal rates up to about 10^{-5} s^{-1} are to be expected for manufactured ENMs. It should be noted that the dissolution of ENMs only changes the chemical form in which this chemical is present in the water phase. Similarly, sedimentation removes the particles from the water phase, but increases their concentration in the sediment, although in an aggregated form.

Table 2.2. Overview of nanomaterial dissolution studies.

Particle Size (method)	Method of measuring dissolved nanomaterials	Suspension matrix	Result or main conclusion	Ref.
Ag 1.9 nm (DLS) 4.8 nm (TEM)	Ultrafiltration (1–2 nm pore size) followed by GFAA.	Deionized water with varying temperature, pH, DOM, and ionic strength in oxic and anoxic conditions	Almost 100% dissolution of 2 mg L ⁻¹ after 125 days equilibrating. Dissolution increases with temperature, up to 37 °C. Dissolution decreases with increasing pH and with increasing DOM content.	⁹¹
Ag 10 nm (-) 2–30 nm (TEM) ----- Ag 10 µm (-)	Filtration (0.2 µm) and centrifugation (14,000 rpm for 30 min) followed by ICP-OES.	Deionized water at pH 6.5, and varying pH 0.5–3.50 with HNO ₃	0.5% dissolution in deionized water at pH 6.5. Dissolution increases with increasing pH. Lower dissolution of bulk compared to nanoparticles.	⁷⁷
Ag 65 nm (TEM) 100 nm (XRD)	Ultrafiltration (1 kDa) followed by ICP-MS analysis	Minimal Davies bacteria growth medium at pH 6, 7.5 and 9.	Less than 2% dissolution for 2 to 2000 µg L ⁻¹ Ag nanoparticle suspensions.	⁸⁶
Ag 6.5–11.7 nm (DLS)	Filtration (0.2 µm) and centrifugation (14000 rpm for 30 min) followed by ICP-OES.	Artificial interstitial fluid and artificial lysosomal fluid as at 38 °C.	0.03–0.07% dissolution of 0.2–2 g L ⁻¹ Ag nanoparticle suspensions after 96 hours.	⁸⁹
Ag 3–20 nm (TEM)	Ultrafiltration (3 kDa) followed by spectrophotometric or ICP-MS analysis	Buffer solutions of Tris-acetic acid, Tris-trifluoroacetic acid and NaOAc-HOAc, with varying concentrations H ₂ O ₂ and pH.	Oxidative dissolution follows first order kinetics (for nanoparticles 5–20 nm in size). Dissolution rate increases with decreasing size, and with increasing [H ₂ O ₂], chloride or bromide ions reduced dissolution.	⁹⁰
Ag 20–30 nm (-) ----- Cu 15–45 nm (-)	Measures the MetPLATE response which is thought to respond only to metal ions.	Deionized water and three types of Suwannee river water.	Cu showed an increased response in river water with increasing ionic strength. Ag only showed a response in river water with highest ionic strength and lowest DOM concentration.	¹⁰⁵

Chapter 2

Particle Size (method)	Method of measuring dissolved nanomaterials	Suspension matrix	Result or main conclusion	Ref.
Al ₂ O ₃ 10.1 nm (BET)	Al ³⁺ by complexation with Eriochromcyanine R and subsequent analysis by spectrophotometry (535 nm).	Deionized water at pH 3 to 11, set with HCl and KOH.	Higher dissolution at pH extremes, high and low. Higher dissolution measured during the first 48 hours of equilibrating followed by a lower stabilized Al ³⁺ concentration.	74
Al ₂ O ₃ 11 nm (TEM) TiO ₂ 12–707 nm (TEM)	Centrifugation (8000g for 1h) and filtration (0.022 µm) followed by ICP-MS analysis.	Unclear, either water or exposure medium.	No TiO ₂ dissolution, 0.3% Al ₂ O ₃ dissolution.	104
Al ₂ O ₃ 300 nm (-)	Filtration (0.02 µm) followed by ICP-MS analysis.	Deionized water at pH 2 to 10 with 0.01 M NaCl and fulvic acid.	0.001% dissolution between pH 5–9 with initial concentration of 50 g L ⁻¹ Al ₂ O ₃ nanoparticles incubated for 72 hours. Dissolution decreased with fulvic acid.	82
CeO ₂ 14–29 nm (BET)	Measures dissolved Ce by ultrafiltration (10kDa) followed by ICP-MS.	Algal growth medium at pH 7.4.	No dissolved Ce could be measured in suspensions of CeO ₂ nanoparticles in algae growth medium.	98
Fe ₂ O ₃ 10 nm (DLS)	Ultrafiltration (pore size not reported) followed by UV-vis spectrophotometry.	Deionized water at pH 2–5	10–35% dissolution at low pH.	106
PbS 14.4 nm (TEM) PbS 3.1 µm (TEM)	Filtration (0.45 µm for 3.1 µm particles and 100 nm and 6 nm for 14.4 nm particles) followed by ICP-AES analysis.	Deionized water at pH 3 under anoxic conditions	Dissolution rates measured are 4.4 × 10 ⁻⁹ mol m ⁻² s ⁻¹ for dispersed 14 nm nanocrystals; 7.7 × 10 ⁻¹⁰ mol m ⁻² s ⁻¹ for dispersed 3.1 µm microcrystals; and 4.7 × 10 ⁻¹⁰ mol m ⁻² s ⁻¹ for aggregated 14 nm nanocrystals.	88
SiO ₂ 3.35 nm (BET)	A spectrophotometric method with molybdic acid	TRIS buffer at pH 7.4–7.8 at 25 °C with 0.11 M NaCl.	Equilibrium concentration of about 100 mg L ⁻¹ SiO ₂ reached within about 50 h of equilibrating. It was not reported if molybdic acid forms complexes at the SiO ₂ nanoparticles interface.	73

Particle Size (method)	Method of measuring dissolved nanomaterials	Suspension matrix	Result or main conclusion	Ref.
TiO ₂ 4.7–28.3 nm (BET)	Centrifugation (4100 rpm for 10 min) and filtration (0.2 µm) followed by Adsorptive Stripping Voltammetry (AdSV)	Deionized water with 0.1 M NaCl	Measured the lowest dissolution at pH 4–10 of about 0.05 µg L ⁻¹ Ti. Higher dissolution was measured at pH 1 and pH 13, up to about 500 µg L ⁻¹ .	⁷²
CuO 30 nm (-) ZnO 70 nm (-)	Response of the recombinant bioluminescent Zn-sensor and Cu-sensor bacteria <i>E. coli</i> .	Artificial freshwater (AFW) and 6 different types of river water	12% of CuO (nanoparticles) and 100% ZnO (bulk and nanoparticles) dissolved in AFW, less in river water. 0.3% of bulk CuO dissolved in AFW.	⁸⁷
ZnO 26 nm (TEM) ZnO 216 nm (TEM)	Filtration (0.1 µm) followed by ICP-OES analysis.	Filtered artificial seawater (salinity: 30‰), pH 8.0.	4.6% nano ZnO and 2% bulk ZnO dissolved after 150 hours equilibration.	⁸⁵
ZnO 30 nm (-) ZnO bulk, unknown size	Dialysis (1 kDa membrane) followed by ICP-AES	Deionized water with 0.01 M Ca(NO ₃) ₂ buffered to pH 7.6 with 2 mM piperazine-N,N'-bis(ethanesulfonic acid)	19% dissolution of bulk and nano ZnO after 72 hours equilibrating. Slightly higher fraction of the nano ZnO is dissolved when filtered 0.1 µm instead of dialysed 1 kDa, 0.4 mg L ⁻¹ difference.	⁸⁴
ZnO 13 nm (BET)	Centrifugation (20000 g for 5 min.) followed by ICP-MS analysis	Deionized water, bronchial epithelial growth medium, with 10% fetal calf serum at near neutral pH.	Up to 7 mg L ⁻¹ Zn dissolved, but possibly the centrifugal method does not separate all nanoparticles from dissolved Zn.	⁸³
ZnO (Electrode coating)	Used electrodes and related conductivity.	Deionized water with 0.5M KCl at pH 1 to 6	Reported dissolution rates ranging from about 10 ⁻⁷ mol cm ⁻² h ⁻¹ for pH 6 to 10 ⁻⁴ mol cm ⁻² h ⁻¹ for pH 1.	⁷⁶

2.4 Possibilities for modeling behavior of nanomaterials in water

In the last couple of years, models and frameworks to describe the fate and distribution of ENMs have been developed, some of which incorporate classical knowledge of colloid science^{38, 65, 107-110} and others which apply principles used for chemical fate modeling and material flow analysis.^{13, 37, 111-114} Gottschalk et al.^{37, 111} provide a model approach that may prove very valuable once more data become available to populate the probabilistic sub-models included. The model developed by Koelmans et al.¹¹², in which they coupled the material flow model of Mueller and Nowack¹¹³ with sedimentation, is one of the first attempts to incorporate a ENM relevant fate process in the modeling of environmental exposure. As described in the present review, a number of particle-specific fate equations will however need to be included in order to obtain “nano relevance”. Among these are sedimentation, agglomeration and dissolution, which all are dynamic, non-equilibrium processes. Future models must therefore focus in kinetics of fate processes. Arvidsson et al.³⁸ have developed such a kinetic model for the aquatic environment based on colloid chemistry principles. A sensitivity analysis of the model using 21 nm TiO₂ nanoparticles showed that the model output was mostly influenced by changes in inflow of nanoparticles to the water compartment and the collision efficiency.

The main challenge is to use the quantitative knowledge of these processes to turn current models “fit for nano”. Can current water quality models be “simply upgraded” with nano-specific process descriptions? Conceptually, if transport of ENMs to and from the water column can be described sufficiently well by first-order kinetics, this should not be difficult, and the main challenge of modeling the behavior of ENMs in water would be to quantify the first-order rate constants of the nano-specific processes. Below, we will discuss possibilities and limitations on the implementation of these first-order rate constants for the important processes sedimentation and dissolution of ENMs.

2.4.1 Sedimentation

Interactions between water and (suspended) sediments have traditionally been described as equilibrium partitioning. At equilibrium, the ratio of concentrations of substance associated with the solid phase $\rho_s C_s$ and the concentration in the water phase C_w is given by a distribution constant K_d , the value of which follows from the difference in Gibbs free energy ΔG between the dissolved and adsorbed states:

$$\rho_s C_s = K_d \cdot C_w \quad \text{with} \quad K_d = e^{-\Delta G / RT} . \quad (\text{Eq. 2.2})$$

This equilibrium partitioning concept has been used for ENMs as well. Koelmans et al.¹¹² have applied K_d -values of 10^3 – 10^5 L kg⁻¹ as reported by Ferguson et al.¹¹⁵ to calculate sedimentation fluxes of CNT. Cornelis et al.¹¹⁶ compared the extent of partitioning of soluble and nanoparticulate Ag and CeO₂ to soil particles by measuring Ag and Ce in filtrates of spiked soil suspensions, reporting the ratio of measured concentrations as a partition coefficient. This is remarkable from a colloid science perspective, where distribution between aggregated and dispersed states is believed to reflect a kinetic limitation, rather than a thermodynamic equilibrium. Colloidal systems are considered thermodynamically unstable in the sense that ΔG between aggregated and dispersed states are generally great, favoring near-complete association of ENMs with the solid surface present in natural water. According to colloid science, observed solid-water concentration ratios of ENMs have little predictive power in describing behavior of ENMs in water-sediment systems.

As discussed in a recent review by Petosa et al.³¹, DLVO theory provides the concepts necessary to model aggregation and deposition of ENMs. The rate of aggregation between two primary nanoparticles at number concentration N (m⁻³) is described by:

$$\frac{dN}{dt} = -kN^2, \quad (\text{Eq. 2.3})$$

of which the solution is:

$$N = N_0 \frac{1}{1 + kN_0 t}, \quad (\text{Eq. 2.4})$$

and in which k (m³ s⁻¹) represents the (second-order) aggregation rate constant, N_0 (m⁻³) the initial number concentration, and t (s⁻¹) the aggregation time. When there is no repulsive (activation) energy to overcome, fast aggregation, limited only by thermal (Brownian) motion of the particles, occurs with the so-called Von Smoluchowski aggregation rate constant. In presence of an energy barrier, only particles with a thermal energy great enough to pass the activated transition state can approach each other close enough for aggregation to occur. Using Boltzmann's law to describe the fraction of particles with sufficient thermal energy, an expression for the aggregation rate (k) is derived:

$$k = \frac{4kT}{3\eta} \alpha_a \approx \frac{4kT}{3\eta} 2\kappa a_p e^{-V_{\max}/k_B T}, \quad (\text{Eq. 2.5})$$

in which α_a (dimensionless) is the attachment efficiency, κ (m⁻¹) is the inverse Debye length (characteristic electric double layer thickness), a_p (m) the particle radius, V_{max} (J) is the energy of inter particle repulsion, k_B (J K⁻¹) is the Boltzmann constant, T (K) is the temperature, and η (N s m⁻²) is the viscosity of the liquid phase.

As aggregation proceeds, particle aggregates grow in size and become more prone to settling by gravity, the settling rate v_s (m s⁻¹) which follows from Stokes' law and can be derived as:

$$v_s = \frac{2a_p^2(\rho_p - \rho_w)g}{9\eta}, \quad (\text{Eq. 2.6})$$

where a_p (m) is the particle radius, ρ represents density (kg m⁻³) of particles and water respectively, g (m s⁻²) is the gravitation constant, and η (N s m⁻²) is the viscosity of water. The net result is that aggregation leads to removal of nanoparticles from water. Deposition of primary nanoparticles onto the larger solid particles plentifully present in all natural waters, of which the majority will tend to settle as well, will similarly result in removal of the ENM from water. Unfortunately, colloid science, in spite of its maturity, cannot theoretically predict the removal rates that should be expected for nanoparticles. As pointed out by Arvidsson et al.³⁸, the main reason is that numerical values for V_{max} cannot be determined easily from classical DLVO theory alone, so that for specific systems attachment efficiencies need to be measured experimentally.

Theory does explain, however, which kinetics are to be expected for the removal of nanoparticles from water. Inter particle collision (and thus aggregation) is second-order in nature. However, as the "amount" of collision capacity (sum of nanoparticles and sum of natural solid surfaces) in natural waters is expected to remain approximately constant throughout the removal process, the second-order nature will tend to reduce to pseudo first-order. Moreover, removal of solids from water by sedimentation is entirely first-order in relation to the concentration of suspended solids. Therefore, the overall kinetics of water-sediment transport of nanoparticles should be close to first-order, which is not necessarily inconsistent with the empirically observed kinetics shown in Figure 2.2. Current exposure models of the behavior of conventional chemicals can thus be upgraded to become "fit for nano" by simply adding a first-order rate constant for transport from water to sediment. Kinetic theory of particle-particle and particle-surface interactions may not be sufficient to quantitatively predict first-order constants, but certainly helps making order-of-magnitude estimates.

2.4.2 Dissolution

In spite of its obvious importance for exposure assessment, little is known about solubility and rates of dissolution of ENMs in water. In absence of such knowledge, modeling dissolution remains highly speculative. As ENMs are engineered to survive in the (often water-rich) environments where they are used, it should not come as a surprise that the chemical substances of which the ENMs are made (oxides, sulfides, metals, carbon) are generally poorly soluble in water. However, the large volumes of water in the environment can and will dissolve relatively small amounts of poorly soluble solids eventually. Removal of ENMs from water is to be modeled by quantifying the rate at which dissolution proceeds.

Dissolution can, at least in principle, be described as a surface-controlled process:

$$\frac{dM}{dt} = -k S A . \quad (\text{Eq. 2.7})$$

The amount M (kg) of ENM that dissolves in water per unit time t (s) is expected to be proportional to the area A (m²) of the nanoparticle's surface and to the concentration of dissolved material near the particle's surface, which should be close to the chemical's water solubility S (kg m⁻³). The dissolution rate constant k (m s⁻¹) reflects the local hydrodynamic conditions near the nanoparticle-water interface, of which little is known. As the rate of dissolution is proportional to the particle's surface area, rather than to the particle's mass, first-order kinetics of dissolution should be expected only when area and mass are proportional. This should not be expected, because the specific surface area (area per unit mass) of particles is expected to increase with the decrease in particle size, resulting from dissolution itself. However, the limited data presented in Figure 2.3 do not positively indicate first order kinetics, mainly because there are no data points below 50% removal. On the other hand the data do not contradict this either. In absence of more adequate data we find that using first-order kinetics for dissolution of ENMs is acceptable. This does indicate the large knowledge gap that remains to be filled before dissolution can be modeled adequately. We suggest to model removal of nanoparticles from water by adding another first-order removal rate constant, the magnitude of which needs to be measured experimentally.

2.4.3 Proposed model for exposure assessment of aquatic organisms to nanomaterials

The water model for chemical substances of Figure 2.1 could be written as:

$$\frac{dC}{dt} = E - \Sigma k C \quad \text{with} \quad \Sigma k = k_{adv} + k_{vol} + k_{deg} + k_{sed} + k_{diss} \quad (\text{Eq. 2.8})$$

where

C = mass concentration of free nanoparticles in water (kg m^{-3})

E = volume-specific release rate of ENM to water ($\text{kg m}^{-3} \text{s}^{-1}$)

k_{adv} = first-order rate constant for removal via advection (s^{-1})

k_{vol} = first-order rate constant for removal via volatilization (s^{-1})

k_{deg} = first-order rate constant for removal via (chemical) degradation (s^{-1})

k_{sed} = first-order rate constant for removal via aggregation/deposition and sedimentation (s^{-1})

k_{diss} = first-order rate constant for removal via dissolution (s^{-1})

Formulated this way, the challenge of modeling is placed entirely in assigning values to the various rate constants, which can be seen as strength and weakness at the same time. The obvious weakness is that a new removal rate needs to be measured for each individual ENM. The advantage is that it provides one single approach to modeling of conventional chemical substances and ENMs. This allows quantitative evaluation of the relative importance of the various removal mechanisms, as they act on substances with different properties (e.g. conventional vs. nano chemicals) in different aquatic environments (e.g. rivers vs. lakes). ENMs do not volatilize, whereas for conventional chemicals dissolution is irrelevant. Removal as a result of transport to sediment is modeled by assigning first-order rate constants to both conventional chemicals and ENMs, albeit on very different mechanistic grounds. Removal by advection follows entirely from the hydrodynamics of the water body; its influence on the concentration in water is independent of the nature of the chemical considered. Table 2.3 lists some typical values of removal rate constants for both conventional chemicals and ENMs in water systems and shows the uncertainty estimations for these rate constants. Rate constants for removal of ENMs by transport to sediment and dissolution were estimated from the material presented in this paper, scaled from the lengths and volumes typical of laboratory experiments to the much greater scales of real water systems. Rate constants for other removal processes were obtained by calculations with the spreadsheet model SimpleBox¹¹⁷ – the EUSES model prescribed for use in REACH (REACH R.16) was derived from this model – applied to the 3000+ organic substances in the USEtox database.^{118, 119} In the typical waters considered in environmental risk assessments under REACH, degradation, volatilization, and transport to sediment play important roles in removal only for conventional chemicals with rather extreme properties. In contrast, transport of

ENMs from water to sediment (and dissolution of ENMs as well) seem to be generally more rapid than volatilization, degradation, and sedimentation of conventional chemicals. Removal of ENMs from water through sedimentation and dissolution seems to be of similar or even greater relative importance than loss by advection.

Table 2.3. Comparison of conventional chemicals and nanomaterials for characteristic rate constants (s^{-1}) with ranges indicated for removal from water by Dissolution, Transport to sediment, Advection, Volatilization and Degradation.

	Conventional chemicals	Nanomaterials
Advection	10^{-6} [$0-10^{-5}$]	10^{-6} [$0-10^{-5}$]
Volatilization	4×10^{-9} [$0-10^{-6}$]	-
Degradation	10^{-7} [$10^{-8}-10^{-5}$]	-
Transport to sediment	8×10^{-10} [$0-10^{-6}$]	? [$0-10^{-4}$]
Dissolution	-	? [$0-10^{-5}$]

In conclusion current exposure assessment models cannot be used for nanomaterials without making adjustments to account for nano-specific processes. The most important of these, sedimentation and dissolution can be incorporated into current exposure assessment methods by adding first-order removal rates. However, theoretical description of the colloidal behavior of nanoparticles is currently insufficient to generically calculate rate constants. In absence of that, rate constants for ENMs need to be measured experimentally for different types and in different environments. Although this is difficult, time consuming and costly, current literature suggests that useful information to this end can be generated. Observations on real environmental systems are required for this purpose. Such information is also required for validation of the predicted exposure concentrations. Obviously, further development of measurement and modeling methods of exposure concentrations of ENMs is beneficial. Specifically experimental data on dissolution of ENMs and the interaction of natural colloids with ENMs and its effect on sedimentation in natural waters are needed.

Acknowledgements

This work was funded by the European Union Sixth Framework Programme NanoInteract NMP4-CT-2006-033231 and the RIVM strategic research programme SOR-S340030. We thank Martien Cohen Stuart for his suggestions.

Chapter 3

Effect of dissolved organic matter on cerium dioxide nanoparticles settling in model fresh water

JORIS T.K. QUIK, ISEULT LYNCH, KAREN VAN HOECKE, CORNELIS
J.H. MIERMANS, KAREL A.C. DE SCHAMPHELAERE, COLIN R. JANSSEN,
KENNETH A. DAWSON, MARTIEN A. COHEN STUART, DIK VAN DE
MEENT

Published as "Effect of natural organic matter on cerium dioxide nanoparticles settling in model fresh water" in Chemosphere 81, 711-715 (2010)

Abstract

The ecological risk assessment of chemicals including nanoparticles is based on the determination of adverse effects on organisms and on the environmental concentrations to which biota are exposed. The aim of this work was to better understand the behavior of nanoparticles in the environment, with the ultimate goal of predicting future exposure concentrations in water. We measured the concentrations and particle size distributions of CeO₂ nanoparticles in algae growth medium and deionized water in the presence of various concentrations and two types of dissolved organic matter (DOM). The presence of DOM stabilizes the CeO₂ nanoparticles in suspension. In presence of DOM, up to 88% of the initially added CeO₂ nanoparticles remained suspended in deionized water and 41% in algae growth medium after 12 days of settling. The adsorbed organic matter decreases the zeta potential from about -15 mV to -55 mV. This reduces aggregation by increased electrostatic repulsion. The particle diameter, pH, electric conductivity and DOM content show significant correlation with the fraction of CeO₂ nanoparticles remaining in suspension.

3.1. Introduction

Engineered nanomaterials (ENMs) are used in a wide variety of applications such as cosmetics, medicine, engineering, electronics, and environmental protection, which will inherently result in their emission into the environment and thereby lead to the exposure of organisms. The ecological risk assessment of chemicals and more recently of nanomaterials is based on the determination of adverse effects on organisms and on evaluation of the environmental concentrations to which biota are exposed.¹² Currently, the awareness of the potential adverse effects of ENMs on organisms is increasing. However, knowledge about the fate of nanomaterials in the environment is developing only slowly.¹²⁰ In particular, the exposure concentration of manufactured nanoparticles (NPs) in the environment is largely unknown and not easily measured in situ. Cerium dioxide (CeO₂) is one of the manufactured NPs focused on by the Organization for Economic Co-operation and Development (OECD) as being a priority NP due to its current use.¹²¹ CeO₂ has several applications, such as a fuel additive in the automotive industry,¹²² and a UV blocking agent in the cosmetic industry.¹²³ Studies on the solubility of CeO₂ nanoparticles are scarce, but they are generally

considered to be insoluble. In a study by Van Hoecke et al.⁹⁸ solubility was below the detection limit of approximately $1 \mu\text{g L}^{-1}$ in deionized water and algae growth medium.

Recently, much attention has been given to the important role that DOM has in the stability of particle suspensions in which DOM generally decreases aggregation. DOM originates from the breakdown of plant and animal tissue in the environment. As such, it varies in composition and concentration depending on the source and location of a water system.¹²⁴ Generally, the main constituents of DOM are humic acids, fulvic acids, and a hydrophilic fraction.^{55, 125} DOM has long been known to adsorb onto colloidal particles and influence their colloidal stability.^{48, 126} In waste water treatment, DOM is known to reduce the coagulation of particles.⁵² It has been shown more recently that carbon nanotubes and fullerenes are suspended in water in the presence of DOM.^{57, 58} Several metal¹²⁷ and metal oxide^{62, 128, 129} NPs are stabilized by the adsorption of DOM. Most studies have shown increased electrostatic repulsion due to adsorption of DOM fractions to the particle surface.^{53, 55} This causes stabilization at moderate ionic strengths due to an absolute increase in the particle charge. Additionally, the adsorbed fraction of DOM is thought to cause steric hindrance, which reduces aggregation irrespective of particle charge and ionic strength.^{53, 55, 62} The increase in colloidal stability is generally thought to affect the exposure of organisms in the aquatic environment to NPs. To predict the particle concentrations in water, we need to quantitatively understand the relationship between the particle concentration and the physicochemical properties of the particles and environment. Unfortunately, little quantitative information exists on the influence of physical and chemical properties on particle concentrations, which seriously hampers our ability to describe and predict the concentrations of nanomaterials in suspension. The known stabilizing potential of DOM for NPs is based on measuring several particle characteristics, like the zeta potential to indicate an increased electrostatic repulsion, and the particle size to see if the addition of DOM reduces aggregation. The aggregation size is related to the suspension concentrations in water.

With the present study, we aim to contribute to a better understanding of the behavior of NPs in the aquatic environment. This will ultimately serve to predict future exposure concentrations of CeO_2 NPs suspended in natural waters. We hypothesize that DOM content greatly influences the particle concentration in suspension due to its known stabilizing effect. In order to test this, we measured the concentration and particle diameter of CeO_2 NPs in suspension during 12 days to be able to relate the effect of DOM stabilization to a concentration of CeO_2 NPs in water. In our experiments we used a well-known algae growth medium¹³⁰ as the model fresh

water, with the addition of DOM to mimic environmental conditions. Most of the recent studies on the interaction of DOM and NPs have focused on DOM from the Suwannee River in Georgia, USA, which is seen as a reference material. In our experiments, we additionally used DOM from Bihain, Belgium to test whether the origin of the DOM matters. The stabilizing effect of DOM on CeO₂ NPs has not been reported yet.

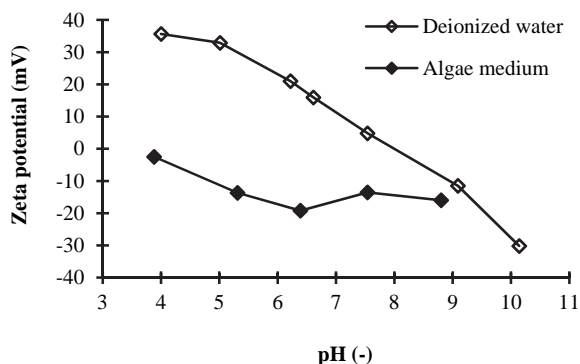


Figure 3.1. The zeta potential measurements of cerium dioxide nanoparticles at various pH, ranging from 4 to 10, in the algae medium and deionized water.

3.2. Materials and methods

3.2.1 Nanoparticles and suspensions

CeO₂ NPs were obtained as 100 g L⁻¹ suspensions at pH 4 (kindly supplied by Umicore Ltd. as part of the NanoInteract project). The manufacturer reported a BET surface area of 42 m² g⁻¹ and calculated a BET surface based particle diameter of 20 nm. The CeO₂ particles have an isoelectric point at pH 8.0 (Figure 3.1), which is similar to the values reported earlier.^{69, 98, 131} The algae growth medium (pH 8.0) was prepared according to the OECD technical guideline 201.¹³⁰ The main electrolytes present in the algae medium were NaHCO₃, NH₄Cl, and CaCl₂. For a full list with concentrations see Table B.1 in Appendix B. The calculated ionic strength was 1.7 mM. DOM from two different sources was used. Suwannee River DOM (SR-DOM) as used by Hyung et al.⁵⁸ was obtained from the International Humic Substances Society (IHSS, St. Paul, MN) as a powder. The SR-DOM stock solution was prepared by weighing 100 mg DOM per liter deionized water (MilliPore Elix 3, Billerica, MA) and stirring for 24 hours at room temperature to equilibrate. Bihain DOM (B-DOM) is retrieved by reverse osmosis from a small river in Belgium and supplied as a concentrate (DOC: ±

400 mg C L⁻¹); see Table B.2 in Appendix B for DOM characterization. All further concentrations of DOM are given as the amount of dissolved organic carbon, in mg C L⁻¹. Solutions with nominal concentrations of 0, 0.5, 1, 5, 10 and 40 mg C L⁻¹ DOM were prepared. All stock solutions were filtered using a 0.22 µm nylon membrane filter prior to use.

3.2.2 Experiment

Suspensions were prepared in glass flasks by adding 10 µL of the stock CeO₂ suspension to 100 mL of algae medium or deionized water, resulting in 10 mg L⁻¹ CeO₂ NP suspensions. Immediately after adding NPs to the algae medium, the pH was adjusted to 8.0 ± 0.2 with NaOH or HCl. The pH was not adjusted in deionized water resulting in a pH of 6.7 ± 0.2 and 7.3 ± 0.5 for suspensions with SR-DOM and B-DOM, respectively (Figure B.1 in Appendix B). Suspensions were allowed to settle under isothermal conditions for 0, 1, 4, and 12 days. Following the settling for the selected time period, samples were taken from the supernatant for analysis. With a pipette, 10 ml of the supernatant was sampled from exactly the same height, 3 cm below the flask opening. The particle size distribution was immediately analyzed.

3.2.3 Characterization

The particle diameter and suspension concentration were measured at each time point. The particle size distributions were measured by nanoparticle tracking analysis using the NanoSight LM 20 (NanoSight Ltd., Salisbury, UK). The method was previously described in Van Hoecke et al.⁹⁸. Nanoparticle tracking analysis software version 2.0 build 25 was used. The nanoparticle tracking analysis was done in expert mode and two sets of analysis parameters were used for samples with and without DOM, see Table B.3 in Appendix B. Three replicate measurements are taken and combined to get a more representative particle size distribution. The average particle diameter is weighted by the number of tracked particles, with a minimum of 100 tracks.

The concentration of CeO₂ NPs was measured by high-resolution inductively coupled plasma mass spectroscopy (Element 2 HR-ICP-MS, Thermo, Bremen, Germany). Before analysis 4 mL sample was weighed into 50 mL tubes for digestion with 7 mL 14.4 M nitric acid and 1 mL 9.8 M hydrogen peroxide at 103 °C for 2 hours.

The zeta potential of all samples was measured at the end of the deposition experiment with a ZetaSizer (nano series, Malvern Instruments Ltd., Worcestershire, UK). The total organic carbon was measured at the beginning of the experiment to

obtain the concentration of DOM in the suspensions (Dohrmann DC-190, Santa Clara, CA). Additionally the humic acid, fulvic acid, hydrophilic acid and hydrophobic neutral organic matter fractions are measured by a rapid batch procedure described in Van Zomeren et al.¹³².

3.2.4 Statistical analysis

Pearson correlation coefficients were calculated using a statistical software package (SPSS v16.0.1, SPSS inc., Chicago, Illinois).

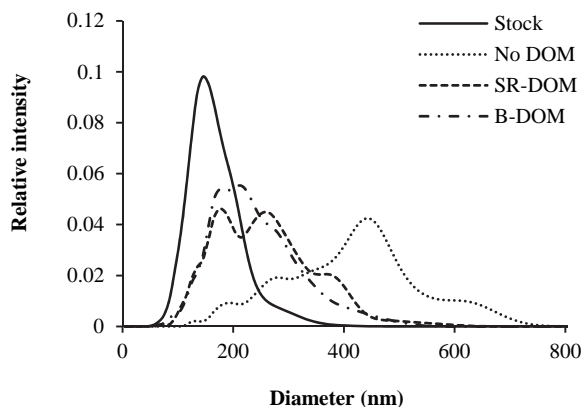


Figure 3.2. The particle size distribution (PSD) of cerium dioxide (CeO_2) nanoparticles (NPs) as measured by nanoparticle tracking analysis. Giving the PSD for the stock suspension of CeO_2 NPs used to prepare all suspensions. The PSD in algae medium without dissolved organic matter (DOM) after one day of settling. The PSD in algae medium with Suwannee River (SR) DOM and Bihain (B) DOM after 12 days of settling.

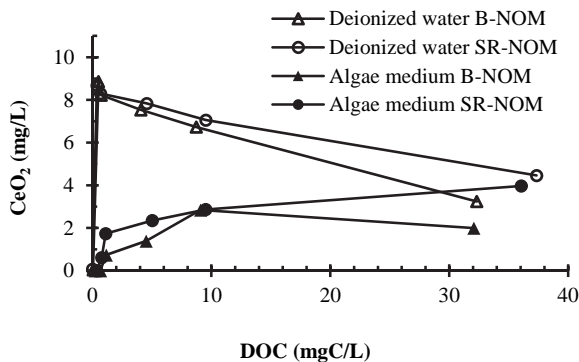


Figure 3.3. The concentration of cerium dioxide nanoparticles in the algae medium (filled symbols) and deionized water (open symbols) after 12 days of settling plotted against the dissolved organic

carbon present from addition of Bihain (B) and Suwannee River (SR) dissolved organic matter (DOM).

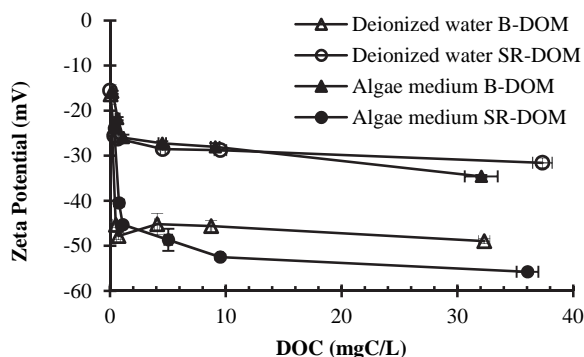


Figure 3.4. The zeta potentials of the cerium dioxide nanoparticles in the algae medium (filled symbols) and deionized water (open symbols) with various concentrations of Bihain (B) and Suwannee River (SR) dissolved organic matter (DOM).

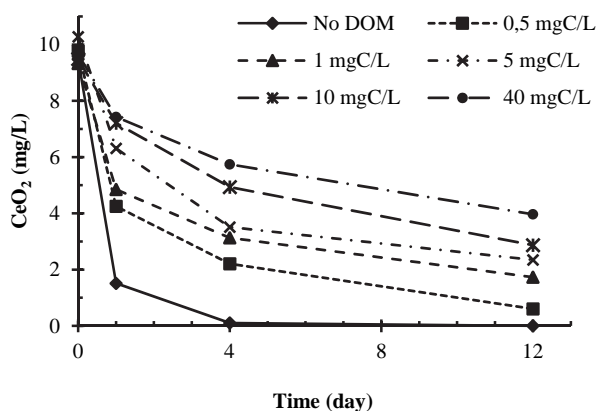


Figure 3.5. The concentration of cerium dioxide in suspension after settling for 0, 1, 4 and 12 days for suspensions prepared in the algae medium and with nominal concentrations of 0, 0.5, 1, 5, 10 and 40 mg C L⁻¹ of Suwannee river dissolved organic matter (SR-DOM).

3.3. Results

3.3.1 Characterization

In deionized water and algae medium almost all CeO₂ NPs had settled out of suspension by day 12. Less than 0.07 mg L⁻¹ of CeO₂ (0.8% of the initially added NPs) remained in suspension. The particle size distribution of the CeO₂ NPs in deionized

water and algae medium showed the formation of aggregates, with an average diameter of 301 and 417 nm in deionized water and algae medium, respectively, after one day of settling. This is larger than the average particle diameter of 169 nm found for the stock suspension at pH 4 (Figure 3.2). In algae growth medium the zeta potential varied between -7 mV and -23 mV with pH ranging from 3.9 to 8.8 (Figure 3.1). The SR-DOM contains less humic acid and more fulvic acid compared to B-DOM. The fractions of total dissolved organic carbon in either DOM type were 6% and 19% humic acid and 60% and 45% fulvic acid in SR-DOM and B-DOM, respectively. The hydrophilic acid and hydrophobic organic matter fractions were similar for both DOM types, see Table B.2 in Appendix B.

3.3.2 Dissolved organic matter in deionized water

Upon addition of DOM to deionized water a large fraction of CeO₂ NPs remained suspended. In deionized water with DOM concentrations ranging from 0.4 to 37 mg C L⁻¹, the CeO₂ concentrations in suspension ranged between 3.2 and 8.9 mg L⁻¹ (36-87%) after 12 days of settling (Figure 3.3). A slightly lower fraction of CeO₂ remained suspended in presence of B-DOM than SR-DOM. The electric conductivity in deionized water with SR-DOM and B-DOM, ranged from 3.4 to 54 $\mu\text{S cm}^{-1}$ and 4.5 to 149 $\mu\text{S cm}^{-1}$, respectively (Figure B.1 in Appendix B). The average particle diameter increases from 173 to 253 nm with increasing DOM concentration, independent of DOM type (Figure B.2 in Appendix B). The zeta potential decreased from -26 to -32 mV and -45 to -49 mV with increasing concentrations of SR-DOM and B-DOM, respectively (Figure 3.4).

3.3.3 Dissolved organic matter in algae growth medium

The sedimentation in the algae medium decreased with increasing DOM content. In algae medium with DOM concentrations ranging from 0.78 to 36 mg C L⁻¹, the CeO₂ concentrations in suspension ranged between 0.61 and 4.0 mg L⁻¹ (6.2-41%) after 12 days of settling (Figure 3.3). The fraction of CeO₂ that remained suspended in algae medium increased with increasing DOM content. Similar to suspensions in deionized water a lower fraction of CeO₂ remained suspended in algae medium when B-DOM was added compared to SR-DOM. The concentrations of CeO₂ in suspension decreased in time for all concentrations of DOM (Figure 3.5). The sedimentation in the algae medium was largest when no DOM was added and decreased with increasing DOM content. This correlation appeared to be more pronounced for SR-DOM compared to B-DOM.

With increasing DOM concentrations, the electric conductivity of the suspensions varied from 160 to 203 $\mu\text{S}/\text{cm}$ and 158 to 226 $\mu\text{S}/\text{cm}$ for SR-DOM and B-DOM, respectively, with the exception of the highest B-DOM concentration, which had an electric conductivity of 412 $\mu\text{S}/\text{cm}$ due to correction of the pH to 8 with hydrochloric acid (Figure B.1 in Appendix B).

In the algae medium with DOM added, the average particle diameter ranged from 248 to 314 nm with very similar particle size distributions up to four days of settling for all of the different concentrations of DOM (Figure 3.2 and Figure B.3). After 12 days of settling, however, there was a clear difference in the particle size distribution and average particle diameter between the lower concentrations of DOM, up to 0.78 mg C L⁻¹, and the higher concentrations of DOM, up to 36 mg C L⁻¹. In algae medium, the presence of DOM reduced the aggregate size of the CeO₂ NPs in suspension. Upon the addition of approximately 10 mg C L⁻¹ DOM to the algae medium, the average particle diameter after 12 days of settling was approximately 260 nm for both DOM types (Figure 3.2).

Similar to deionized water, the zeta potential decreased upon addition of DOM (Figure 3.4). The decrease was larger for suspensions containing SR-DOM, (-40.5 to -55.8 mV) compared to suspensions containing B-DOM (-21.8 to -34.6 mV). Significant correlations were found between the electric conductivity, pH, average particle diameter and the fraction CeO₂ in suspension ($P < 0.01$) using all data. Only in algae medium the fraction of CeO₂ in suspension significantly correlated with log normal transformed SR-DOM ($P < 0.01$) and B-DOM ($P < 0.05$) content.

3.4. Discussion

The addition of DOM to the particle suspensions had a clear effect on the concentration of CeO₂ NPs remaining suspended after a prolonged period of settling. Dissolved organic matter clearly increases the stability of CeO₂ NPs in water as previously indicated for other types of NPs.^{128, 129} The main mechanism explaining the increased stability is the adsorption of DOM to the particle surface. The strong adsorption of DOM to iron oxide, titanium dioxide, aluminum oxide, and zinc oxide surfaces was reported previously.^{53, 128} In our experiments, the absolute zeta potential increased with an increasing DOM concentration, which was also previously reported for other nanomaterials.¹⁰⁶ We observed this for both the SR-DOM and B-DOM. However, there was a difference in the magnitude of the zeta potential increase depending on the type of DOM and medium used (Figure 3.4). This difference in zeta potential is related to a larger or smaller fraction of humic or fulvic acid present in

these two DOM types, a similar difference was shown by Harbour et al.⁵⁵ for alumina particles.

An absolute increase in the zeta potential increases the electrostatic repulsion, which in turn reduces aggregation. In deionized water there is a clear increase in aggregation with an increasing DOM content. This is strongly related to an increased electric conductivity due to electrolytes present in the DOM stocks. This strong dependency on electrolyte content is in accord with the DLVO theory of colloid stability,²³ which fully explains such a dependence. This means that steric hindrance is not likely to have a large effect on the increased stability of the CeO₂ suspension with DOM. But the role of steric hindrance cannot be totally ruled out because we did not test very high ionic strengths. Several other studies have indicated the possibility of steric hindrance caused by DOM.^{53, 55, 62} The similar particle size distributions in the presence of either SR-DOM or B-DOM indicate similar stabilizing effects for both DOM types (Figure 3.2).

Aggregation and sedimentation are known to control the fate and transport of natural colloids.^{39, 41} The removal of particles from suspension depends on the sedimentation velocity. The sedimentation velocity depends on the particle diameter, density, and friction factor. In this case, aggregation means that particles settle to a greater extent and more rapidly. Ultimately, the aggregation rate limits sedimentation.

The CeO₂ NP suspensions in the algae medium that showed the greatest sedimentation had particle diameters ranging from about 150 to 800 nm in size with an average particle diameter between 400 and 490 nm. The addition of DOM reduced aggregation, which lead to an average diameter of about 275 nm and a narrower particle size distribution (Figure 3.2).

The relationship between the fraction CeO₂ NPs remaining suspended after 1, 4 and 12 days of settling and the DOM concentration was only significant in algae medium and when the DOM content was transformed by taking the natural logarithm. This can be readily understood from the non-linear relationship between the DOM content and suspended fraction of CeO₂, presented in Figure 3.3. Furthermore significant correlations were found between important parameters, like particle size, electric conductivity and the stabilized fraction of CeO₂ nanoparticles at different time points. The underlying mechanisms of these relationships, which describe the behavior of nanoparticles in aquatic systems, are not fully understood. In the natural aquatic environment other interactions most likely also play an important role in the fate of nanoparticles, e.g. with natural colloids.

In light of risk assessment further research is needed to be able to predict environmental concentrations of nanoparticles based on environmental conditions. A predicted environmental concentration for CeO₂ can be compared to a predicted no effect concentration. Van Hoecke et al.⁹⁸ reported an aquatic no effect concentration of between 0.052 and 0.108 mg L⁻¹ CeO₂. This is 7 to 14 times lower than the concentration CeO₂ remaining in suspension after 12 days settling in presence of 1 mg C L⁻¹ DOM. This no effect concentration was measured without DOM present, but this needs to be investigated.

Acknowledgements

This work was carried out as part of the European Union Sixth Framework Programme NanoInteract (NMP4-CT-2006-033231). We thank Alex de Haan from the Research and Development department of the Netherlands Vaccine Institute for help with the zeta potential measurements. We thank Rob Comans and André van Zomeren from ECN for the characterization of the dissolved organic matter.

Chapter 4

Natural colloids are the dominant factor in the sedimentation of nanoparticles

JORIS T.K. QUIK, MARTIEN COHEN STUART, MARJA WOUTERSE,
WILLIE PEIJNENBURG, A. JAN HENDRIKS AND DIK VAN DE MEENT

Published in Environmental Toxicology and Chemistry 31 (5): 1019-1022 (2012)

Abstract

Estimating the environmental exposure to engineered nanomaterials (ENMs) is part of risk assessment. Because nanoparticles aggregate with each other (homoaggregation) and with other particles (heteroaggregation), the main route of the removal of most nanoparticles from water is aggregation followed by sedimentation. We used water samples from two rivers in Europe, the Rhine and Meuse. To distinguish between small (mainly DOM) and the remainder of the natural colloids present, both filtered and unfiltered river water was used to prepare the particle suspensions. The results show that the removal of nanoparticles from natural river water follows first-order kinetics towards a residual concentration. This was measured in river water with less than 1 mg L^{-1} CeO_2 nanoparticles. We inferred that the heteroaggregation with or deposition onto the solid fraction of natural colloids was the main mechanism causing sedimentation. In contrast, the DOM fraction in filtered river water stabilized the residual nanoparticles against further sedimentation. The proposed model could form the basis for the improved exposure assessment for nanomaterials.

4.1 Introduction

The large scale production of nanomaterials⁹ has raised concerns about their potential environmental risks.¹³³ Typical colloidal processes need to be taken into account when estimating the exposure concentration of nanomaterials.¹³⁴⁻¹³⁶ Although individual colloidal processes like aggregation and sedimentation have been studied to a reasonable extent, this is usually done only with well-defined model systems, which lack the complexity present in the natural environment.^{31, 46} Here, we study the effect of natural colloids on the sedimentation of CeO_2 nanoparticles in river water.

Natural colloids comprise an ubiquitous component of natural surface water, and they are likely to affect the fate of nanoparticles.^{16, 134, 137} Natural colloids are generally categorized into three main components:⁴¹ (i) inorganic solids, (ii) small organic compounds (a few nm), and (iii) larger, rigid biopolymers ($0.1\text{-}1 \mu\text{m}$). The interaction of nanoparticles with the full range of natural colloids has been poorly studied, and most studies have emphasized the dissolved organic matter (DOM) fraction, which consists of relatively small organic compounds, such as fulvic and humic acids.^{57, 58, 70, 128, 138} However, several studies have shown that nanoparticles tend to associate with biofilms^{96, 97} and wastewater biomass,^{68, 69} indicating that heteroaggregation and

deposition are important aspects of the fate of nanoparticles in the aquatic environment.⁴⁶

Estimating the exposure concentration of nanoparticles requires a quantitative model describing the removal processes in the water phase. We previously proposed to use first-order rate constants for this.¹³⁵ This suggestion is based on the assumption that first-order kinetics apply when heteroaggregation with or deposition onto natural colloids is the dominant process affecting aggregation and sedimentation. We use the sedimentation data of CeO₂ nanoparticles in natural river water to test our proposed model. This model describes the removal of nanoparticles by first-order kinetics toward a residual concentration in the water phase. This is the first time such a model could be verified by experimental data.

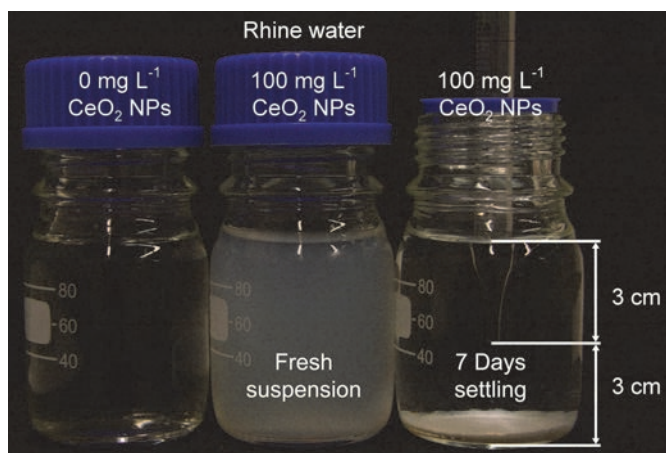


Figure 4.1. Experimental setup showing particle suspensions that were left to settle for 12 days in flasks; at set time points, a sample of the supernatant was collected for analysis at 3 cm above the bottom of the flask.

4.2 Materials and methods

4.2.1 Sampling and sedimentation

River water was sampled at the Dutch water monitoring pontoons in Eijsden (Meuse) and Lobith (Rhine). The samples were stored at 4 °C, and the experiments were started the day after sample collection. Before suspension preparation, the river water was shaken to resuspend any sedimented natural colloids, and a portion of the river water was filtered over 0.2- μ m PALL nuclepore filters as pretreatment. The suspensions were prepared by adding different doses of CeO₂ nanoparticles to 100 mL

river water to reach 1, 10, and 100 mg L⁻¹ mass concentrations of CeO₂, respectively. The sedimentation behavior was followed for 12 days by sampling the supernatant (Figure 4.1). Samples from the supernatant were taken at 6 different time points during the experiment at 3 cm above the bottom of the glass flasks, and the total height of the water column was 6 cm (Figure 4.1). This method was adapted from two previous studies describing the stabilizing effect of DOM.^{58, 70}

4.2.2 Nanoparticles and analysis

CeO₂ nanoparticles were obtained as a 100 g L⁻¹ suspension at pH 4 (kindly supplied by Umicore Ltd., as part of the NanoInteract project). The particles were dried after synthesis and were redispersed into Milli-Q water by ball milling. Prior to the redispersion, the pH of the Milli-Q water was adjusted to 4 using diluted nitric acid. The manufacturer reported a BET surface area of 42 m² g⁻¹ and a calculated BET surface based particle diameter of 20 nm. The CeO₂ particles have an isoelectric point at pH 8.0.^{70, 98, 131}

The measurements of the water quality parameters were obtained from the freely accessible waterbase application¹³⁹ (see Table C.1 in Appendix C). The concentration of suspended solids was measured by filtering with 1.2-μm Whatman GF/C filters and weighing after drying. The concentration of CeO₂ nanoparticles was measured by high-resolution inductively coupled plasma-mass spectroscopy (Element 2 HR-ICP-MS, Thermo). Before analysis, 4 mL of the sample was weighed into 50-mL tubes for digestion with 7 mL 14.4 M HNO₃ and 1 mL 9.8 M H₂O₂ at 103 °C for 2 h. The particle diameter was measured by nanoparticle tracking analysis using the NanoSight LM 20 (NanoSight Ltd.) using a previously described method.⁷⁰ This method tracks the Brownian motion of nanoparticles in water using a laser and camera. The zeta potential of all of the samples was measured at the end of the deposition experiment with a ZetaSizer (nano series, Malvern Instruments Ltd.) as an indication of the electrostatic stabilization against aggregation. As measure for DOM the dissolved organic carbon was measured by adding HNO₃ and purging with O₂ using HiPerTOC total organic carbon analyzer (Thermo). The statistical calculations were performed using R (v2.12.2).¹⁴⁰

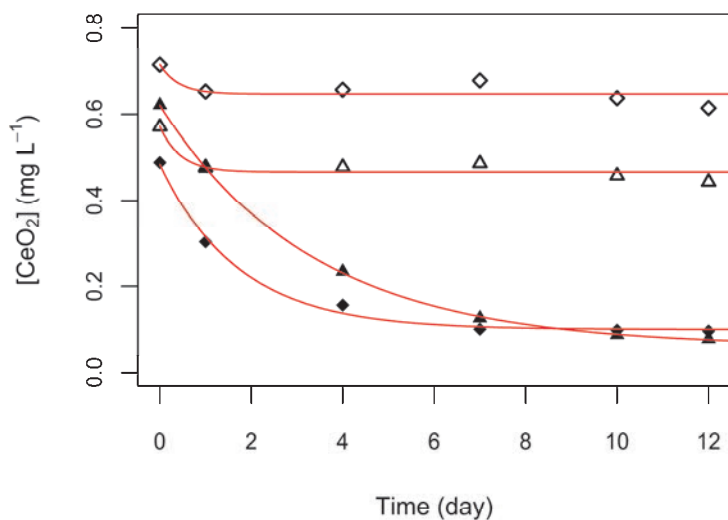


Figure 4.2. CeO_2 nanoparticle sedimentation over time for the lowest initial concentration of CeO_2 in the Rhine (triangles) and Meuse (diamonds). Water samples with natural colloids (filled) show increased sedimentation compared to filtered river water (open). The lines indicate least squares fit of equation 4.2 to the data points ($N=6$).

4.3 Results and discussion

The physico-chemical parameters of the Rhine and Meuse water samples were similar (see Table C.1 in Appendix C). Natural colloids in the Rhine and Meuse water samples contained 12 mg L^{-1} and 5 mg L^{-1} of larger suspended solids and DOM consisted of 4.5 mg L^{-1} and 3.7 mg L^{-1} dissolved organic carbon, respectively.

For the most dilute sample ($1 \text{ mg L}^{-1} \text{ CeO}_2$), between 80 to 86% of CeO_2 was removed in 12 days from the unfractionated river water, as compared to a removal of only 14 to 22% from the filtered river water (Figure 4.2). This can be explained by the CeO_2 nanoparticle heteroaggregation with or the deposition onto natural colloids, followed by sedimentation. However, it cannot be excluded that homoaggregation also plays a role prior to sedimentation at this CeO_2 nanoparticle concentration. The natural colloids themselves settled out of suspension, as was confirmed by a decrease in the aluminum concentration from $454 \text{ } \mu\text{g L}^{-1}$ to $15 \text{ } \mu\text{g L}^{-1}$ and $69 \text{ } \mu\text{g L}^{-1}$ to $8 \text{ } \mu\text{g L}^{-1}$ after 10 days sedimentation for the Rhine and Meuse water samples, respectively (Figure C.1 in Appendix C). At the higher initial CeO_2 concentrations (10 and 100 mg L^{-1}), more than 99% of the CeO_2 nanoparticles sedimented out of the unfiltered suspensions within 12 days of settling (Figure 4.3). At these higher nanoparticle

concentrations, homoaggregation was likely to be more important than interaction with the natural colloids. Although the residual concentration of CeO_2 in the 10 mg L^{-1} CeO_2 suspension was still the lowest for the presence of natural colloids in both the Rhine and Meuse samples, more than 98% of the CeO_2 nanoparticles sedimented out of the filtered river water (Figure 4.3).

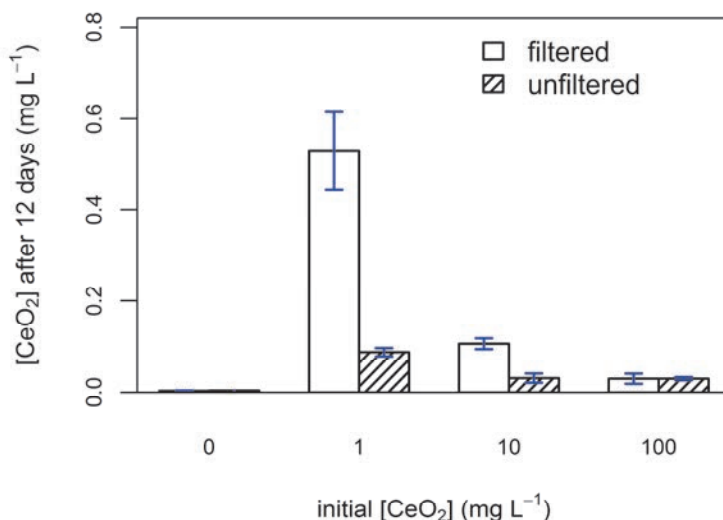


Figure 4.3. Residual concentration of CeO_2 nanoparticles after 12 days of settling in relation to the initial CeO_2 concentration for filtered and unfiltered river water, average of concentration in Rhine and Meuse.

The 1 mg L^{-1} CeO_2 suspension in the filtered river water showed almost no sedimentation (Figure 4.2). However, the zeta potential in relation to an electric conductivity of approximately $670 \mu\text{S cm}^{-1}$ of the river water was too low to explain this stability in terms of electrostatic repulsion, thereby suggesting steric repulsion due to the adsorbed DOM. The zeta potentials of colloids from the Rhine and Meuse samples and for both the 1 and 10 mg L^{-1} suspensions were very similar (between -17.9 and -15.4 mV). Only the 100 mg L^{-1} suspension showed a slightly less negative zeta potential (between -12.9 and -11.5 mV). We suggest as an explanation that in this case, the DOM fraction of natural colloids decreased the attachment efficiency of nanoparticles. At higher CeO_2 nanoparticle concentration this effect in filtered river water is not observed due to the limited amount of DOM available. Even though a relatively low sedimentation rate was measured, the particle sizes in suspension were

somewhat larger than the original material, ranging between 372 nm to 806 nm and 387 to 519 nm for the Rhine and Meuse river water samples, respectively, as compared to 171 nm for the stock CeO₂ suspension.

The data showed that both the residual concentration (C_{res}) and the rate of sedimentation (k_{sed}) were related to the initial nanoparticle concentration (C_0) or the collision frequency. This is known from colloid science theories describing aggregation and sedimentation.^{31, 38, 67} Consistent with the theories, the results show that an increasing initial nanoparticle concentration resulted in an increasing rate of sedimentation⁶⁷ and a decreasing residual CeO₂ nanoparticle concentration (Figure 4.3 and Figures C.2 and C.3). We reason that, in addition to the collision frequency, the attachment efficiency also affected the aggregation rate. This is shown by the relatively stable suspension of 1 mg L⁻¹ CeO₂ nanoparticles in filtered river water in absence of suspended solids, but in presence of DOM. The DOM is known to reduce the attachment efficiency,^{67, 129, 141} although increases due to bridging have been reported at higher DOM concentrations.^{142, 143} As we have shown earlier,⁷⁰ an increase in the DOM content can reduce the sedimentation rate for similar CeO₂ nanoparticles. In general, the initial particle concentration, which affect the collision frequency, and the macromolecular components (e.g., the DOM), which affects the attachment efficiency, are the two main parameters that affect the aggregation and subsequent sedimentation of nanoparticles in water.

Homoaggregation is the dominant process when relatively high initial nanoparticle concentrations are present. The rate at which homoaggregation takes place is faster than what first-order kinetics describe.^{27, 31, 38} Conversely, when heteroaggregation is dominant, the following first-order kinetics apply:

$$\frac{dN_{ENM}}{dt} = -k_{agg}N_{ENM}N_{NC} \quad [m^{-3}s^{-1}], \quad (\text{Eq. 4.1})$$

where k_{agg} [$m^3 s^{-1}$] is the aggregation rate constant. This model is commonly used for deposition in porous matrices.^{31, 144}

Considering the sedimentation process, we propose to use

$$C_t = (C_0 - C_{res})e^{-k_{sed}t} + C_{res} \quad [mg L^{-1}] \quad (\text{Eq. 4.2})$$

as a simplified model for estimating the concentration of nanoparticles over time. To test how this first-order model describes the measurements quantitatively, the model parameters, C_0 , C_{res} , and k_{sed} , were estimated by the nonlinear least squares regression (see Table 4.1). For this model, we assumed that heteroaggregation was the dominant process, which is the case at relatively low concentrations of nanoparticles. The model fit for the lowest initial particle concentration in the unfiltered river water was very

good (Figure 4.2), however, in the filtered river water, the residual concentration was already attained after the first day of settling. Thus, at relatively high initial particle concentrations, it is clear that the removal of particles from the suspension during the first day is faster than can be explained by first-order sedimentation kinetics, likely due to the increased homoaggregation at these higher nanoparticle concentrations. Consequently, the first measurement was omitted from the regression because the model was not valid under those circumstances (Figures C.2 and C.3). It should also be noted that the model describes the mass concentration of CeO₂ nanoparticles in time. This means that the CeO₂ nanoparticles in the residual concentration likely do not have the same physico-chemical characteristics as the initially added nanoparticles. In time nanoparticles are subject to changes in e.g. aggregate size and coating.

Table 4.1. The nonlinear least-squares estimates of the sedimentation rate constant (k_{sed}), residual concentration (C_{res}), and begin concentration (C_0) for equation 4.2 with standard error and significance for $N=6$ samples in the fractionated (F) and unfractionated (NC) Rhine and Meuse river water samples.

	$C_{0,added}$ (mg L ⁻¹)	Natural colloids	k (d ⁻¹)	C_{res} (mg L ⁻¹)	C_0 (mg L ⁻¹)
Rhine	1	NC	$0.30 \pm 0.007^{***}$	$0.06 \pm 0.003^{***}$	$0.62 \pm 0.003^{***}$
		F	2.24 ± 1.91	$0.47 \pm 0.010^{***}$	$0.57 \pm 0.019^{***}$
	10 ^a	NC	$0.83 \pm 0.040^{**}$	$0.05 \pm 0.005^{**}$	$2.10 \pm 0.083^{**}$
		F	$0.87 \pm 0.049^{**}$	$0.10 \pm 0.01^{**}$	$4.27 \pm 0.204^{**}$
	100 ^a	NC	$0.98 \pm 0.006^{***}$	$0.02 \pm 0.001^{**}$	$5.74 \pm 0.036^{***}$
		F	$1.06 \pm 0.012^{***}$	$0.02 \pm 0.002^*$	$8.78 \pm 0.104^{***}$
Meuse	1	NC	$0.58 \pm 0.069^{**}$	$0.10 \pm 0.008^{**}$	$0.48 \pm 0.013^{***}$
		F	2.44 ± 5.07	$0.65 \pm 0.014^{***}$	$0.57 \pm 0.019^{***}$
	10 ^a	NC	$0.67 \pm 0.002^{***}$	$0.02 \pm 0.0002^{***}$	$0.68 \pm 0.001^{***}$
		F	$0.79 \pm 0.010^{***}$	$0.12 \pm 0.002^{***}$	$2.89 \pm 0.028^{***}$
	100 ^a	NC	$0.99 \pm 0.052^{**}$	0.05 ± 0.016	$3.20 \pm 0.714^*$
		F	$1.06 \pm 0.229^*$	$0.05 \pm 0.010^*$	$6.98 \pm 0.354^{**}$

Significance: 0.001^{***}, 0.01^{**} and 0.05^{*}, a: $N=5$, concentration at $T=0$ omitted from the regression due to the high concentration of CeO₂.

This is the first experimental data demonstrating the effect of natural colloids on the rate of the removal of foreign nanoparticles from the water phase. According to our results using Rhine and Meuse water samples, the rate at which these particles disappear from the solution followed first-order kinetics and was strongly reduced by

prefiltering, that is, the removal of the natural colloids. For the generalization to other nanoparticles and systems, the increased complexity of the natural environment should be kept in mind, for example, the increased shear stress or interaction with organisms.^{98, 100} We further propose that the model will adequately describe the clearance of nanoparticles from the water phase under various conditions. As low initial concentrations of nanoparticles are expected to be the most common, the natural colloids present are likely to play an important role in the nanomaterial sedimentation. The heteroaggregation with or the deposition onto these natural colloids, followed by their sedimentation from the water phase, is likely to be the main removal mechanism of nanoparticles in natural water. Therefore, this approach is a valuable observation for the future modeling of exposure concentrations of nanoparticles for the purpose of risk assessment.

Acknowledgement

We thank the Research and Development Department of the Netherlands Vaccine Institute for the use of the Malvern ZetaSizer, the Centre for Environmental Health Research at the RIVM for the use of the NanoSight LM 20, and Cornelis Miermans of the Laboratory for Environmental Monitoring at the RIVM for assisting with the ICP-MS measurements. This work was funded by the European Union Sixth Framework Program NanoInteract NMP4-CT-2006-033231 and the RIVM strategic research program SOR-S340030.

Chapter 5

Nanomaterials in natural waters: Sedimentation rates and attachment efficiencies for heteroaggregation

JORIS T.K. QUIK, ILONA VELZEBOER, MARJA WOUTERS, ALBERT A.
KOELMANS AND DIK VAN DE MEENT

Submitted

Abstract

Exposure modeling of engineered nanomaterials (ENMs) requires input parameters such as sedimentation rates and attachment efficiencies. Here, we estimate these using quiescent settling experiments under environmentally relevant conditions. We investigated 4 different ENMs (C_{60} , CeO_2 , SiO_2 -Ag and PVP-Ag) in 6 different water types ranging from a small stream to sea water. Sedimentation rates in the presence of natural colloids (NC) showed significant differences among particle and water types. The sedimentation rates ranged from 0.0001 m d^{-1} for SiO_2 -Ag to 0.14 m d^{-1} for C_{60} . NC-ENM apparent heteroaggregation rates and attachment efficiencies were estimated using a novel method that separates heteroaggregation from homoaggregation using a simplified Smoluchowski-based aggregation-settling equation applied to data from unfiltered and filtered waters. The attachment efficiencies for heteroaggregation ranged between 0.0067 and 1, with the highest values observed in seawater. We argue that such system specific parameters are key to the development of dedicated water quality models for ENMs.

5.1 Introduction

The production and use of engineered nanomaterials (ENMs) are growing, which increases their emission to environmental compartments.¹⁵ Consequently, understanding the safety, environmental and human health implications of nanotechnology-based products is of worldwide importance.^{145, 146} Although the benefits of ENMs have shown to be plentiful, the implication of large quantities of ENMs entering the environment has yet to be understood.^{9, 147} There is a growing need for risk assessment of different nanomaterials in order to support their safe production and use.¹⁴⁸ The environmental risk assessment is based on the determination of adverse effects on organisms and on evaluation of the environmental concentrations to which biota are exposed.^{64, 135} Recently, several modeling approaches for estimating the environmental exposure concentration of nanomaterials have been suggested.^{36-38, 135} However, these studies acknowledge a lack of input parameters valid for environmentally relevant conditions, such as attachment efficiencies for collisions between natural colloids (NCs) and ENMs (α_{hetero}),^{36, 38} and sedimentation rates in natural waters.^{37, 135} Since there is no validated framework for calculation of these parameters for ENMs, they need to be estimated experimentally.^{46, 134, 149, 150}

Heteroaggregation rates are usually measured by directly measuring the increase in particle size in time.^{151, 152} The attachment efficiency is often calculated from the ratio between the rate of aggregation under unfavorable conditions compared to the rate under favorable conditions,³¹ although in a recent study it was deemed unfeasible to apply this method for estimating the attachment efficiency for heteroaggregation due to not measuring the aggregation rate under favorable conditions.¹⁵² For studying heteroaggregation in complex natural systems, direct measurement of aggregation rates is problematic due to the limitations of measurement techniques for such complex systems. For this reason, it has been shown that sedimentation can be used to estimate the attachment efficiency.⁶⁷

In the present study we provide sedimentation rates and estimates of attachment efficiencies for heteroaggregation, based on sedimentation data for 4 different ENMs in the presence and absence of NCs in 6 different natural water types. A novel method to estimate these attachment efficiencies from sedimentation data is proposed. We used fullerenes (C₆₀) as a carbon based ENM, Cerium dioxide (CeO₂) ENM as a metal oxide and Silver (Ag) ENM with two different coatings, polyvinylpyrrolidone (PVP) and silicon dioxide (SiO₂). Quiescent settling was followed in water from six different water bodies ranging from a small pond and stream to lake and seawater. Earlier work showed that NCs governed the sedimentation of ENMs in river water (Rhine and Meuse).¹⁵³ Here, this mechanism is studied for a much wider range of water types, including brackish tidal water and marine water. Sedimentation rates, heteroaggregation rates and attachment efficiencies for heteroaggregation between ENMs and NCs are reported. To our knowledge, this is the first study that reports these parameters on the interaction of ENMs with NCs in surface waters.

5.2 Materials and Methods

5.2.1 Engineered nanomaterials

Polyvinylpyrrolidone coated silver (PVP-Ag) nanoparticles (hydrodynamic diameter (d_h): 102 nm) and SiO₂ coated silver (SiO₂-Ag) nanoparticles (d_h: 148 nm) were purchased from nanoComposix (San Diego, CA). Ceriumdioxide (CeO₂) nanoparticles (d_h: 167 nm) were kindly supplied by Umicore Ltd. (Brussels), as part of the EU NanoInteract project. CeO₂ nanoparticles from the same batch have previously been used in several fate and effect studies.^{70, 98, 153, 154} Fullerene (C₆₀, d_h: 217 nm), 99 wt% purity was obtained as powder from Cheaptubes (Brattleboro, VT). A C₆₀ nanoparticles stock suspension was prepared by dispersing 1 g L⁻¹ C₆₀ in deionized

water by shaking (150 rpm) for 4 weeks in a glass bottle screened from sunlight. Other properties and electron microscopy images of the ENMs are provided as Supporting Information (Table D.1, Figure D.1 and D.2 in Appendix D).

Particle size distribution and particle number concentration were measured using nanoparticle tracking analysis (NTA). This was done after 1, 6 and 10 days of settling using the NanoSight LM 20 (NanoSight Ltd., Salisbury, UK) using a previously described method⁷⁰ and NTA software version 2.2. Electrophoretic mobility of all samples was measured after day 0, 2 and 13 of settling with a ZetaSizer instrument (nano series, Malvern Instruments Ltd., Worcestershire, UK). Throughout this paper, the term ‘concentration’ refers to mass concentration unless indicated otherwise.

Table 5.1. Characteristics of the natural waters.

Sample	KG	AA	RL	IJ	MS	NZ
pH (-)	4.61	6.69	7.95	8.33	7.89	7.78
EC ($\mu\text{S cm}^{-1}$)	67.1	434	584.3	763	7200	47000
O ₂ (mg L^{-1})	8.94	7.55	9.27	10.83	7.92	8.38
Cl (mg L^{-1})	9.9	57.5	126	146	3970	28600
NO ₃ +NO ₂ (mg N L^{-1})	0.2	6.25	2.75	1.88	2.44	0.26
PO ₄ ($\mu\text{g P L}^{-1}$)	48.2	102.4	36.1	28.4	103.4	n.a. ^a
NH ₃ (mg N L^{-1})	0.18	0.59	0.03	0.1	0.07	0.02
Total P (mg P L^{-1})	0.01	0.16	0.04	0.02	0.12	0.12
Total N (mg N L^{-1})	0.34	5.14	1.68	1.45	1.72	0.06
Ca (mg L^{-1})	3.7	36	55.7	55.4	104	401
K (mg L^{-1})	1.2	13.7	4.4	7.4	50	371
Mg (mg L^{-1})	1.94	7.7	10.6	12.3	160	1233
Na (mg L^{-1})	13.9	22.7	46.2	59.1	1370	10630
DIC (mg C L^{-1})	0.69	23.02	24.62	30.23	31.22	40.91
DOC (mg C L^{-1})	5.45	25.98	2.45	5.62	2.85	0.17
NCs ^b (mg L^{-1})	1.9	7.1	10.3	2.9	11.9	2.6
NCs ^c (10^8 L^{-1})	0.65	3.39	0.72	0.51	0.54	0.10
Density NC ^d (kg m^{-3})	1350	1879	2363	1513	2262	1993
Radius NC ^c (nm)	351 ± 46	286 ± 31	291 ± 47	225 ± 30	319 ± 49	348 ± 163

a: No data available

b: Measured using dry weight after filtration.

c: Measured using nanoparticle tracking analysis.

d: Calculated from ash free dry weight ($\rho=1250 \text{ kg m}^{-3}$) and ash weight ($\rho=2700 \text{ kg m}^{-3}$)¹⁵⁵

5.2.2 Water sampling

Six different natural waters were sampled using polyethylene containers. Samples were taken from the North Sea (NZ, coastal sea), Rhine (RL, river), Brabantse Aa (AA, small stream), IJsselmeer (IJ, freshwater lake), Nieuwe Waterweg (MS, tidal water), and Karregat (KG, small acid pond), all located in the Netherlands. Details on sampling and exact locations are provided as Supporting Information (Table D.2 in Appendix D). Sedimentation experiments were started on the same day of sampling. To remove NCs, part of the water was filtered with 0.2 μm membrane filters (Nuclepore filters, PALL), following earlier studies.^{58, 153} This filtration technique reduces NC concentrations to negligible levels (Figure D.4). After measuring pH, EC and O_2 content, samples were stored at -20°C before further elemental analysis. Dissolved organic carbon (DOC) was measured by adding HNO_3 and purging with O_2 using HiperTOC (Thermo, Delft, NL). The six water types mainly differed in ionic strength, pH and DOC content (Table 5.1). Electric conductivity as an indicator of ionic strength ranged between $47000\ \mu\text{S cm}^{-1}$ for sea water (NZ), followed by brackish water (MS) and the different fresh water types (IJ, RL, AA, KG) of which the lowest value was $67.1\ \mu\text{S cm}^{-1}$ (Table 5.1). DOC concentration was highest at AA ($26\ \text{mg C L}^{-1}$) and lowest at NZ ($0.17\ \text{mg C L}^{-1}$). The pH was lowest at KG ($\text{pH}=4.6$) whereas the pH of the five other water types ranged from 6.7 to 8.3. MS and RL water had the highest concentration of natural particulate matter ($>10\ \text{mg L}^{-1}$), whereas NZ, KG and IJ water had the lowest concentration of natural particulate matter ($< 3\ \text{mg L}^{-1}$). An overview of all chemical characteristics of the water samples is provided in Table 5.1.

5.2.3 Sedimentation experiments

Sedimentation of CeO_2 , PVP-Ag, SiO_2 -Ag and C_{60} nanoparticles was studied during 15 days with a method adapted from earlier work.^{70, 153} Our experiments used a considerably longer sedimentation time than many other studies, in order to increase realism and accuracy in medium to long timescales. Three different doses of ENMs were added to each of the six water types in order to obtain dispersions of 0.5, 2.5 and $10\ \text{mg L}^{-1}$ for the metal ENMs, and 5, 25 and $100\ \text{mg L}^{-1}$ for the C_{60} nanoparticles. For C_{60} nanoparticles a higher dose was used because of the higher detection limit of the UV_{vis} method. After 0, 1, 2, 6, 10 and 15 days, samples were taken for characterization and analysis of ENM. Samples of 5 mL were carefully taken by pipette at 3 cm below the water surface and used for measurement of concentration, particles size and electrophoretic mobility, see above. Concentrations of Ce and Ag were taken as a proxy for ENM mass, and were measured by high-resolution inductively coupled

plasma-mass spectroscopy (Element 2 HR-ICP-MS, Thermo, Bremen, Germany). Before analysis, 4 mL of the supernatant sample was weighed into 50-mL tubes for digestion with 7 mL 14.4 M nitric acid and 1 mL 9.8 M hydrogen peroxide at 103 °C for 2 h (Ce measurements). For Ag measurement, 7 mL 37% w/w HCl was added. Concentration of C₆₀ were measured by extraction using 0.01 M Mg(ClO₄)₂ from water to 2.5 mL toluene after shaking for 30 minutes. Subsequently, the absorbance in 1 mL toluene C₆₀ extracts was measured at 335nm in triplicate.

5.2.4 Dissolution

At the start and after 15 days the dissolved fraction of metals in the water phase was measured by centrifugal filtering for 15 min. at 14000 rpm. Particulate and dissolved fractions were separated by means of 3kDa filters (PALL). To prevent reported effects of Ag⁺ loss from adsorption to the filter, filters were pre-treated with Cu solution.¹¹⁶ 1 mL samples were collected from two filters and Ag and Ce concentration was measured using HR-ICP-MS (see above). The chemical speciation program CHEAQS¹⁵⁶ was used to calculate chemical species present at the measured water composition.

5.2.5 Estimating sedimentation rates

Sedimentation data were interpreted using a semi-empirical model adapted from Newman et al.¹⁵⁷ and Quik et al.¹⁵³, which describes the concentrations of ENMs in the supernatant (C_t [g L⁻¹]) as a function of time:

$$C_t = (C_0 - C_{ns})e^{-(\frac{V_s}{h} + k_{dis})t} + C_{ns} \quad (\text{Eq. 5.1})$$

The non-settling concentration (C_{ns} [g L⁻¹]) represents the ENM concentration after infinite time based on data measured at 15 days. V_s [m d⁻¹] is the apparent sedimentation rate, h [m] is the sedimentation length, k_{dis} [d⁻¹] is the dissolution rate constant and t is time [d]. This model was fitted to the data using the nonlinear least squares method in package stats in R.¹⁴⁰ Due to the design of the sedimentation experiment, dissolution (k_{dis} in equation 5.1) could not be inferred from the elemental concentration measurement in the supernatants of the settling experiments (section 5.2.5). After all, Ce, Ag or C₆₀ in the supernatant were measured as total concentration, thus any decrease in concentration in time has to relate to sedimentation (V_s) and not to dissolution (k_{dis}). Instead, dissolution was studied by analyzing the Ag and Ce ion concentrations in ultra-filtered water.

In order to compare the obtained sedimentation rates (Table 5.2, V_s) to literature data, we converted previously reported sedimentation rate constants [d⁻¹]^{67, 92, 158} to

true sedimentation rates [m d⁻¹] using a sedimentation length measured from the water surface to the measurement depth (calculations provided table D.4 in Appendix D).

5.2.6 Estimating the heteroaggregation rate and attachment efficiency

The basis for the calculation of the heteroaggregation rate and attachment efficiency is the combined Von Smoluchowski–Stokes equation:²⁴

$$\frac{dN_j}{dt} = \frac{1}{2} \sum_{i=1}^{j-1} \alpha_{i,j-i} K_{i,j-i} N_i N_{j-i} - N_j \sum_{i=1}^{\infty} \alpha_{i,j} K_{i,j} N_i - \alpha_{NC,j} K_{NC,j} N_{NC} N_j - \frac{v_{s,j}}{d_s} N_j \quad (\text{eq. 5.2})$$

in which $\alpha_{i,j}$ is the attachment efficiency between ENM aggregates i and j , $\alpha_{NC,j}$ the attachment efficiency between ENM and NCs, j the number of primary nanoparticles in ENM aggregate, $K_{i,j}$ the collision frequency between ENM aggregates i and j [m³ s⁻¹], $K_{NC,j}$ the collision frequency between ENM particle aggregate j and NCs [m³ s⁻¹], N_j is the number concentration of the ENM aggregate j [m⁻³], N_{NC} is concentration of NCs [m⁻³], $v_{s,j}$ is the sedimentation rate of ENM aggregate j [m s⁻¹] and d_s is the sedimentation length [m]. In Eq. 5.2, the first two terms account for growth to and loss from ENM size class j due to homoaggregation, the third term accounts for heteroaggregation, and the last term for sedimentation of ENM aggregates. The concentration of natural colloids C_{NC} is assumed to decrease due to Stokes settling:^{40,}

155

$$\frac{dN_{NC}}{dt} = -\frac{v_{s,NC}}{d_s} N_{NC} \quad (\text{eq. 5.3})$$

Eq. 5.2 is simplified based on a series of informed assumptions, which subsequently are validated against simulations obtained using the full deterministic Eq. 5.2 (provided as supporting information in Appendix E). Following Farley and Morel³⁵, it is assumed that aggregation is the rate limiting process for the observed removal of ENMs from the water phase. This is based on the concept that aggregates first need to be large enough for sedimentation to occur. This means that the aggregation terms in Eq. 5.2 are considered to be rate determining and that the last term in Eq. 5.2 can be omitted. Secondly, it is assumed that the summations in Eq. 2 can be replaced by single terms accounting for the apparent critical collision behavior for sedimentation. This is motivated as follows. The summation in Eq. 5.2 accounts for numerous collisions that will not (yet) lead to homo- or heteroaggregates large enough to settle. However, a certain fraction of all possible collisions will at some point reach a critical limit after which rapid settling occurs. The measured removal in the sedimentation experiments relate to this apparent removal of settleable ENMs only (ENM_{crit}).

Because size distributions of these settling ENM aggregates will probably not be monodisperse, the single terms are governed by apparent parameters reflecting average properties of the particles at the onset of settling. Thirdly, it is assumed that the ENM concentration change in the overlying water is determined by aggregation to settling particles only i.e. is not affected by progressive aggregation to larger particles. Progressive aggregation cannot affect $C_{ENM,crit}$ concentrations beyond the critical size for sedimentation because they would have settled out already. This implies that the first two terms for aggregation in Eq. 5.2 can be combined. Consequently, Eq. 5.2 can be simplified to describe removal from the water column:

$$\frac{dC_{ENM,crit}}{dt} = -\alpha_{hom,crit}K_{hom,crit}C_{ENM,crit}^q - \alpha_{het,crit}K_{het,crit}C_{NC}C_{ENM,crit} \quad (\text{eq. 5.4})$$

in which $C_{ENM,crit}$ is the concentration of settleable ENMs [g L^{-1}], $k_{hom,crit}$ is the apparent collision rate constant for the formation of settleable ENM homoaggregates [$(\text{L g}^{-1})^{1-q} \text{ s}^{-1}$], $\alpha_{hom,crit}$ is the apparent attachment efficiency for settleable ENM homoaggregates, $\alpha_{het,crit}$ is the apparent attachment efficiency for settleable ENM-NC heteroaggregates, and $K_{het,crit}$ is the apparent collision rate constant for the formation of settleable ENM heteroaggregates [$\text{L g}^{-1} \text{ s}^{-1}$]. The exponent q defines the kinetics for homoaggregation and was estimated as $q \approx 1$, by fitting the analytical solution of equation 5.4 against simulations based on Eq. 5.2 (details provided as supporting information in Appendix E). In summary, Eq. 5.4 describes how the concentration of the (operationally defined) settling ENM fraction changes over time, as a function of the processes that drive the production of aggregates. Aggregates that do not settle substantially in the time interval over which settling is monitored (15 days in the present experiments) are also formed. Primary particles may also be stabilized and not settle at all. The latter two categories of processes lead to an operationally defined non-settling fraction (C_{ns} in Eq. 5.1). Eq. 5.4 can be solved with $q=1$ and with Eq. 5.3 for the time dependence of C_{NC} to yield the analytical solution:

$$C_{ENM,crit}(t) = C_{0,ENM,crit}e^{-At+B}(e^{-Dt}-1) \quad (\text{eq. 5.5})$$

where $A = \alpha_{hom,crit}K_{hom,crit}$, $B = \alpha_{het,crit}K_{het,crit}C_{0,NC}d_s/v_{s,NC}$ and $D = v_{s,NC}/d_s$. The rate for heteroaggregation to settleable particles, $\alpha_{het,crit}K_{het,crit}$, can be estimated by fitting Eq. 5.5 to the sedimentation data from the unfiltered systems using values for $\alpha_{hom,crit}K_{hom,crit}$ obtained from fitting Eq. 5.5 to sedimentation data for the filtered systems, with $C_{0,NC} = 0$. The fitting procedures may use all measured sedimentation data or may use C_0 and a single time point $C(t)$, for instance after 15 d only. The latter approach is better if the differences between sedimentation in filtered vs. unfiltered water are too small for the early time points. After obtaining $\alpha_{hetero,crit}K_{het,crit}$, this can

be adjusted for differences in collision frequency through dividing by K_{het} , which is the collision frequency between ENMs and NCs based on Brownian motion and differential settling (details provided as supporting information in Appendix E, Eq. E.7 and Table E.2). This assumes that shear is negligible due to the quiescent settling conditions. The relative $\alpha_{hetero,crit}$ can be estimated using these adjusted apparent heteroaggregation rates. A validation of the two fitting approaches (i.e. full curve vs. single time point) against simulations using Eq. 5.2 is provided in Appendix E.2.

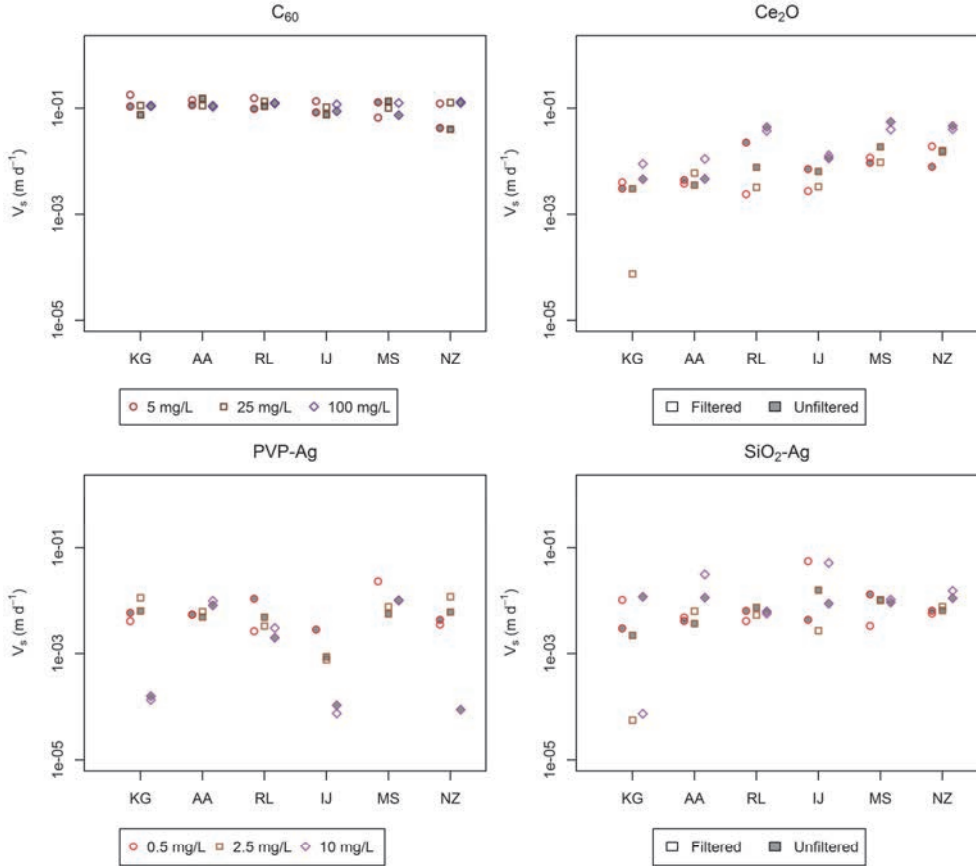


Figure 5.1. Sedimentation rates (V_s) for C_{60} , CeO_2 , PVP-Ag and SiO_2-Ag nanoparticles in 6 different water types with (unfiltered) and without (filtered) natural colloids present, for 3 different initial ENM concentrations (0.5, 2.5 and 10 $mg L^{-1}$ for metal ENMs and 5, 25, 100 $mg L^{-1}$ for C_{60}). Water types: Karregat (KG), Brabantse Aa (AA), Rhine (RL), IJsselmeer (IJ), Nieuwe Waterweg (MS) and North Sea (NZ).

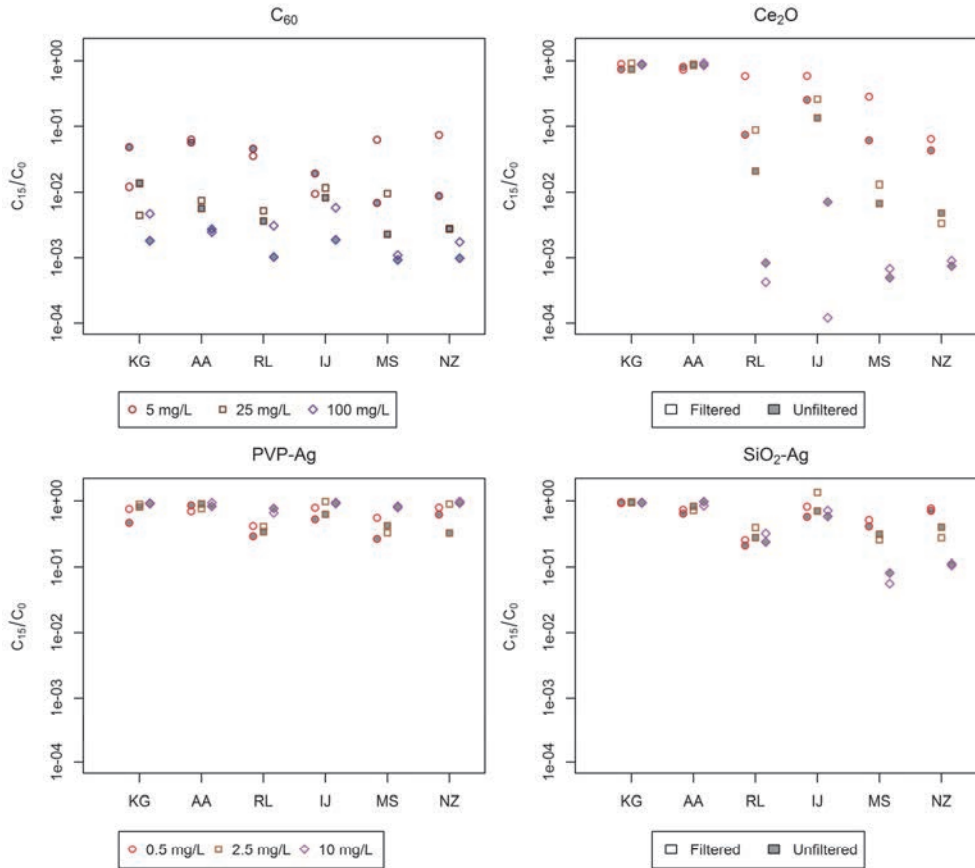


Figure 5.2. Non-settling fractions (C_{15}/C_0) for C_{60} , CeO_2 , PVP-Ag and SiO_2 -Ag ENMs in 6 different water types with (unfiltered) and without (filtered) natural colloids (NCs) present for 3 different initial ENM concentrations. Water types: Karregat (KG), Brabantse Aa (AA), Rhine (RL), IJsselmeer (IJ), Nieuwe Waterweg (MS) and North Sea (NZ).

5.3 Results and discussion

5.3.1 Natural colloids and water types

In general, NCs increased sedimentation of ENMs, although the obtained ENM sedimentation rates were not significantly affected by the presence of NCs in the surface waters, nor by the different water types (paired t-test, $p > 0.05$, Figure 5.1). However, for the non-settling fraction after 15 days (C_{15}/C_0), a significant decrease was observed in the presence of NCs ($p < 0.01$, Figure 5.2). Significant differences between the C_{15}/C_0 were also observed between most water types, except in the

subsets RL, MS, NZ, and AA, KG, IJ (Figure 5.2). This suggests a communality in the characteristics of the water types in these sets. The KG, AA and to lesser extent IJ water show significantly higher non-settling fractions in the water phase after 15 days compared to RL, MS and NZ. The first mentioned group also possesses the more favorable conditions for stability against aggregation, such as higher DOC, lower EC, more extreme pH and lower NC mass.^{46, 67, 159} In addition to ENM sedimentation being affected by the presence of NCs, the sedimentation of NCs may also be affected due to heteroaggregation with ENMs. However, using Al as a proxy for NCs, we observed no significant effect of presence of ENMs on NC settling (Figure D3 in Appendix D).

To better isolate the effect that NCs may have on the sedimentation of ENMs from the water phase, we subtracted the C_{15}/C_0 in unfiltered water from that in filtered river water. This shows that NCs generally increase sedimentation of ENMs (Figure 5.3) for the most environmentally relevant initial particle concentration (0.5 or 5 mg L⁻¹ ENM). The fraction removed due to presence of NCs varies per water type and particle type. In AA water the difference is negative for both CeO₂ and PVP-Ag ENMs suggesting a decrease in sedimentation in presence of NCs. This is not in line with the total amount of NCs present in AA water, which has the highest available surface area for interaction with ENMs compared to the other water types (Figure 5.4 and Figure D.4). This suggests that the NCs present in AA water do not directly affect the sedimentation within 15 days. This could be due to the size of the NCs in AA water, which were measured to be smaller than NCs in the other water types. In the other waters, the larger NCs settle much faster (Figure D.3). The low fraction removed for AA water may also relate to the high DOC content of the water. DOC may indicate the presence of lower density NCs, which might not settle within 15 days. Furthermore, DOC (as a proxy for dissolved organic matter) is known to reduce the attachment efficiency of ENMs resulting in a decrease in aggregation and sedimentation.^{70, 160}

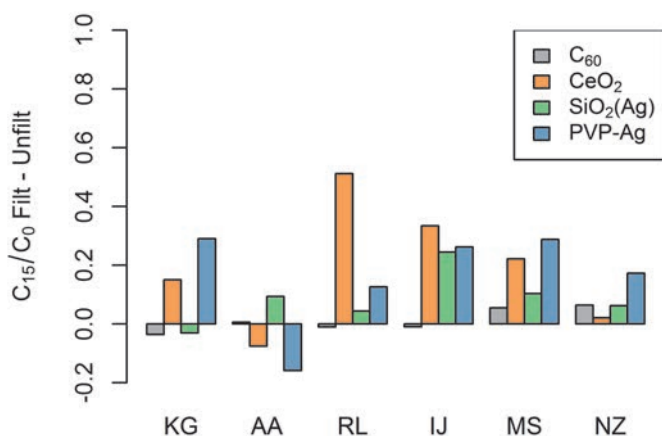


Figure 5.3. Fraction of ENM removed from the water phase due to the presence of NCs. Calculated by subtraction of C_{15}/C_0 for unfiltered water from C_{15}/C_0 of filtered water, for 0.5 mg L^{-1} (metal ENM) and 5 mg L^{-1} (C_{60}) initial ENM concentration. Water types: Karregat (KG), Brabantse Aa (AA), Rhine (RL), IJsselmeer (IJ), Nieuwe Waterweg (MS) and North Sea (NZ).

5.3.2 Sedimentation and stability of ENMs

The different ENMs showed significant differences in apparent sedimentation rate and C_{15}/C_0 (paired t-test, $p < 0.01$; Figure 5.1). The sedimentation rates ranged from 0.0048 m d^{-1} for PVP-Ag to 0.12 m d^{-1} for C_{60} . The apparent non-settling fractions (given as $C_{15}/C_0 \times 100\%$) after 15 d varied from 0.01% to 92% for the metal based ENMs. Only for C_{60} particles consistently low values of C_{15}/C_0 were observed in all water, from 1 to 7 %. A full overview of all the sedimentation rates and C_{15}/C_0 can be found in Table D.5. In addition to differences in chemical composition, these ENMs differed in particle coating, size and initial particle number concentrations. The observed number concentrations (Figure 5.4) are discussed here because it is important for relative contributions of homo- and heteroaggregation, discussed in the next section. The differences in particle size cause differences in particle number concentration for the same 0.5 mg L^{-1} mass concentration (Figure 5.4). The 0.5 mg L^{-1} PVP-Ag and $\text{SiO}_2\text{-Ag}$ have similar particle number concentrations. CeO_2 however, shows significantly lower particle number concentrations. The 5 mg L^{-1} C_{60} particle number concentration (not shown) is even lower, but this is probably not representative due to limitations of the NTA measurement method with regard to large C_{60} aggregates ($> 1\mu\text{m}$). Because (a) the initial ENM concentration appears to affect the sedimentation rate and C_{15}/C_0 of the ENMs (Figures 5.2 and 5.3), and (b) the

lower concentrations have a higher environmental relevance, the discussion below will focus on the data obtained at the lowest initial ENM concentrations (Table 5.2).

Generally, sedimentation rates from other studies span a higher range compared to the range observed in our experiments with 6 different water types in the presence of NCs (Figure 5.5). Only the sedimentation rates reported by Keller et al.⁶⁷ span down to similarly low values. There are too many differences between these studies to unambiguously explain all differences. However, generally these earlier studies used higher initial ENM concentrations, which may explain the higher sedimentation rates for these ENMs. Remarkably, the highest sedimentation rates are observed for multi walled carbon nanotubes,⁹² regardless of the presence of DOC in the water. This agrees to the much higher sedimentation rates observed for C₆₀ in the present study. Furthermore the study of Battin et al.⁹⁶ showed relatively high sedimentation rates: between 0.10 and 0.28 m d⁻¹ using stream microcosms, with and without a biofilm present, as opposed to quiescent settling in the current study. The adsorption of the ENM to the biofilm may have caused these higher sedimentation or removal rates. In our previous studies sedimentation of the same CeO₂ ENM as in the present study were tested in algae medium with and without DOC⁷⁰ and in two natural water samples from the Rhine and Meuse rivers.¹⁵³ The sedimentation rates for 1 mg L⁻¹ CeO₂ suspensions in natural water were similar to the rates observed in the present study.

Given the importance of the particle number concentration on aggregation, the contribution of heteroaggregation can only be significant when there are more NC than ENM particles present in suspension. This idea has been postulated^{36, 135} as a basis for exposure modeling where heteroaggregation is assumed to be the dominant process due to the abundance of NCs being much higher than that of ENMs, given their current and anticipated levels of ENM emission.¹⁶¹ For exposure modeling this simplifies equation 5.2 to only the heteroaggregation term. However, we observed the particle number concentration of both of our Ag nanoparticle types to be higher than the NC number concentrations present in the different water types (Figure 5.4). Only for CeO₂ similar or higher NC number concentrations than ENM number concentrations are observed. Nevertheless, for both Ag and CeO₂ ENMs a higher sedimentation is observed in most water types when NCs are present (Figure 5.3). This shows that even at these rather high ENM concentrations, NCs affected sedimentation. However, homoaggregation cannot be excluded as shown by the removal of ENMs in filtered water. Note that, unlike Eqs. 5.2 and 5.5, the empirical model used to estimate apparent sedimentation rates (Eq. 5.1) does not explicitly

account for all the processes affecting sedimentation, such as homo- and heteroaggregation.

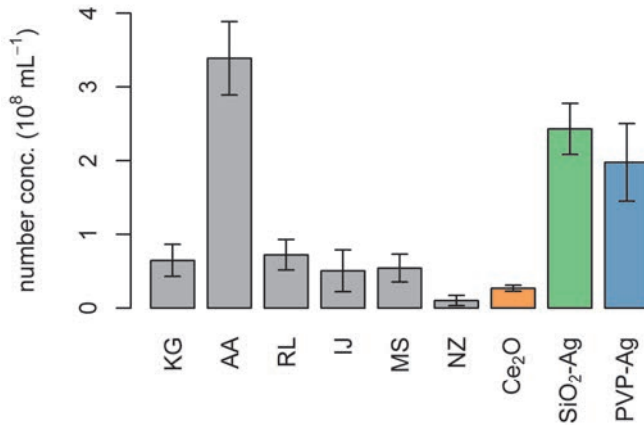


Figure 5.4. Number concentration of NCs in original water for 0.5 mg L^{-1} (metal ENM) and 5 mg L^{-1} (Ce_{60}) ENMs in deionized water as measured by nanoparticle tracking analysis. Water types: Karregat (KG), Brabantse Aa (AA), Rhine (RL), IJsselmeer (IJ), Nieuwe Waterweg (MS) and North Sea (NZ).

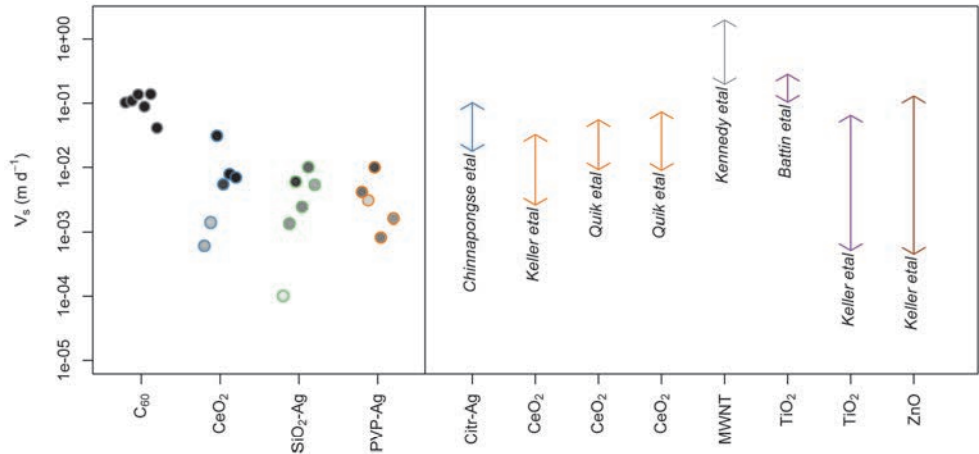


Figure 5.5. Comparison of sedimentation rates (points, this study) to ranges recalculated from literature data (arrows with citation).^{67, 70, 92, 96, 153, 158}

5.3.3 Dissolution

It has been reported that Ag dissolution is affected by Ag nanoparticle coating as well as by pH, oxygen content and ionic composition of the water.^{90, 162, 163} CeO_2 is not

expected to show any significant dissolution.¹³⁵ In general, dissolution was very limited, with values < 1.5 % for AA, RL, IJ and MS and similar for both PVP and SiO₂ coated Ag nanoparticles. Higher dissolution was measured in the acid pond water (KG), i.e. between 0.7 and 4% with a slightly higher dissolution of SiO₂-Ag than PVP-Ag in these acidic conditions (Figure 5.6 and Figure D.4 in Appendix D). Additionally, KG water is the only water type with a detectable fraction dissolved Ce: < 0.4 %. The highest percentage of dissolved Ag (7 - 12 %), is measured in sea water (NZ).

The measured dissolved fraction of Ag and Ce after 15 days was in most cases lower than at the start of the experiment (Figure D.3). This suggests that the stable species of Ag is not a dissolved ion complex, but that precipitation occurs, most likely of AgCl(s). Equilibrium speciation calculations suggest that in all water types except seawater, AgCl makes up more than 95% of the silver species present. For seawater, CHEAQS showed that 98.6% of Ag present should be in the form of AgCl₄³⁻, which explains the higher dissolution in seawater consistent with literature, which indicated only minor effects of sulfide in seawater.¹⁶³ The diameter of the PVP-Ag particles was significantly lower after 10 days compared to day 1 (Figure D.5). This supports the idea that there is continued dissolution causing the shrinking of the Ag NPs in time. It is likely that the increase in the fraction dissolved Ag is not seen in the filtrate due to the formation of other Ag-containing solids after aging, which do not pass the 3 kDa filter. These observations illustrate the importance of addressing aging and alteration of ENMs under environmental conditions.¹⁶⁴

These results imply that for CeO₂ we can neglect k_{dis} in Eq. 5.1 compared to the sedimentation term (V_s/h), i.e. we may consider coagulation-sedimentation as the dominating removal process in fresh and brackish water types. This is not always the case for Ag ENMs. However, the dissolution data do not allow the estimation of k_{dis} . Further measurements aimed at measuring the dissolution kinetics are needed to estimate the dissolution rates under a range of different environmentally relevant conditions. Note that the fact that k_{dis} for Ag is indeterminate, does not imply that sedimentation rate estimates are inaccurate, as was explained in the materials and methods section.

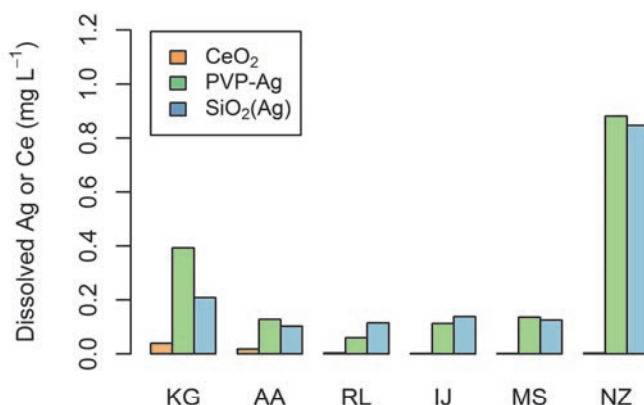


Figure 5.6. Dissolved metal ions, Ce and Ag, in 10 mg L⁻¹ ENM suspensions of CeO₂, SiO₂-Ag and PVP-Ag in six different water types. Water types: Karregat (KG), Brabantse Aa (AA), Rhine (RL), IJsselmeer (IJ), Nieuwe Waterweg (MS) and North Sea (NZ).

5.3.4 Heteroaggregation rates and attachment efficiencies

The largest range of apparent heteroaggregation rates ($K_{\text{hetero,crit}}\alpha_{\text{hetero,crit}}$) is observed for C₆₀ ENMs, followed by CeO₂, PVP-Ag and SiO₂-Ag ENMs. The lowest apparent heteroaggregation rates are observed in AA water, indicating a stabilizing effect of the high DOC concentration in this water (Table 5.2). The highest heteroaggregation rates occur in different water types for different ENM types. In order to better compare the apparent heteroaggregation rates, they can be adjusted for the differences in collision frequency due to differences in NC and ENM sizes and densities, by calculating and correcting for the collision frequency (K_{hetero}) (Table 5.2). The result is that the heteroaggregation rate is converted to an apparent attachment efficiency for heteroaggregation ($K_{\text{hetero,crit}}\alpha_{\text{hetero,crit}} / K_{\text{hetero}} = \alpha_{\text{hetero,crit}}$). However, due to the general inaccuracy of the estimate of the collision frequency, the obtained attachment efficiencies cannot be regarded as accurate estimates of $\alpha_{\text{hetero,crit}}$. One way of adjusting for this inaccuracy is to assume that the conditions affecting the collision frequency (e.g. shear or temperature) are similar within the experimental setup and therefore justify the calculation of a relative $\alpha_{\text{hetero,crit}}$ that is scaled to the highest corrected collision frequency ($K_{\text{hetero,crit}}\alpha_{\text{hetero,crit}} / K_{\text{hetero}}$). The apparent heteroaggregation rate and attachment efficiency obtained in this way were estimated using the simplified Smoluchowski equation (Eq. 5.5) using the single best measured data point in time (Table 5.2). Although this method uses only one data point, it gave more accurate results in our validation test compared to using all data (see Table E.1).

For the validation test we selected values for α_{hetero} (0.01, 0.1, 0.5 and 1), which then were used in simulations of combined homoaggregation, heteroaggregation and sedimentation, based on the full Smoluchowski-Stokes model (Eq 5.2). Subsequently, $\alpha_{\text{hetero,crit}}$ values were back calculated with the simplified Eq 5.5 for the scenarios with and without NC present. The resulting $\alpha_{\text{hetero,crit}}$ values for a $C_{0,\text{ENM}}$ of 0.5 mg L⁻¹ deviated between 0 and 22 % from the original α_{hetero} values, using a single data point. When all simulation data were used to fit Eq 5.5, the lowest $\alpha_{\text{hetero,crit}}$ value (original $\alpha_{\text{hetero}}=0.01$) could not be calculated and the deviation was larger; between 0 and 39 %. This is explained from the fact that for the final time point, the difference between removal with and without NCs present is largest and less prone to random error. However, the $\alpha_{\text{hetero,crit}}$ values estimated by the two methods still are reasonably similar. Furthermore, the validation showed that the actual $\alpha_{\text{hetero,crit}}$ values were underestimated by the approximation, a deviation that increased with increasing initial ENM concentration. Consequently, our estimated α_{hetero} values are most reliable for the lowest initial ENM concentrations. The higher underestimation of $\alpha_{\text{hetero,crit}}$ values at higher ENM concentrations follows from the fact that the high ENM concentrations cause homoaggregation to dominate over sedimentation. Consequently, the effect of heteroaggregation is too small to yield meaningful estimates for $\alpha_{\text{hetero,crit}}$.

Taking these limitations into account, the $\alpha_{\text{hetero,crit}}$ values show that for all ENMs, the NCs in seawater have the highest $\alpha_{\text{hetero,crit}}$, which is expected because of the high ionic strength of seawater (Table 5.2). This is in line with other methods of estimating attachment efficiencies related to favorable aggregation conditions.¹⁶⁵ Because of the saline conditions of seawater, favorable aggregation conditions are expected, which agrees to a study by Keller et al.⁶⁷ with an α of 1 for CeO₂, TiO₂ and ZnO ENMs in seawater. Other water types with a relatively high $\alpha_{\text{hetero,crit}}$ were: KG and RL with $\alpha_{\text{hetero,crit}}$ of 0.69 and 1 for PVP-Ag and CeO₂ respectively, and MS with $\alpha_{\text{hetero,crit}}$ between 0.6 and 0.85 for CeO₂, SiO₂-Ag and PVP-Ag. The rest of the $\alpha_{\text{hetero,crit}}$ values ranged between 0.01 and 0.44. In general KG and AA have the lowest number of $\alpha_{\text{hetero,crit}}$ values estimated, which is explained from the stabilization of ENMs in these waters, which therefore showed low sedimentation of ENMs in either filtered or unfiltered systems (Figure 5.2). For this reason it is remarkable that PVP-Ag and SiO₂-Ag have such a high $\alpha_{\text{hetero,crit}}$ in KG and AA water respectively. The small $\alpha_{\text{hetero,crit}}$ in DOM rich AA water is in line with a decrease in α from 1 to 0.05 for the deposition of C₆₀ on a silica surface upon addition of humic acid or alginate to a 1 mM CaCl₂ solution.¹⁶⁶ Additionally, Huynh et al.¹⁵¹ showed the total inhibition of

heteroaggregation between multi walled carbon nanotubes and hematite nanoparticles upon addition of 0.5 mg L⁻¹ humic acid. In general these results seem to indicate that water types that generally stabilized ENMs also resulted in lower $\alpha_{\text{hetero,crit}}$.

Table 5.2. Sedimentation rates (V_s), non-settling concentration (C_{ns}), apparent heteroaggregation rates ($K_{\text{het,crit}}\alpha_{\text{het,crit}}$) and heteroaggregation attachment efficiency ($\alpha_{\text{het,crit}}$) for C_{60} , CeO_2 , SiO_2 -Ag and PVP-Ag nanoparticles in natural waters in presence of natural colloids.

		KG	AA	RL	IJ	MS	NZ
C_{60}	V_s (m d ⁻¹)	0.102	0.109	0.136	$8.81 \cdot 10^{-2}$	0.139	$4.11 \cdot 10^{-2}$
	C_{ns} (mg L ⁻¹)	$4.06 \cdot 10^{-2}$	$7.17 \cdot 10^{-2}$	$6.09 \cdot 10^{-2}$	$1.78 \cdot 10^{-2}$	$1.81 \cdot 10^{-2}$	$2.29 \cdot 10^{-2}$
	$K_{\text{het,crit}}\alpha_{\text{het,crit}}$ (L mg ⁻¹ day ⁻¹) ^a	n.a. ^b	$6.82 \cdot 10^{-4}$	n.a. ^b	n.a. ^b	$1.49 \cdot 10^{-2}$	$6.00 \cdot 10^{-2}$
	$\alpha_{\text{het,crit}}$ (-) ^c	n.a. ^b	$6.75 \cdot 10^{-3}$	n.a. ^b	n.a. ^b	0.231	1
CeO_2	V_s (m d ⁻¹)	$6.10 \cdot 10^{-4}$	$1.39 \cdot 10^{-3}$	$3.09 \cdot 10^{-2}$	$5.44 \cdot 10^{-3}$	$7.83 \cdot 10^{-3}$	$6.94 \cdot 10^{-3}$
	C_{ns} (mg L ⁻¹)	0.270	0.309	$2.46 \cdot 10^{-2}$	$9.60 \cdot 10^{-2}$	$1.68 \cdot 10^{-2}$	$9.37 \cdot 10^{-3}$
	$K_{\text{het,crit}}\alpha_{\text{het,crit}}$ (L mg ⁻¹ day ⁻¹) ^a	$2.63 \cdot 10^{-3}$	n.a. ^b	$1.45 \cdot 10^{-2}$	$5.12 \cdot 10^{-3}$	$1.04 \cdot 10^{-2}$	$1.14 \cdot 10^{-2}$
	$\alpha_{\text{het,crit}}$ (-) ^c	0.161	n.a. ^b	0.996	0.121	0.854	1
SiO_2 -Ag	V_s (m d ⁻¹)	$1.01 \cdot 10^{-4}$	$1.34 \cdot 10^{-3}$	$5.97 \cdot 10^{-3}$	$2.42 \cdot 10^{-3}$	$1.00 \cdot 10^{-2}$	$5.33 \cdot 10^{-3}$
	C_{ns} (mg L ⁻¹)	0.285	0.179	$5.16 \cdot 10^{-2}$	0.152	$7.94 \cdot 10^{-2}$	0.164
	$K_{\text{het,crit}}\alpha_{\text{het,crit}}$ (L mg ⁻¹ day ⁻¹) ^a	n.a. ^b	$8.74 \cdot 10^{-4}$	$1.34 \cdot 10^{-3}$	$2.16 \cdot 10^{-3}$	$1.54 \cdot 10^{-3}$	$2.40 \cdot 10^{-3}$
	$\alpha_{\text{het,crit}}$ (-) ^c	n.a. ^b	0.222	0.444	0.252	0.603	1
PVP-Ag	V_s (m d ⁻¹)	$4.12 \cdot 10^{-3}$	$3.06 \cdot 10^{-3}$	$9.98 \cdot 10^{-3}$	$8.22 \cdot 10^{-4}$	n.a.	$1.61 \cdot 10^{-3}$
	C_{ns} (mg L ⁻¹)	0.141	0.316	$4.57 \cdot 10^{-2}$	0.116	$4.06 \cdot 10^{-2}$	0.218
	$K_{\text{het,crit}}\alpha_{\text{het,crit}}$ (L mg ⁻¹ day ⁻¹) ^a	$6.96 \cdot 10^{-3}$	n.a. ^b	$2.54 \cdot 10^{-3}$	$2.47 \cdot 10^{-3}$	$5.01 \cdot 10^{-3}$	$6.98 \cdot 10^{-3}$
	$\alpha_{\text{het,crit}}$ (-) ^c	0.692	n.a. ^b	0.292	0.102	0.678	1

n.a.: no data available.

a: Start and single, final time point used in Eq. 5.5 to estimate $\alpha_{\text{hetero,crit}}K_{\text{hetero,crit}}$

b: no calculation of $\alpha_{\text{hetero,crit}}$ possible due to difference between data from filtered vs unfiltered water (leading to negative $\alpha_{\text{hetero,crit}}K_{\text{hetero,crit}}$).

c: $\alpha_{\text{hetero,crit}}$ calculated from an estimate of K_{het} obtained using equation E.7.

5.3.5 Implications and conclusions

This study provided sedimentation rates, operationally defined non-settling fractions, heteroaggregation rates and critical attachment efficiencies for heteroaggregation for several representative ENMs and a wide range of natural water types. Heteroaggregation with NCs has been shown to play a key role in the sedimentation of ENMs. Furthermore, dissolution has been shown to be relevant for specific combinations of ENM and water types. We argue that these data as well as the approach to derive them will advance the development of fate and exposure models for ENMs, as was suggested in recent literature.^{36, 38, 135} For instance, Praetorius et al.³⁶ recently provided widely varying river transport scenarios for ENMs, with attachment efficiency as the major unknown. We suggest that the $\alpha_{\text{hetero,crit}}$ derived in the present study may be used to judge the probability of such scenarios.

Several disclaimers should be identified with respect to the use of the data from this study. First, variation in NC characteristics are likely to have a large effect on the estimated $\alpha_{\text{hetero,crit}}$ and the concentrations of NCs in rivers may be higher than those in our samples due to turbulence and constant input. Under such conditions ENM sedimentation rates will be different, which is currently being addressed in a separate study. Secondly, this work used pristine ENMs, whereas ENM input to natural waters may concern particles that already are aged, altered and clustered to larger agglomerates. Other differences in surface chemistry of the ENMs may result in changes in the attachment efficiency. Therefore, the applicability of the current $\alpha_{\text{hetero,crit}}$ values to other systems still has to be assessed. Probably, model implementations have to use system specific parameters, which then may be derived following procedures like those in this present work.

Acknowledgments

We thank Ruud Jeths, Gerrie Pieper, Leo van Hal, Erik Steenbergen and Mieke Verheij for their assistance and cooperation regarding sampling of the different water types. This work was funded by the European Union Sixth Framework Program NanoInteract NMP4-CT-2006-033231 and the RIVM strategic research program SOR-S340030. This work is supported by NanoNextNL, a micro and nanotechnology consortium of the Government of the Netherlands and 130 partners.

Chapter 6

Rapid settling of nanoparticles due to heteroaggregation with suspended sediment

ILONA VELZEBOER, JORIS T.K. QUIK, DIK VAN DE MEENT AND
ALBERT A. KOELMANS

In preparation

Abstract

Sedimentation of engineered nanomaterials (ENMs) has been studied mainly in artificial media and stagnant systems mimicking natural waters. This neglects the role of turbulence and heteroaggregation with sediment. We studied the apparent removal rates of selected ENMs (CeO₂, PVP-Ag and SiO₂-Ag) in agitated sediment-water systems resembling fresh, estuarine and marine water types. Experimental set-up was designed to mimic low energy and periodically resuspended sediment water systems (14 days), followed by a long term aging, resuspension and settling phase (6 months), as would occur in receiving shallow lakes. ENMs in systems with periodical resuspension of sediment were removed with settling rates between 0.038 - 1.5 m d⁻¹ for fresh and estuarine waters, or > 1.6 m d⁻¹ for marine waters. Higher settling rates of about 1 - 2 m d⁻¹ are observed after 6 months of aging in the sediment bed at all salinities, which is explained from ENMs being progressively captured in sediment flocs. The removal rates are 1 - 2 orders of magnitude higher than those reported for aggregation-sedimentation in stagnant systems without suspended sediment. Attachment efficiencies for heteroaggregation were estimated and ranged between 0.6 - 1. The high removal rates in turbulent conditions are explained from heteroaggregation being the rate determining step in scavenging of ENMs from the water column.

6.1 Introduction

The increasing use of engineered nanomaterials (ENMs) urges for refined exposure and risk assessment approaches for these materials.^{15, 145} For risk assessment, environmental concentrations of ENMs need to be known and compared to the predicted no-effect concentration.¹¹³ Measurement of ENMs, however, is challenging, due to a lack of suitable methods for measuring low concentrations ENMs in complex environmental matrices like natural waters, sediments or soils.¹⁶⁷ Consequently, exposure assessment may have to rely on modeling. Modeling the fate of ENMs in surface waters, however, is still in its infancy and faces difficulties such as lack of data on ENM specific aggregation and sedimentation parameters. ENM fate models should quantify aggregation and sedimentation,^{67, 112, 153} which are crucial processes in natural waters. However, key factors that govern these processes like ENM attachment efficiencies, particle geometries and size distributions, as well as the influence of dissolved organic matter (DOM) and natural colloids typically are unknown.^{36, 38, 63, 168, 169} Only recently, studies start to focus on apparent conditional

aggregation-sedimentation behavior in laboratory tests mimicking natural waters in order to find characteristic ranges of sedimentation behavior as a function of particle type and main water characteristics.^{138, 153, 167, 168, 170}

Several aquatic fate studies considered ENM sedimentation in stagnant systems focusing on the effects of water characteristics, including DOM.^{31, 67, 70, 153, 168} In stagnant i.e. non-agitated conditions, particles smaller than 10 μm , which includes the ENM range, settle very slowly. In waters with a depth ranging from a meter to several hundreds of meters they would remain in the water column for weeks to years if there are no other deposition mechanisms than the Stokes' law of gravity settling and Brownian motion.¹⁷¹ Attached to DOM, it has been shown that nanoparticles can form stable colloidal suspensions in the aqueous phase.⁵⁸

While slow aggregation/sedimentation is of obvious importance in stagnant waters, colloid stabilization may be also a relevant issue in more turbulent waters, where interaction occur with much larger particles that enter the water column upon wind-induced resuspension or bioturbation. Turbulence may increase shear and hence, the collision frequency, leading to faster and more extensive aggregation. Presence of resuspended sediment particles (suspended solids, SS) may further increase the heteroaggregation and scavenging of ENMs that subsequently settle at much higher rates. Consequently, when sediment is present, like in natural systems, nanoparticles are likely to end up in the sediment.¹¹² Stolzenbach et al.¹⁷² argued that fine particles are preferentially removed from suspension by heteroaggregation in a hydrodynamically active "fluff" layer (porous and mobile layer) at the sediment-water interface driven by the near-bottom water motion or by activities of benthic organisms. Hence, realistic conditions include turbulence and (periodic) resuspension of sediments in the water column. Especially in rivers and shallow lakes, SS loads have been reported to range from 5 to 200,000 mg L^{-1} in some rivers.¹⁷³ This will affect obviously the cycling of ENMs in water systems, and may overwhelm the settling rates observed in stagnant, low SS systems.^{35, 157} As mentioned before, DOM can stabilize ENMs in the water phase, but SS can also increase the settling rates of ENMs or agitation can bring settled nanomaterials into suspension again. However, to date the question whether resuspension leads to net mobilization or removal of nanoparticles compared to stagnant systems, has not been addressed. If resuspension of sediment plays an important role in scavenging ENMs from the water phase, it may be argued that water – only exposure is not relevant for ENM risk assessment.^{167, 174}

This study aims at quantifying the removal rates of selected ENMs from the water column in dynamic sediment-water systems for three water types; fresh, estuarine

and marine, under realistic hydrodynamic conditions. Here, removal may include homo- and heteroaggregation, sedimentation and dissolution.³⁶ ENM settling rates and ENM-SS attachment efficiencies for heteroaggregation were inferred from the removal data. Experimental systems and conditions were designed to mimic low energy agitation and periodical resuspension of sediment water systems (14 days), followed by a long term aging phase (6 months), in which the systems were periodically in a short resuspension and settling phase, as would occur in a receiving stagnant reservoir, e.g. a shallow lake. After 6 months the systems were resuspended once again, but not agitated anymore, to mimic settling in such a truly stagnant reservoir. Aim was to quantify the removal rate for aged ENMs from the water column, including sediment interaction. Natural waters and sediment were used to mimic environmental realistic systems. By using three types of water we could test the possible importance of aquatic geochemical variables. The observed removal rates were evaluated against literature data recently reported for the same ENMs and waters under stagnant conditions.

6.2 Material and methods

6.2.1 Chemicals

Ceriumdioxide (CeO_2) nanoparticles (20 nm) were supplied by Umicore Ltd. (Brussels), as a 100 g L⁻¹ suspension of in HNO_3 at pH 4. The CeO_2 ENM contained 81.4 wt% Ce, based on the defined ratio and molecular weight. Silica coated silver (SiO_2 -Ag) nanoparticles, with a stock suspension in water of 4.66 g L⁻¹ and polyvinylpyrrolidone capped silver (PVP-Ag) nanoparticles, with a stock suspension of 10.23 g L⁻¹ were purchased from nanoComposix (San Diego, CA). These nanoparticles represent important ENM classes and included two different functionalization types for one of the ENMs (Ag). The SiO_2 -Ag NPs consist of a 40.5 ± 20.5 nm silver core and a 24.6 nm silica shell. Based on these dimensions, 86.9 wt% of SiO_2 -Ag NP is calculated to be silver. The capped PVP layer of the PVP-Ag NP (51 ± 22.1 nm) is thin and the mass contribution to the whole NP is negligible compared to the silver core.

6.2.2 Water and sediment sampling

Water types were selected to cover a wide range of salinities. Marine water (NZ) was collected during surveys on the North Sea. Estuarine water (MS) was sampled with a bucket from Nieuwe Waterweg at Maassluis ($51^\circ 54' 51.7''\text{N}$, $4^\circ 14' 59.7''\text{E}$). Fresh

water (RL) was sampled via a pump from river Rhine at Lobith (51°51'13.8"N, 6°5'28'E). All samples were stored in polyethylene containers. Experiments were started immediately after arrival in the laboratory. Chlorine, anions, cations, dissolved inorganic and organic carbon (DIC, DOC), dry weight (DW) and ash free dry weight (AFDW) were determined.

Sediment was sampled with a van Veen grabber at lake Ketelmeer (52°36'40.8"N, 5°39'35.8'E). This lake represents shallow buffered lakes as well as fresh tidal waters with fluctuations in water run-off and sedimentation area.¹⁷⁵ The sediment was sieved using a 500 μm mesh stainless-steel sieve to remove pebbles, shells and large organic debris. Particle size distribution (PSD) was measured with a Beckman Coulter LS 230 laser diffraction particle size analyzer with Polarization Intensity Differential of Scattered Light (PIDS). Four distinctive fractions were identified: <1 μm , 4.9%; 1 – 20 μm , 54.6%; 20 – 100 μm , 31.2% and 100 – 400 μm , 9.3%; there were no particles detected in the 400 – 2000 μm fraction. The average particle size was 15.7 μm (Figure F.3 in Appendix F). Calcium carbonate (CaCO_3) was determined volumetrically according to Schreiber (NEN-ISO 10693) and was $8.66 \pm 0.05\%$ ($n=4$). Organic carbon (OC) and black carbon (BC) were measured using chemothermal oxidation (CTO-375 method)^{176, 177} using a CHN analyzer (EA 1110 CHN Elemental Analyzer, CE Instruments, Milan, Italy). OC was $2.24 \pm 0.61\%$ ($n=5$, one data point was considered an outlier based on Dillons Q test, $p<0.05$) and BC was $0.22 \pm 0.06\%$ ($n=6$). Based on Elimelech et al.¹⁷⁸ a density of 2.58 g cm^{-3} could be calculated.

6.2.3 Sediment resuspension and aging systems

To create the systems, 7 g sediment (wet weight), 1 L water and one of the nanoparticle types CeO_2 , PVP-Ag or SiO_2 -Ag were added to 1 L glass jars (see schematic representation in Figure F.1 in Appendix F). Stock suspensions of the NPs were diluted with MilliQ water, immediately prior to starting the experiments. Per water type, NPs were added in three doses (0.5, 2.5 and 10 mg L^{-1}). A blank system (sediment and water, no NPs) was included.

At time zero the systems were homogenized by shaking thoroughly for a minute, after which they were placed on a table shaker (100 rpm). On the table shaker the systems developed three phases: a bed sediment ($\sim 0.5 \text{ cm}$ layer), a transitional zone of settled but still slowly moving sediment particles ($\sim 3 \text{ cm}$ 'fluff' layer) and an overlying water phase ($\sim 10 \text{ cm}$), which remained slightly turbid throughout the experiment, but did not contain macroparticles. This mimicked the conditions of a natural sediment bed under continuous flow. During the 14 day experiment, 5 times

per week a resuspension event was simulated by shaking the system 5 times upside down by hand. Just before the resuspension events on days 0, 1, 7 and 14, overlying water samples (15 mL) were taken 7 cm under the water surface using a 25 mL pipet. This means that all water column samples in this phase relate to a phase separation time of 24 h after resuspension, where phase separation was created by gravitational settling under semi-quiescent conditions. To mimic settling and aging in a stagnant reservoir, for the subsequent 6 months resuspension was continued 5 times a week, but the systems were not agitated in between resuspension events. After these 6 months, the systems were resuspended once and water column samples were taken as described above, after 1, 4 and 24 h for the 10 mg L⁻¹ ENM systems and after 24 hours for the 0.5 and 2.5 mg L⁻¹ ENM systems. Consequently, these latter samples relate to phase separation due to gravitational settling under stagnant conditions. All overlying water samples were used for measurement of ENM colloid stability (zeta potential), ENM abundance (high-resolution inductive coupled plasma mass spectroscopy, hr-ICP-MS, element analysis), particle- and aggregate size (nanoparticle tracking analysis, NTA) and general water characteristics (pH, EC). Element analysis of water column samples included Si and Al as a proxy for clay minerals¹⁷⁹ to be able to compare their behavior to that of the ENMs. Prior to these analyses, subsamples were sonicated for 15 minutes, shaken on a shaker table for 10 minutes and sonicated again for 10 minutes.

6.2.4 Characterization of ENMs

Particle size distributions (PSD) were measured by NTA on a NanoSight LM20 (NanoSight Ltd., Salisbury, UK) with Nanoparticle Tracking Analysis software version 2.1 using a previously described method.⁷⁰ The zeta potential (ZP) was measured with a ZetaSizer (nano series, Malvern Instruments Ltd., Worcestershire, UK). The elemental concentrations of Ce, Ag, Al and Si in the samples were measured by hr-ICP-MS (Element 2 HR-ICP-MS, Thermo, Bremen, Germany). For the CeO₂ NPs, 4 mL of sample was weighed in 50 mL tubes and destructed with 7 mL 14.4M HNO₃ and 3 mL 9.8 M H₂O₂ at 103°C for 2 hours. For Ag NPs, samples were destructed with 2 mL 14.4M HNO₃ and 7 mL 37% w/w HCl at 103°C for 1 hour. Subsamples were also measured with single particle ICP-MS, using a Thermo Scientific X series 2 spectrometer equipped with a Babington type nebulizer and a quartz impact bead spray chamber, to check on initial size and amount of nanoparticles. CeO₂ nanoparticles had an average diameter of 19 nm, which agrees to the manufacturer specifications. PVP-Ag ENMs had an average diameter of 64 nm, which agrees with the

51.0 ± 22.1 nm size distribution as specified by the manufacturer, based on TEM measurement.

6.2.5 Data analysis

ENM removal data were interpreted using a semi-empirical first order settling rate model, describing ENM sedimentation in time.^{153, 157, 158} First-order kinetics is consistent with collision based aggregation theory when homoaggregation is limited. In other words, first-order kinetics should be expected when the nanoparticles aggregate or agglomerate with other particulate matter present, i.e. in case of heteroaggregation. Typically, a residual or non-settling concentration of ENMs is observed,¹⁵³ which leads to:

$$C_t = C_{res} + (C_0 - C_{res}) \cdot e^{-\left(\frac{v_s}{h} + k_{diss}\right) \cdot t} \quad (\text{Eq. 6.1})$$

in which C_t [mg L⁻¹] is the concentration at time t , C_{res} [mg L⁻¹] is the residual concentration at infinite time, C_0 [mg L⁻¹] is the initial concentration, v_s [m d⁻¹] is the sedimentation rate, h [m] is the sedimentation length, the distance from the water surface till the height where the samples were taken, k_{diss} is a dissolution rate constant [d⁻¹] and t [d] is time. Dissolution is best described by shrinking particle models, which however can be approximated by first order kinetics^{90, 180, 181}.

The experimental setup does not allow for estimating the C_{res} due to the total resuspension of ENMs and SS 24 hours prior to the measurement of the ENM concentration. In order to estimate the residual concentration longer sedimentation times are needed. However the average concentrations measured, 24 hours after resuspension, are below 3% of the initial concentration. This means that equation 6.1 is reduced to the following:

$$C_t = C_0 e^{-\left(\frac{v_s}{h}\right) \cdot t} \quad (\text{Eq. 6.2})$$

Using Eq. 6.2, the sedimentation rate was calculated directly at four different time points, 1, 7 and 14 days during agitation and after 6 months in quiescent conditions. In all cases C_0 was the concentration ENMs as measured at start of the experiment.

Attachment efficiencies between ENMs and SS (α_{hetero}) were estimated following a method recently described by Quik et al.¹⁶⁸. A detailed description of the method and calculations used for estimating the attachment efficiency for heteroaggregation are provided in Appendix E. In summary this method calculates the attachment efficiency relative to the water type with the highest $\alpha_{hom,crit}$ calculated with equation 6.3. This equation is simplified based on a series of assumptions, which are validated by

simulations with the full Von Smoluchowski – Stokes equation (provided in Appendix F):

$$\frac{dC_{ENM,crit}}{dt} = -\alpha_{hom,crit}K_{hom,crit}C_{ENM,crit}^q - \alpha_{het,crit}K_{het,crit}C_{SS}C_{ENM,crit} \quad (\text{Eq 6.3})$$

where $C_{ENM,crit}$ is the concentration of settleable ENMs, $K_{hom,crit}$ is the apparent collision rate constant for the formation of settleable ENM homoaggregates, $\alpha_{hom,crit}$ is the apparent attachment efficiency for settleable ENM homoaggregates, $\alpha_{het,crit}$ is the apparent attachment efficiency for settleable ENM-SS heteroaggregates, $K_{het,crit}$ is the apparent collision rate constant for the formation of settleable ENM heteroaggregates, the exponent q defines the kinetics for homoaggregation. The first part of equation 6.3 represents the removal due to homoaggregation and the second part due to heteroaggregation. In this case removal due to homoaggregation is considered negligible. This is on the one hand due to the concentration of DOC present which is known to stabilize ENMs against aggregation, effectively reducing the attachment efficiency.³⁶ On the other hand the large concentration of SS present ($>3.4 \text{ g L}^{-1}$) results in formation of heteroaggregates instead of homoaggregates.

6.3 Results and discussion

6.3.1 Water characteristics

The three water types RL, MS and NZ showed a wide variation in composition (Table F.1). Electric conductivity (EC) ranged from $584 \text{ } \mu\text{S cm}^{-1}$ (RL) to $47000 \text{ } \mu\text{S cm}^{-1}$ (NZ). pH of the waters was comparable at 7.8 - 7.9. Particulate matter was $>10 \text{ mg L}^{-1}$ for RL and MS, whereas NZ had a much lower concentration ($<3 \text{ mg L}^{-1}$). After addition of sediment to the systems, the systems reached a stable pH of 7.2 - 7.3, buffered by calcium carbonate in the sediment. EC increased with 9 - 15 % and was stable per water type during the 14 day experiment with an average of $642 \text{ } \mu\text{S cm}^{-1}$ for RL, $8009 \text{ } \mu\text{S cm}^{-1}$ for MS and $51730 \text{ } \mu\text{S cm}^{-1}$ for NZ. Added nanoparticles had no influence on system pH or EC.

6.3.2 ENM removal from the water column

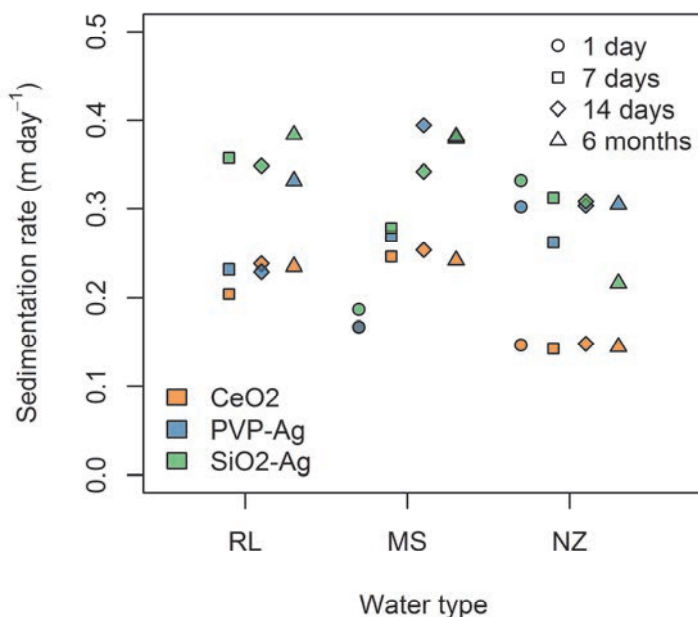


Figure 6.1. Sedimentation rates for 3 ENMs at 0.5 mg L^{-1} suspension concentration in 3 water types in presence of suspended sediment observed after 1, 7, 14, and 6 months of incubation.

The recoveries for measurement of CeO₂ ENMs in the water samples is $> 90\%$ when compared to the nominally added CeO₂ concentration. For PVP-Ag and SiO₂-Ag, however, recovery remains a bit lower at $\sim 80 - 90\%$. In marine water recoveries are lower ($>30\%$) due to the higher salt content which needed extra dilutions. However, this does not directly affect the calculation of sedimentation rates or attachment if the recovery can be assumed similar for each individual ENM water type combination. E.g. the sedimentation for PVP-Ag in marine water is calculated from the concentration measured after 14 days and at start of the experiment, both measurements with a recovery of 30% will result in the same sedimentation rate compared to the case where the recovery was 90% hypothetically.

The concentrations ENMs measured at the four time points were low and close to detection limits; on average 2.19% of C_0 (range $0.15 - 12.49\%$). The concentrations of ENMs likely do not only consist of particulate ENMs, but also their dissolved form,

because dissolution cannot be fully discarded. However, in parallel work using the same ENMs and waters, dissolution was indeed shown to be negligible for CeO₂ NPs.¹⁶⁸ In the same study, 1.5 – 12% dissolution was reported for both Ag NPs,¹⁶⁸ which is higher than observed in the current experiments. This implies silver settled in our experiments, either through aggregation-sedimentation with SS, and/or through (limited) dissolution and subsequent sorption to the SS or precipitation with Chloride or Sulphide. In either case, the removal data can be interpreted as a result of sedimentation. The low ENM concentration is in line with the decreased residual concentration in presence of natural colloids (NC) compared to filtered water,^{153, 168} albeit that the current concentrations are considerably lower. This is interpreted as fast aggregation and sedimentation with SS in the systems, which has a higher concentration than the NCs in Quik et al.¹⁶⁸ and thus yields lower concentrations.

The sedimentation rates all ranged between 0.14 – 0.5 m d⁻¹ for the different water and ENM types and aging times. No clear differences were seen when comparing sedimentation rates for the different water and ENM types, except for the 0.5 mg L⁻¹ CeO₂ ENM suspension in marine water, which showed the lowest sedimentation rates (Figure 6.1), also observed at higher CeO₂ ENM concentration, although not as pronounced (Figure F.2). This lower sedimentation rate in marine water is contradictory to the expectation that the high salinity of marine water would increase the aggregation rate and sedimentation rate compared to river and estuarine water. However, it seems that 12 % of the CeO₂ ENMs remain stable in suspension after 24 hours, even after 6 months of aging. This stable CeO₂ ENM fraction is likely in the particulate form because dissolution of CeO₂ ENMs was not detectable (< 1 µg L⁻¹) in marine water.¹⁶⁸ The other ENMs do not show any difference in sedimentation rates between water types, with sedimentation rates ranging from 0.16 to 0.50 m d⁻¹. There seem to be some difference between the water types with regard to an increase or decrease in sedimentation rate with incubation time of the Ag ENMs. However, only the sedimentation rates after 1 day incubation in estuarine water are significantly different from the 7, 14 day or 6 month incubation times ($p < 0.004$, $n = 9$, paired t-test).

Table 6.1. Sedimentation rates and attachment efficiencies for 3 ENMs (0.5 mg L^{-1}) in 3 water types in suspended sediment (SS) systems from the current study and previously reported values¹⁶⁸ for quiescent settling systems with the same ENMs and water types without SS, but with Natural Colloids (NCs).

		RL	MS	NZ
CeO ₂	$V_{s, \text{water}+\text{NCs}} \text{ (m d}^{-1}\text{)}$	0.031	0.0078	0.0069
	$V_{s, \text{water} + \text{SS}} \text{ (m d}^{-1}\text{)}^a$	0.24	0.25	0.15
	ENM-NC $\alpha_{\text{hetero.crit}} \text{ (-)}$	1.0	0.85	1.0
	ENM-SS $\alpha_{\text{hetero.crit}} \text{ (-)}^a$	0.96	1.0	0.85
SiO ₂ -Ag	$V_{s, \text{water}+\text{NCs}} \text{ (m d}^{-1}\text{)}$	0.0060	0.010	0.0053
	$V_{s, \text{water} + \text{SS}} \text{ (m d}^{-1}\text{)}^a$	0.35	0.34	0.31
	ENM-NC $\alpha_{\text{hetero.crit}} \text{ (-)}$	0.44	0.60	1.0
	ENM-SS $\alpha_{\text{hetero.crit}} \text{ (-)}^a$	0.98	1.0	0.93
PVP-Ag	$V_{s, \text{water}+\text{NCs}} \text{ (m d}^{-1}\text{)}$	0.010	n.a.	0.0016
	$V_{s, \text{water} + \text{SS}} \text{ (m d}^{-1}\text{)}^a$	0.23	0.39	0.3
	ENM-NC $\alpha_{\text{hetero.crit}} \text{ (-)}$	0.29	0.68	1.0
	ENM-SS $\alpha_{\text{hetero.crit}} \text{ (-)}^a$	0.82	1.0	0.88

a: measured after 14 days incubation.

6.3.3 Attachment efficiencies for heteroaggregation of ENMs with suspended sediment

The attachment efficiencies for heteroaggregation were estimated based on the assumptions that homoaggregation is negligible and that aggregation is rate limiting for sedimentation. The brief validation of the method, reported in Appendix F.2, showed that with these assumptions the method for estimating the heteroaggregation attachment efficiency is accurate. However, the obtained attachment efficiencies from the sedimentation measurements are less accurate due to several uncertainties, such as measurement error of the ENM or SS concentrations.

The $\alpha_{\text{het,crit}}$ measured for these three ENM and water types ranged between 0.82 and 1 for the three suspension concentrations. The most relevant conditions are in presence of the lowest ENM concentration (0.5 mg L^{-1}). In this case the $\alpha_{\text{het,crit}}$ in estuarine water is 1, and for fresh and marine water slightly lower (0.82-0.98). Thio et al.¹⁸² observed negligible attachment of PVP-Ag ENMs in fresh or marine water on a bare silica surface. This could indicate that the attachment of PVP-Ag ENMs to SS is to other components than silica.

6.3.4 Comparison of sedimentation rates and attachment efficiencies of ENMs and natural colloids

The sedimentation rates and attachment efficiencies from the systems with SS (Table 6.1) can be compared directly to those provided by Quik et al.¹⁶⁸, who used the same water types and ENMs with the same initial concentrations as in the present study. The range of sedimentation rates observed with the periodic resuspension of sediment and turbulent settling conditions are significantly higher ($p < 2 \times 10^{-5}$, $n=8$, paired t-test) than in the non-agitated systems studied by Quik et al.¹⁶⁸, where only a low level of natural colloids and solids was present in unfiltered water samples. The higher sedimentation rates can be explained by the much higher particle concentration in presence of SS compared to the NCs (Figure F.4). The sedimentation rates reported here are 7 to 187 fold higher, indicating the large impact resuspended sediment can have on removal of ENMs from the water phase. Consequently, we suggest that as soon as there is a resuspension event, heteroaggregation with SS occurs and the sedimentation of ENM will coincide with that of SS.

Where Quik et al. calculated the attachment efficiencies for heteroaggregation of ENMs and NCs, here they are calculated for ENMs and SS (Table 6.1). The CeO₂ ENMs had high attachment efficiencies between both SS and NCs.

6.4 Conclusion and implications

This study demonstrates that presence of SS in turbulent aquatic systems governs the sedimentation rates of ENMs irrespective of salinity and ENM type studied. Heteroaggregation of ENMs with SS followed by sedimentation explains the significantly shorter process time compared to the stagnant systems without SS or with low SS concentrations. We propose that in our experiments, prolonged aging in the sediment bed with incidental resuspension resulted in particles with even higher sedimentation rates. These data suggest that ENM fate in river systems may be described as sedimentation-resuspension of SS with sedimentation rates between 0.1 – 0.5 m d⁻¹. We argue that ENMs entering water systems, most probably also already are aggregated to particles and flocks. Only if (a) ENMs are entering water systems as nano-sized particles like soot i.e. through atmospheric deposition, and (b) suspended solids are absent or have a low concentration as in stagnant deep lakes, homoaggregation may prevail. Homoaggregation thus may be relevant for the fate of airborne ENMs in deep lakes.

In most aquatic systems, sediment is not resuspended to the total height of the water column, this leads to two possible ENM scavenging regimes in rivers or lakes. One regime in the upper water layers with heteroaggregation and sedimentation in the aqueous phase where DOM can stabilize NPs, which is comparable to stagnant waters with low settling rates (10^{-4} - 10^{-2} m d⁻¹).¹⁶⁸ Closer to the sediment bed, a second regime may exist, where turbulence, bioturbation and wind induced resuspension will cause resuspension of larger particles at high concentrations, which will increase collision efficiency and shear, leading to faster aggregation, heteroaggregation with micrometer sized particles and rapid subsequent sedimentation and settling rates of 0.1 – 0.5 m d⁻¹. Water quality models that implement these regimes will increase realism of ENM fate scenario studies.³⁶ Furthermore, ENM aging in the sediment bed suggests strong aggregation with SS, rendering them practically unavailable for transport as would be when present in the water phase. Transport of ENMs via sediment resuspension and horizontal bed load transfer, like in rivers, is possible, but not in the same order of magnitude as in the upper layer without SS. Due to association of ENMs with SS, ENM transport can be predicted using sediment transport models.

Acknowledgements

We would like to thank Marja Wouterse of the Laboratory for Ecological Risk Assessment (RIVM) for her assistance during the experiments, Cornelis Miermans of the Laboratory for Environmental Monitoring (RIVM) for the ICP-MS measurements, Frits Gillissen and Wendy Beekman-Lucassen of the Aquatic Ecology and Water Quality Management Group (Wageningen University) for their help and advice with measuring water quality parameters, Ruud Peters of RIKILT for the sp-ICP-MS measurements, the Research and Development Department of The Netherlands Vaccine Institute for the use of the Malvern ZetaSizer and the Centre for Environmental Health Research (RIVM) for the use of the NanoSight LM20.

Chapter 7

Empirical versus mechanistic modeling of engineered nanomaterial aggregation and sedimentation in water

JORIS T.K. QUIK, ALBERT A. KOELMANS AND DIK VAN DE MEENT

In preparation

7.1 Introduction

The main difference between conventional chemicals and engineered nanomaterials (ENMs) in the environment is the chemical form in which they are present. For conventional chemicals this is the dissolved or adsorbed state, compared to the solid phase of ENMs. Although ENMs can dissolve, the solid state is what makes them a particle with specific physico-chemical properties. For this reason current exposure assessment models need to be adapted to take into account particle behavior. Almost a century ago Von Smoluchowski²⁷ was the first to describe a theory for particle aggregation. This was the basis for Friedlander²⁴ and Farley and Morel³⁵ to combine aggregation kinetics with sedimentation theory by Stokes²⁵ to calculate the removal rates for particles from the water phase.

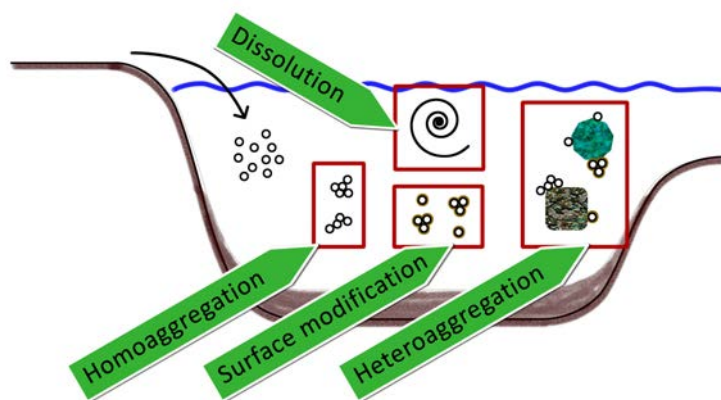


Figure 7.1. Processes affecting fate of ENMs in the aquatic environment.

Overall the fate processes affecting ENMs upon entering the aquatic environment are dual in nature: (a) transformation and (b) transport. The transformation processes are surface modification, homoaggregation, heteroaggregation and dissolution (Figure 7.1) and the transport processes are advection and sedimentation. Based on experimental observations we have identified heteroaggregation to be one of the most important processes affecting the fate of ENMs.^{153, 168}

We have introduced an empirical model to describe the sedimentation of low concentrations of ENMs in presence of natural colloids, which however was not derived from the above mentioned colloidal theories for particle-particle interactions, but uses a simplified first order removal towards a non-settling fraction of ENMs. Primary aim of this chapter is to interpret and define limitations for this empirical

model by comparing model outputs with scenarios calculated with a combined Smoluchowski-Stokes type mechanistic model^{24, 35} with added processes describing heteroaggregation.³⁸ This model describes the transport of ENMs from the water phase to the sediment, which consists of two steps. First transformation of free ENMs to either larger homoaggregates of only ENMs or heteroaggregates with NCs followed by the second process, sedimentation of these two aggregate types. The sedimentation kinetics are thus largely dependent on the rate of homo- and heteroaggregation. The rates of these two aggregation processes are based on the collision frequency and attachment efficiency. The collision frequency is calculated from the physical characteristics of the ENMs or NCs and their particle concentrations. The attachment efficiency however cannot be calculated based on the physical or chemical characteristics of the environment, ENM or NC, although all of these affect the attachment efficiency.^{46, 67}

Using this mechanistical model we simulate our simple test systems as used in the experiments described in chapter 3 to 5. We will discuss the effect of homoaggregation and heteroaggregation on the sedimentation of ENMs out of the water phase and give a brief comparison between the mechanistical and empirical model used in chapters 4 and 5. And finally we discuss the parameterization of particle based exposure assessment models focusing on the measurement of the attachment efficiency between ENMs and NCs (α_{hetero}).

7.2 Mechanistic model

7.2.1 Model design

Basic colloidal theories on particle aggregation by Von Smoluchowski²⁷ and sedimentation by Stokes²⁵ allow modeling of the concentration of particles in water.²⁴ In this case three distinct processes are modeled, homoaggregation of the nanoparticles, heteroaggregation of nanoparticles with natural colloids and sedimentation of homo- and heteroaggregates.

Homoaggregation is described by second order reaction kinetics:

$$\frac{dn_j}{dt} = \frac{1}{2} \sum_{i=1}^{j-1} \alpha_{\text{homo}} K_{i,j-i} n_i n_{j-i} - n_j \sum_{i=1}^{\infty} \alpha_{\text{homo}} K_{i,j} n_i \quad (\text{Eq. 7.1})$$

where the concentration of particles consisting of j primary particles, n_j [m^{-3}] changes with the aggregation rate constant K [$\text{m}^3 \text{s}^{-1}$]. The aggregation rate constant is based on the collision rate of nanoparticles and the attachment efficiency, α [-]. There are three main processes of motion that affect the collision rate: (1) Brownian motion

(peri-kinetic), (2) fluid motion (ortho-kinetic) and (3) differential settling. The aggregation rate constant $K_{i,j}$ for homoaggregation is given by:

$$K_{i,j} = \frac{2k_b T}{3\mu} \frac{(a_i + a_j)^2}{a_i a_j} + \frac{4}{3} G (a_i + a_j)^3 + \pi (a_i + a_j)^2 |v_{s,i} - v_{s,j}| \quad (\text{Eq. 7.2})$$

where k_b is the Boltzman constant [$\text{m}^2 \text{ kg s}^{-2} \text{ K}^{-1}$], T the temperature [K], a is the particle radius of aggregates consisting of j or i primary particles, μ is the viscosity [$\text{kg s}^{-1} \text{ m}^{-1}$] of the suspending medium, G is the shear rate [s^{-1}] and v_s the sedimentation rate [m s^{-1}] which is given by:

$$v_s = \frac{2a_j^2(\rho_{p,j} - \rho_w)g}{9\mu} \quad (\text{Eq. 7.3})$$

where g is the gravitational acceleration [m s^{-2}], ρ_p the density of the particle or aggregate [kg m^{-3}] and ρ_w is the density of water [kg m^{-3}]. The removal by sedimentation relative to the sedimentation length (d [m]) is given by:

$$\frac{dn_j}{dt} = - \frac{v_{s,j}}{d} n_j. \quad (\text{Eq. 7.4})$$

Heteroaggregation of nanoparticles with natural colloids is described by first order kinetics:

$$\frac{dn_j}{dt} = -\alpha_{hetero} K_{NC,j} n_{NC} n_j \quad (\text{Eq. 7.5})$$

where the aggregation rate constant for heteroaggregation ($K_{NC,j}$) is given by:

$$K_{NC,j} = \frac{2k_b T}{3\mu} \frac{(a_{NC} + a_j)^2}{a_{NC} a_j} + \frac{4}{3} G (a_{NC} + a_j)^3 + \pi (a_{NC} + a_j)^2 |v_{s,NC} - v_{s,j}| \quad (\text{Eq. 7.6})$$

where α_{hetero} is the attachment efficiency between natural colloids and nanoparticles, a_{NC} is the radius of the natural colloids and $v_{s,NC}$ their sedimentation rate.

The aggregate size (a_j) is calculated from the primary ENM size [a_1], the number of primary ENMs (j) and the fractal dimension (D_f), $a_j = a_1 * j^{(1/D_f)}$. Because of computational limitations a maximum j is calculated based on a given maximum ENM aggregate radius ranging from 0.35 μm to 1 μm .

7.2.2 Model parameters

The hydrological model parameters were chosen to resemble the flasks used in the settling experiments from chapters 3 to 5, such as a sedimentation length of 3 cm. As there is no inflow or outflow a single dose of ENMs and NCs is used. As default a monodisperse CeO_2 nanoparticle suspension with radius of 15 nm was used at an initial concentration between 1 $\mu\text{g L}^{-1}$ and 10 mg L^{-1} . Various parameters were varied

to further understand the effect of heteroaggregation on the fate of ENMs in water. Such as α_{homo} , α_{hetero} , C_{ENM} , C_{NC} , a_{ENM} , a_{NC} , G , D_f , ρ_{NC} . In this case only CeO_2 ENMs were simulated, as this is the main particle for which experimental data are available. These differential equations were solved using the DeSolve package v 1.10-3¹⁸³ for R v15.0.¹⁴⁰ Model output was generated at 10 minute time steps, simulating 14 days of aggregation and sedimentation.

Table 1. Parameter ranges used for model analysis.

Parameter	Range	Default
α_{homo} (-)	0 – 1	0 or 1 ^a
C_{ENM} ($\mu\text{g L}^{-1}$)	1 - 10 ⁴	10
a_{ENM} (nm)	10 - 25	15
G (s^{-1})	0 – 10	0
D_f (-)	1.5 – 2.5	2.5
α_{hetero} (-)	0 – 1	1
C_{NC} (mg L^{-1})	1 – 100	100
ρ_{NC} (kg m^{-3})	1100 – 2000	1250
a_{NC} (μm)	0.5 – 2	0.5
a: $\alpha_{\text{homo}} = 0$ if $C_{\text{ENM}} < 10 \mu\text{g/L}$ otherwise $\alpha_{\text{homo}} = 1$		

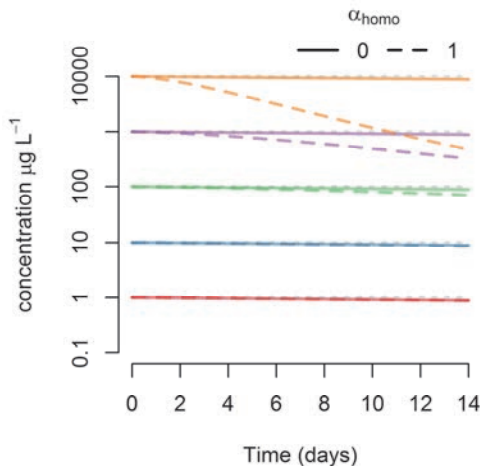


Figure 7.2. Calculated CeO_2 nP concentration in time for $C_{0\text{nP}}$ ranging from $1 \mu\text{g L}^{-1}$ to 10mg L^{-1} taking only homoaggregation and sedimentation into account.

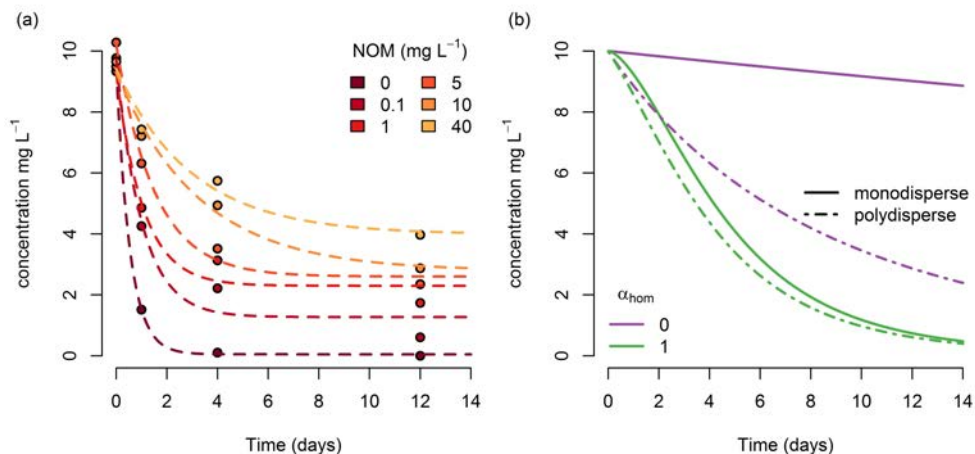


Figure 7.3. Sedimentation of 10 mg L^{-1} CeO_2 NPs as observed in algae medium with DOM concentration ranging from 0 to 40 mg L^{-1} (a). Dashed lines in panel a are a fit of the first order empirical model to the concentration data. Calculated CeO_2 NP concentration using the mechanistical model (b). Polydisperse (dashed lines) and monodisperse (solid lines) 15 nm CeO_2 NP size distributions are used in panel b.

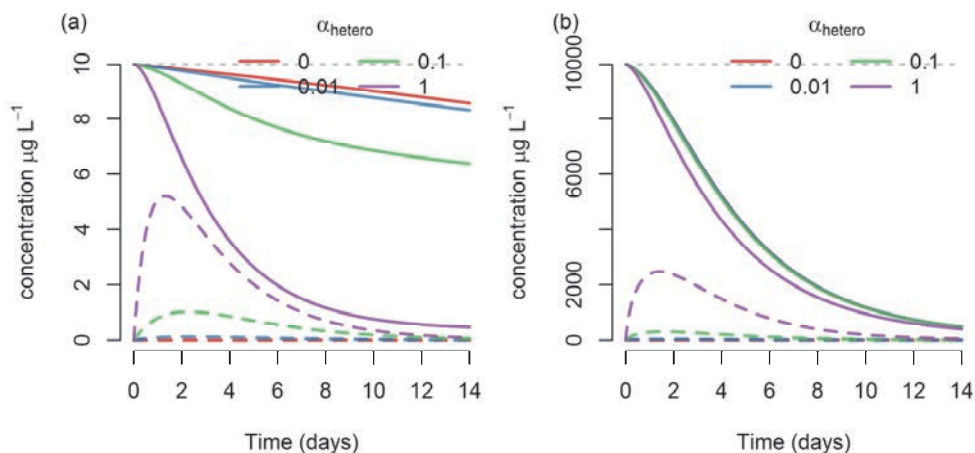


Figure 7.4. Calculated concentration CeO_2 NPs freely suspended (solid line) or attached to NCs (dashed line) in the water phase at $\alpha_{\text{homo}} = 1$ and α_{hetero} ranging between 0 and 1 with different $C_{0\text{NP}}$ of 10 $\mu\text{g L}^{-1}$ (a) and 10 mg L^{-1} (b). Default parameters given in Table 7.1. Grey dashed line is the sum of ENMs hetero and homo-aggregates in the water phase and sediment.

7.3 Model analysis and comparison with experimental results

7.3.1 Homoaggregation and sedimentation

In this mechanistic model, homoaggregation is the most elaborate process taken into account as every particle interaction is calculated up to a maximum number based on the defined maximum aggregate size (a_{\max}). The current state of the art exposure assessment methods do not incorporate homoaggregation based on the assumption that relevant environmental ENM concentrations will be very low and the ubiquitous presence of NCs will lead to heteroaggregation instead of homoaggregation.^{36, 135} Results from our model indeed show that if we disregard heteroaggregation ($\alpha_{\text{hetero}}=0$), the removal of ENMs from the water phase due to homoaggregation ($\alpha_{\text{homo}}=1$) followed by sedimentation is negligible ($< 5\%$ difference between $\alpha_{\text{homo}}=1$ and $\alpha_{\text{homo}}=0$) at $C_{0\text{ENM}}$ below $10 \mu\text{g L}^{-1}$ (Figure 7.2). This confirms the assumption that homoaggregation does not play a role in the overall fate of ENMs in the environment because ENM concentrations higher than $1 \mu\text{g L}^{-1}$ CeO_2 ¹⁸⁴ or $16 \mu\text{g L}^{-1}$ TiO_2 ^{113, 161, 185} are not expected in the environment. Additionally, the α_{homo} is likely not going to be 1 in many natural fresh waters as has been shown by the stabilizing effect of DOM.^{58, 67, 70} In the experiment described in chapter 3 we observed a decrease in sedimentation rate and increase in residual non-settling concentration with increasing DOM concentration (Figure 3.5 in Chapter 3). This stabilizing effect is caused by a decrease in attachment efficiency due to the presence of DOM. As the experiments were done with filtered DOM extracts ($0.2 \mu\text{m}$) and artificial water no heteroaggregation is expected. However, when we try to mimic the experimental results by varying α_{homo} , the fast initial decrease in CeO_2 concentration observed in the experiment (Figure 7.3a) is not observed in the modeling results (Figure 7.3b). Using a poly-disperse size distribution at the start of the calculations results in a more immediate decrease in ENM concentration, however the overall initial decrease is still not close to that observed in the experiments. Additionally the experimental results show an increasing residual concentration with increasing DOM content, which is not observed to the same degree in the model data. This seems to indicate some kind of added heterogeneity in the stabilization of CeO_2 ENMs under these conditions. This heterogeneity could have several reasons:

1. There could be a temporary increase in aggregation rate directly after adding the ENMs to the suspension flask. Because the flask is briefly shaken and thereby increasing the shear stress and consequently

temporarily also the aggregation rate. This can cause larger initial aggregates that settle quickly.

2. The stabilizing effect of DOM is not homogeneously distributed among all CeO₂ ENMs, resulting in a plateau of well stabilized CeO₂ ENMs or smaller aggregates and removal of a less stabilized fraction.
3. Differences in fractal dimension (Df) of initial aggregates in the stock (likely high) and the aggregates formed during the experiment (likely low).

These discrepancies between the modeled and experimental data could be further investigated by implementing the above mentioned heterogeneities in the mechanistic model. Although this would increase our understanding of the aggregation and sedimentation process of pristine CeO₂ ENMs under these experimental conditions, such work is not immediately necessary for exposure modeling of ENMs due to the small likelihood that homoaggregation plays a role under environmentally relevant conditions. The modeling of homoaggregation clearly shows that at low ENM concentration the aggregation rate is so low that it would not affect sedimentation at environmentally relevant concentrations and timescales. This gives the opportunity to simplify the modeling of ENMs by excluding homoaggregation ($\alpha_{\text{homo}}=0$) at CeO₂ ENMs concentrations below approximately 10 $\mu\text{g L}^{-1}$.

7.3.2 Heteroaggregation and sedimentation

As previously mentioned heteroaggregation is deemed one of the most important processes in the fate of ENMs in the natural environment. The mechanistic model enables us to investigate the NC and ENM characteristics affecting this process. To start the model confirms earlier experimental results from chapter 4 where heteroaggregation does not have a large effect on the removal of ENMs from the water phase at high ENM concentrations (10 or 100 mg L^{-1}), but does at lower ENM concentrations (Figure 7.4). It clearly shows the high removal of CeO₂ ENMs from the water phase due to heteroaggregation at the lower initial particle concentration (Figure 7.2a), where homoaggregation is negligible. At 10 mg L^{-1} CeO₂ ENMs the increased removal due to heteroaggregation is minimal as was also seen in the experimental data presented in (Figure 4.3 in chapter 4).

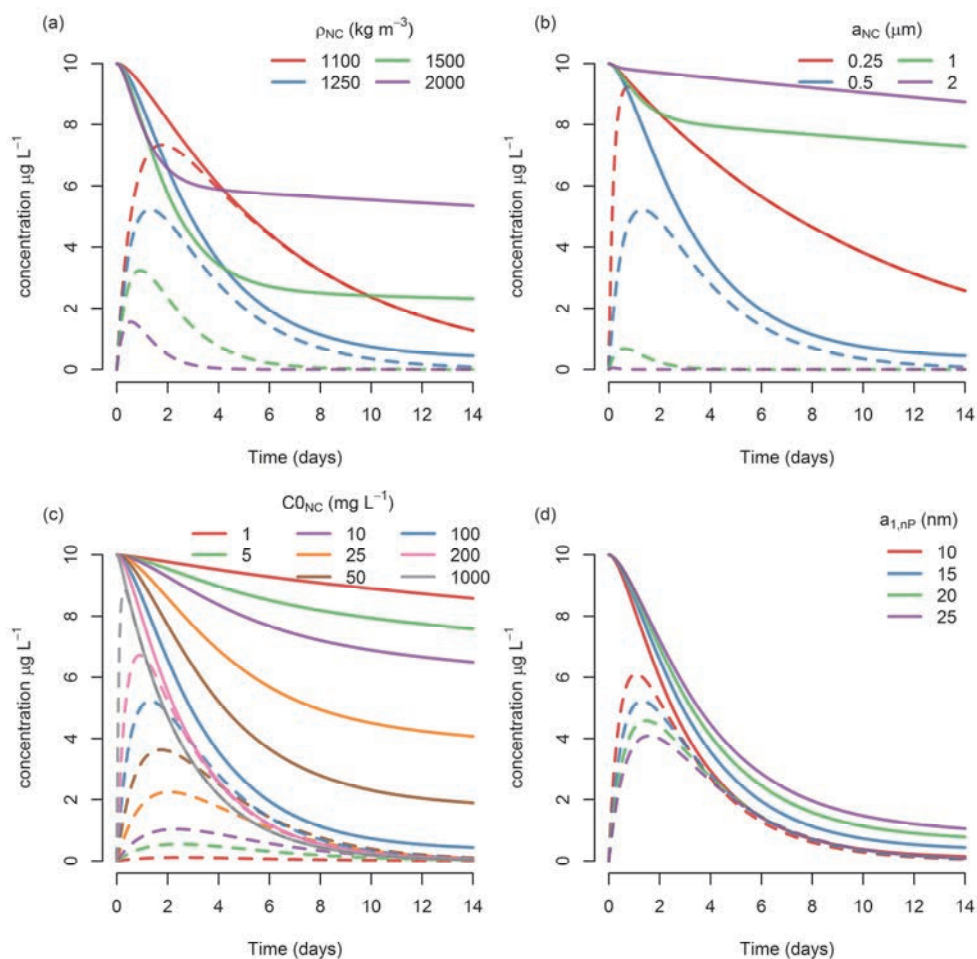


Figure 7.5. Calculated concentration CeO_2 NPs freely suspended (solid line) or attached to NCs (dashed line) in the water phase at different ρ_{NC} (a), a_{NC} (b), $C_{0\text{NC}}$ (c) and a_{NP} (d). The default parameters are given in Table 7.1.

Using a default scenario we tested the influence of NC characteristics such as a_{NC} , ρ_{NC} , $C_{0\text{NC}}$, on the removal due to heteroaggregation of a $10 \mu\text{g L}^{-1}$ CeO_2 ENM suspension. In Figure 7.5a, b, and c it is shown that these NC characteristics can make a big difference in the removal of ENMs from the water phase. Basically a_{NC} , ρ_{NC} affect the residence time of NCs in the water phase during which heteroaggregation can occur and the higher the $C_{0\text{NC}}$ the larger the fraction ENM-NC aggregates compared to free ENMs. Depending on the number concentration of NCs, the ENM's removal

follows the sedimentation of the ENM-NC heteroaggregates, such as at low ρ_{NC} (Figure 7.5a), low a_{NC} (Figure 7.5b) and at high $C_{0\text{NC}}$ (Figure 7.5c). In addition to NC characteristics, the influence of particle characteristic a_{NP} was tested (Figure 7.5d). This showed a relatively small variation in ENM concentration after 14 days, with an increase in ENM concentration with increasing a_{NP} . Although ρ_{NC} is another main ENM characteristic to consider, a change in ρ_{NC} would also depict a change in ENM chemical composition, e.g. Ag instead of CeO_2 . This is not further considered here at this point because of our focus on CeO_2 ENMs.

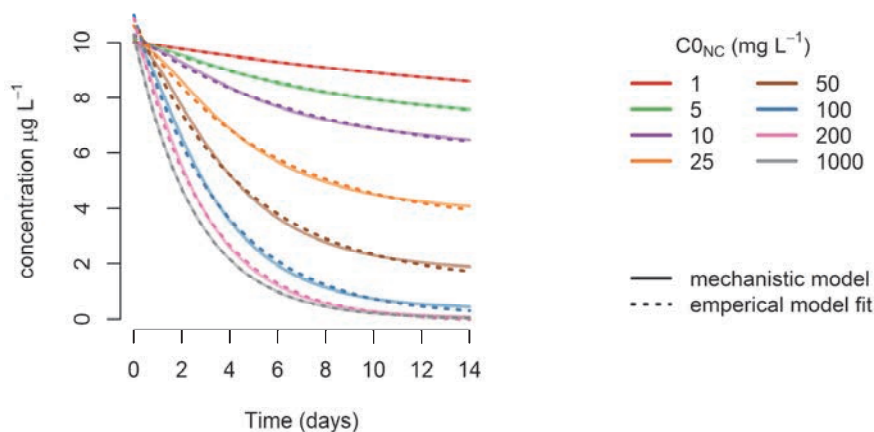


Figure 7.6. Calculated CeO_2 NP concentration in time at different $C_{0\text{NC}}$ concentrations ranging from 1 mg L^{-1} to 1000 mg L^{-1} . Additionally the empirical model as given in chapter 5 is indicated by the dashed line.

From our empirical data we found that sedimentation of ENMs is described well by a model describing first order removal towards a residual ENM concentration (Eq 4.2). This was explained by heteroaggregation of ENMs with NCs. From the mechanistic modeling results we know that at low ENM concentrations indeed heteroaggregation is the main processes affecting sedimentation. However in addition to heteroaggregation there are still several processes playing a role in the removal of ENMs from the water phase, such as: sedimentation of NCs, sedimentation of ENMs and sedimentation of ENM-NC heteroaggregates. We tested to see if the empirical model indeed can also describe the simulated data obtained using the mechanistic model by fitting equation 4.2 to the simulated data. This resulted in a generally good description of the simulated data (Figure 7.6). The largest deviation from the simulated data is seen at the start ($t=0$), although still relatively small. The decrease in

concentration due to sedimentation of heteroaggregates is captured well. Because there is only a limited amount of NCs in this scenario, a plateau is formed due to depletion of NCs leaving only the CeO₂ ENMs themselves, which sediment very slow. This shows that indeed the removal of ENMs due to heteroaggregation and sedimentation can be described by the empirical model.

7.5 Conclusion

The most important processes affecting the behavior of ENMs in water are taken into account in the mechanistic model introduced here: homoaggregation, heteroaggregation and sedimentation. Although such a model is not usable for assessment of the exposure concentration of ENMs in water, it can be used to simulate experiments and better understand the processes affecting sedimentation of ENMs from the water phase. The current model however could still be improved to better describe the experimental data observed, specifically when homoaggregation is important. Although this is the case, we could show that the empirical model from chapter 4 is adequate for describing removal due to heteroaggregation and sedimentation. The importance of heteroaggregation means that the NC types present in natural waters play an important role in the fate of ENMs in the aquatic environment. This is further illustrated by the large variation in sedimentation rate with different NC characteristics. This means that we need to have some basic information on the NC characteristics affecting heteroaggregation in order to better estimate the ENM exposure concentration.

Chapter 8

Synthesis

In order to adapt or develop new exposure assessment methods we need to fully understand the fate of ENMs in the natural environment and we should be able to derive quantitative descriptions of the relevant fate processes. In one of the first critical reviews in 2008, Klaine et al.¹⁶ states that the sediment is the most likely sink for ENMs due to interaction with NCs. However, at the time this was purely based on what was known about the behavior of different types of NCs.⁴¹

The aim of this thesis was to increase the understanding of ENM removal from the water phase using sedimentation experiments under environmentally relevant conditions and improve the exposure assessment of ENMs in the aquatic environment.

8.1 Engineered nanomaterial specific fate processes

Upon emission of ENMs to the aquatic environment, transformation processes take place followed by transport (**Chapter 2**). Both these processes can affect the exposure concentration of ENMs. All the transformation processes such as aggregation, dissolution and changes in particle coating, potentially affect the transport of ENMs. However, only dissolution has the potential to directly reduce the exposure concentration of ENMs by transforming the particulate form to the dissolved form of a chemical. This was shown in **Chapter 5** where significant dissolution of Ag ENMs was observed in seawater and to lesser extent in fresh water. The other transformation processes mainly affect aggregation which in turn results in the sedimentation of ENMs out of the water phase. Measuring the removal of ENMs from the water phase proved to be a useful endpoint for estimating the effect of DOM and NCs on the sedimentation of ENMs (**Chapters 3-6**). The DOM fraction of NCs extracted from two natural sources stabilized CeO₂ ENMs against aggregation and reduced removal from the water phase with increasing DOM concentration (**Chapter 3**). A similar stabilizing effect was seen in natural water with only DOM present (**Chapters 4 and 5**). When, however the whole range of NCs were present, the stabilizing effect of DOM was reduced. This indicated that heteroaggregation played an important role in removal of ENMs from the water phase, even in presence of DOM (**Chapter 4 and 5**). In addition to NCs, suspended sediment had an even greater effect on the removal of ENMs from the water phase (**Chapter 6**). This showed that sediments have the potential to efficiently scavenge ENMs out of the water phase upon resuspension of these sediments into the water phase.

These findings show that heteroaggregation of ENMs with NCs or suspended sediments followed by sedimentation of these heteroaggregates will cause transport of ENMs from the water phase to the sediment.

8.2 Quantitative description of engineered nanomaterial sedimentation

It was already expected that sedimentation of ENMs from the water phase could be described using first order kinetics, because of the potential dominant effect of heteroaggregation in natural systems (**Chapter 2**). From the sedimentation experiments (**Chapters 3-6**) it was found that the decrease in ENM concentration could be well described using first order kinetics, however the ENM concentration did not decrease to 0, but a residual concentration of ENMs remained (**Chapter 4**). This resulted in the empirical model (**Eq. 4.2**) which could be used to quantify the sedimentation rate of ENMs. The sedimentation rates observed in presence of NCs were considerably lower ($0.002\text{--}0.02\text{ m d}^{-1}$) than those observed in presence of suspended sediments ($0.04\text{--}1.6\text{ m d}^{-1}$) for the same water and ENM types (**Chapters 5 and 6**). However the direct application of the observed sedimentation rates is problematic due to the experimental conditions being far from realistic.

This can be overcome by calculating the sedimentation rate based on Stokes' law for modeling exposure concentrations of ENMs. This however requires the aggregation process to be quantitatively described as well. For heteroaggregation however, the main unknown parameter is the attachment efficiency.³⁶ For this reason a method for calculation of the attachment efficiency of heteroaggregation between ENMs and NCs was derived for use with the results obtained from the sedimentation experiments (**Chapter 5**). The resulting attachment efficiencies ranged from 0.012 to 1 depending on water and ENM type. The large range in $\alpha_{\text{hetero,crit}}$ indicated that heteroaggregation does not have the same effect on removal of ENMs from the water phase in all cases.

8.3 Modeling engineered nanomaterial fate processes

In the experimental studies presented in this thesis heteroaggregation was found to be the main process affecting the sedimentation of ENMs from natural waters. However, at higher ENM concentrations homoaggregation was thought to still play a role. In **Chapter 7**, a mechanistic model coupling homo- and heteroaggregation to sedimentation showed that indeed at low concentrations of ENMs ($< 10\text{ }\mu\text{g L}^{-1}\text{ CeO}_2$) heteroaggregation with NCs was the main removal process. Using this mechanistic model, it was shown that indeed heteroaggregation and subsequent sedimentation can be described using first order kinetics towards a residual non-settling ENM concentration. This is mainly due to the fact that the calculations replicated the

experimental setup, where only a limited concentration of NCs was present. Under realistic conditions a more constant concentration of NCs is expected, which means that pure first order removal kinetics is adequate for exposure modeling.

8.4 Concluding remarks

In this thesis we have identified three removal processes affecting the concentration of ENMs in the water phase. First, removal due to dissolution; second, removal due to heteroaggregation with NCs and subsequent sedimentation; third, removal due to heteroaggregation of ENMs with resuspended sediments and subsequent sedimentation. These processes can form the basis for an exposure modeling framework.³⁶ The method that quantified the interaction between NCs and ENMs by estimating one of the generally unknown model parameters: α_{hetero} , is the first step in better parameterization of exposure assessment models for ENMs. With some more information on the physico-chemical characteristics of the NCs combined with data on ENMs emissions we can truly calculate local exposure concentrations of ENMs in water and sediment.

Appendices

Appendix A

A: Supporting information to chapter 2: How to assess exposure of aquatic organisms to engineered nanomaterials?

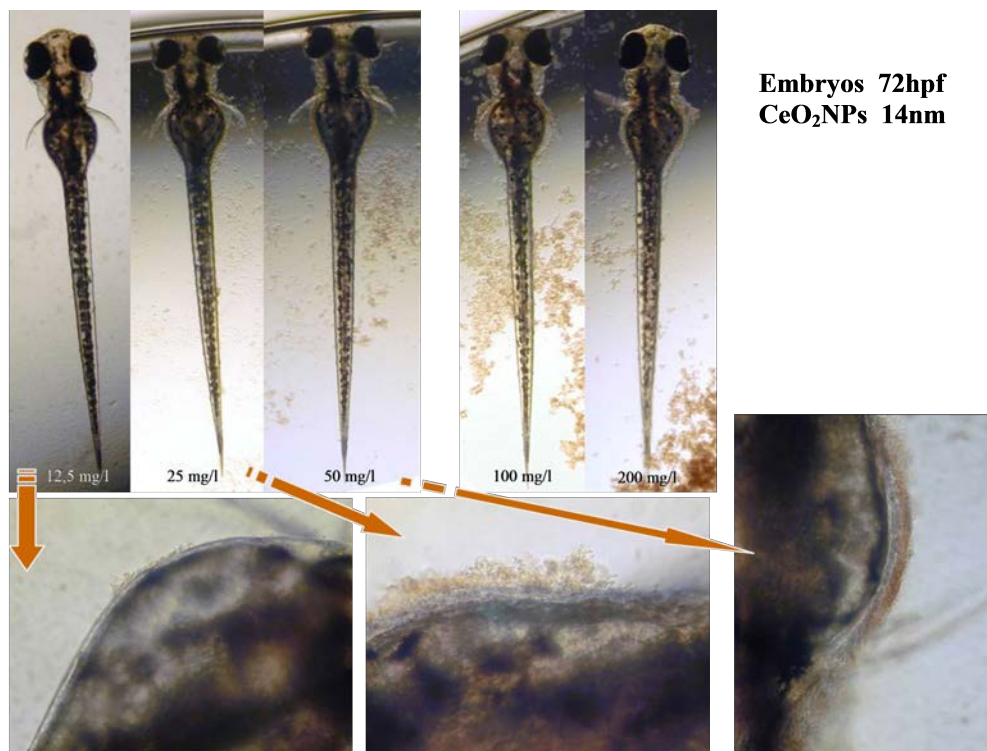


Figure A.1. CeO₂ nanoparticles aggregated and attached to zebrafish embryo's, Work published in Van Hoecke et al.⁹⁸

Table A.1. Sedimentation data as presented in figure 2.2.

	Time (Hours)	Time (Seconds)	C_{susp}/C_0	Discription	Source
TiO₂ (Battin 2009)	1	3.60E+03	0.26	TiO ₂ HOM	Figure 1 in Battin et al. ⁹⁶
	2	7.20E+03	0.11	TiO ₂ HOM	
	3	1.08E+04	0.05	TiO ₂ HOM	
CeO₂ (a, Quik 2010)	24	8.64E+04	0.16	CeO ₂ (a)	Directly from author, published in Quik et al. ⁷⁰
	96	3.46E+05	0.01	CeO ₂ (a)	
	288	1.04E+06	0.00	CeO ₂ (a)	
CeO₂ (b, Quik 2010)	24	8.64E+04	0.44	CeO ₂ 0.5 mg/L DOM	Directly from author, published in Quik et al. ⁷⁰
	96	3.46E+05	0.23	CeO ₂ 0.5 mg/L DOM	
	288	1.04E+06	0.06	CeO ₂ 0.5 mg/L DOM	
CeO₂ (c, Quik 2010)	24	8.64E+04	0.76	CeO ₂ 10 mg/L DOM	Directly from author, published in Quik et al. ⁷⁰
	96	3.46E+05	0.52	CeO ₂ 10 mg/L DOM	
	288	1.04E+06	0.30	CeO ₂ 10 mg/L DOM	
MWCNT (a, Kennedy 2008)	0.1	4.20E+02	0.65	MWCNT	Directly from author, published in Kennedy et al. ⁹²
	0.3	1.08E+03	0.36	MWCNT	
	0.5	1.80E+03	0.27	MWCNT	
	1.0	3.60E+03	0.21	MWCNT	
	1.5	5.40E+03	0.19	MWCNT	
	2.0	7.20E+03	0.17	MWCNT	
MWCNT (b, Kennedy 2008)	0.2	6.00E+02	0.94	MWCNT + DOM	Directly from author, published in Kennedy et al. ⁹²
	0.3	1.20E+03	0.86	MWCNT + DOM	
	0.5	1.80E+03	0.83	MWCNT + DOM	
	1.0	3.60E+03	0.81	MWCNT + DOM	
	1.5	5.40E+03	0.80	MWCNT + DOM	
	2.0	7.20E+03	0.79	MWCNT + DOM	
MWCNT (Hyung 2007)	96	3.46E+05	0.03	MWCNT + DOM	Table 1 in Hyuang et al. ⁵⁸
Fe⁰-SM (a Phenrat 2009)	1.7	6.11E+03	0.30	nZVI	Figure 4 in Phenrat et al. ⁹³
	6.7	2.40E+04	0.08	nZVI	
	13	4.80E+04	0.03	nZVI	
	23	8.40E+04	0.01	nZVI	
Fe⁰ (b, Phenrat 2009)	1.7	6.11E+03	0.50	Aged nZVI	Figure 4 in Phenrat et al. ⁹³
	6.7	2.40E+04	0.30	Aged nZVI	
	13	4.80E+04	0.22	Aged nZVI	
	23	8.40E+04	0.18	Aged nZVI	
Fe⁰ (c, Phenrat 2009)	1.7	6.11E+03	0.90	SM-nZVI	Figure 4 in Phenrat et al. ⁹³
	6.7	2.40E+04	0.80	SM-nZVI	
	13	4.80E+04	0.70	SM-nZVI	
	23	8.40E+04	0.63	SM-nZVI	
TiO₂ (Keller 2010)	0.7	2.52E+03	0.78	TiO ₂	Figure 5 in Keller et al. ⁶⁷
	1.6	5.77E+03	0.58	TiO ₂	
	3.8	1.36E+04	0.20	TiO ₂	
	6.0	2.15E+04	0.12	TiO ₂	
ZnO (Keller 2010)	0.7	2.52E+03	0.88	ZnO	Figure 5 in Keller et al. ⁶⁷
	1.6	5.77E+03	0.80	ZnO	
	3.8	1.36E+04	0.71	ZnO	
	6.0	2.16E+04	0.60	ZnO	
CeO₂ (Kellers 2010)	0.7	2.52E+03	0.84	CeO ₂	Figure 5 in Keller et al. ⁶⁷
	1.6	5.77E+03	0.75	CeO ₂	
	3.8	1.37E+04	0.52	CeO ₂	
	6.0	2.15E+04	0.36	CeO ₂	

Table A.2. Dissolution data as presented in figure 2.3.

	Time (Hours)	Time (Seconds)	C_{susp}/C_0	Discription	Source
TiO2 (Schmidt 2009)	500	1.80E+06	1.00	TiO2	Figure 5 in Schmidt et al. ⁷²
Al2O3 (Roelofs 2006)	200	7.20E+05	1.00	Al2O3	Table 5 in Roelofs et al. ⁷⁴
ZnO (a, Franklin 2007)	6	2.26E+04	0.90	nano ZnO	Figure 2 in Franklin et al. ⁸⁴
	24	8.47E+04	0.84	nano ZnO	
	31	1.10E+05	0.82	nano ZnO	
	48	1.72E+05	0.81	nano ZnO	
	72	2.60E+05	0.80	nano ZnO	
ZnO (b, Franklin 2007)	6	2.26E+04	0.91	Bulk ZnO	Figure 2 in Franklin et al. ⁸⁴
	24	8.47E+04	0.85	Bulk ZnO	
	31	1.10E+05	0.84	Bulk ZnO	
	48	1.72E+05	0.82	Bulk ZnO	
	72	2.60E+05	0.81	Bulk ZnO	
ZnO (a, Wong 2010)	8	2.73E+04	0.96	nano ZnO	Figure 3 in Wong et al. ⁸⁵
	24	8.64E+04	0.96	nano ZnO	
	48	1.73E+05	0.95	nano ZnO	
	72	2.59E+05	0.94	nano ZnO	
	96	3.46E+05	0.94	nano ZnO	
	120	4.32E+05	0.94	nano ZnO	
ZnO (b, Wong 2010)	8	2.73E+04	0.98	Bulk ZnO	Figure 3 in Wong et al. ⁸⁵
	24	8.64E+04	0.98	Bulk ZnO	
	48	1.73E+05	0.97	Bulk ZnO	
	72	2.59E+05	0.97	Bulk ZnO	
	96	3.46E+05	0.98	Bulk ZnO	
	120	4.32E+05	0.97	Bulk ZnO	
Ag (a, Liu 2010)	6	2.12E+04	0.75	Ag, low ionic strength	Figure 7 in Liu et al. ⁹¹
	24	8.64E+04	0.61	Ag, low ionic strength	
	96	3.46E+05	0.48	Ag, low ionic strength	
	192	6.91E+05	0.46	Ag, low ionic strength	
Ag (b, Liu 2010)	6	2.12E+04	0.86	Ag, high ionic strength	Figure 7 in Liu et al. ⁹¹
	24	8.64E+04	0.78	Ag, high ionic strength	
	96	3.46E+05	0.66	Ag, high ionic strength	
	192	6.91E+05	0.60	Ag, high ionic strength	
Ag (c, Liu 2010)	24	8.64E+04	0.67	Ag + 5 mg/L DOM	Figure 7 in Liu et al. ⁹¹
	24	8.64E+04	0.74	Ag + 10 mg/L DOM	
	24	8.64E+04	0.81	Ag + 20 mg/L DOM	
	24	8.64E+04	0.98	Ag + 50 mg/L DOM	
Ag (Fabrega 2009)	24	8.64E+04	0.997	Ag	Table 1 in Fabrega et al. ⁸⁶

Table A.1 Sedimentation data as presented in figure 2.2.

This table can be found in the online version of this thesis or at:

<http://goo.gl/4Vnzb> or <http://iquik.nl/thesis/tableA1.pdf>



Table A.2 Dissolution data as presented in figure 2.3.

This table can be found in the online version of this thesis or at:

<http://goo.gl/OhHXR> or <http://iquik.nl/thesis/tableA2.pdf>



Appendix B

B: Supporting information to chapter 3: Effect of dissolved organic matter on cerium dioxide nanoparticles settling in model fresh water

Table B.1. The contents of the test medium according to OECD guidelines.

Substance	Concentration (mmol L ⁻¹)
H ₃ BO ₃	2.990*10 ⁻³
NH ₄ Cl	0.280
NaHCO ₃	0.595
Na ₂ EDTA.2H ₂ O	0.269*10 ⁻³
Na ₂ MoO ₄ .2H ₂ O	0.029*10 ⁻⁶
KH ₂ PO ₄	0.012
MgSO ₄ .7H ₂ O	0.061
MgCl ₂ .6H ₂ O	0.059
CaCl ₂ .2H ₂ O	0.122
MnCl ₂ .4H ₂ O	2.100*10 ⁻³
FeCl ₃ .6H ₂ O	0.237*10 ⁻³
CoCl ₂ .6H ₂ O	0.006*10 ⁻³
CuCl ₂ .2H ₂ O	0.060*10 ⁻⁶
ZnCl ₂	0.022*10 ⁻³
Ionic strength	1.70

Table B.2. Fractionation of dissolved organic matter given as percentage of total dissolved organic matter present.

	Humic acid	Fulvic acid	Hydrophilic acid	Hydrophobic natural organic matter
SR-DOM	6%	60%	14%	21%
B-DOM	19%	45%	16%	20%

Table B.3. The nanoparticle tracking analysis settings.

	With DOM	Without DOM
Pulldown	15	20
Gain	2.00	1.33
Blur	3	3
DetectThresh	40	40
MaxBlob	3000	3000
MinTrackLength	20	30
MaxParticleJump	8.6	6.0
BinWidth	4	4

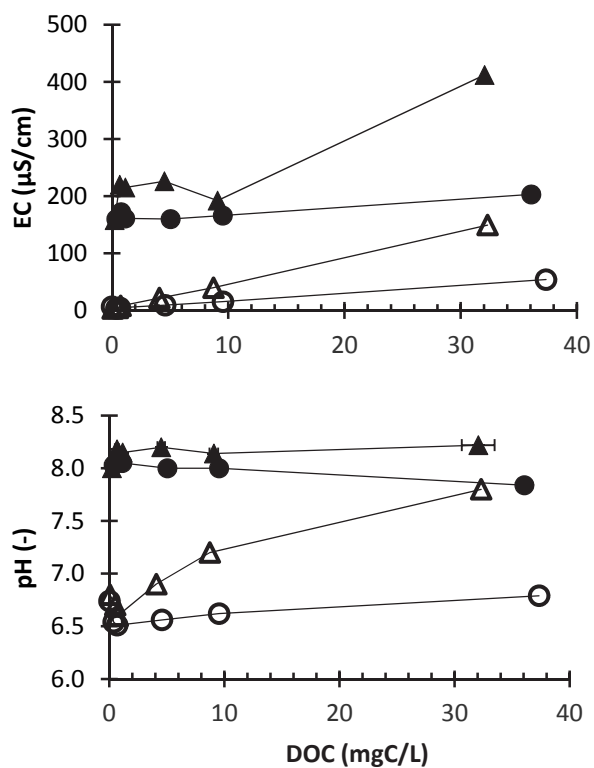


Figure B.1. The electrical conductivity (top) and pH (bottom) in the algae medium (filled symbols) and pure water (open symbols) with Bihain (▲) and Suwannee River (●) dissolved organic matter.

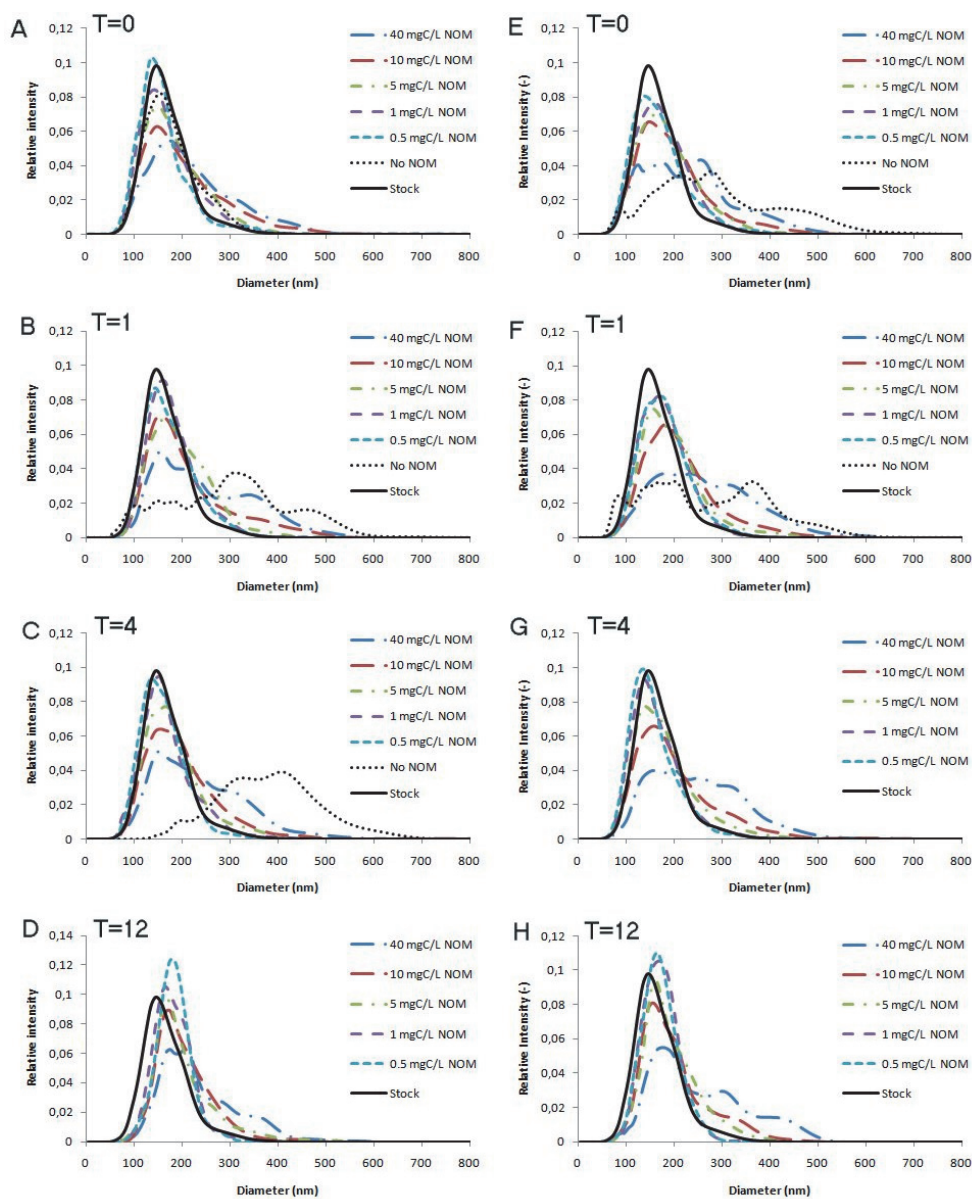


Figure B.2. The particle size distributions of CeO_2 nanoparticles in deionized water at $T = 0, 1, 4$, and 12 days with SR-DOM (A-D) and B-DOM (E-H).

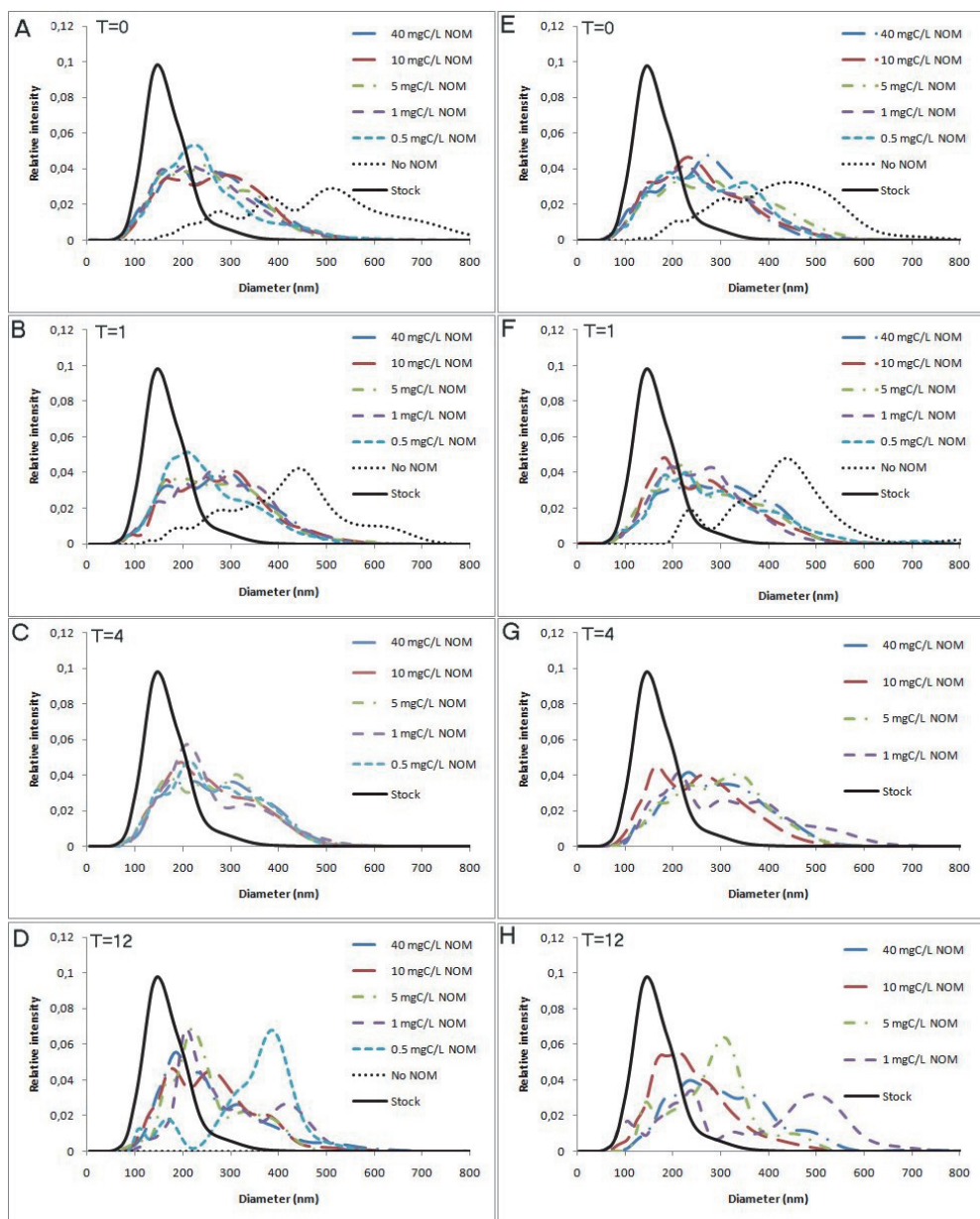


Figure B.3. The particle size distributions of CeO_2 nanoparticles in the algae medium at $T = 0, 1, 4$, and 12 days with SR-DOM (A-D) and B-DOM (E-H).

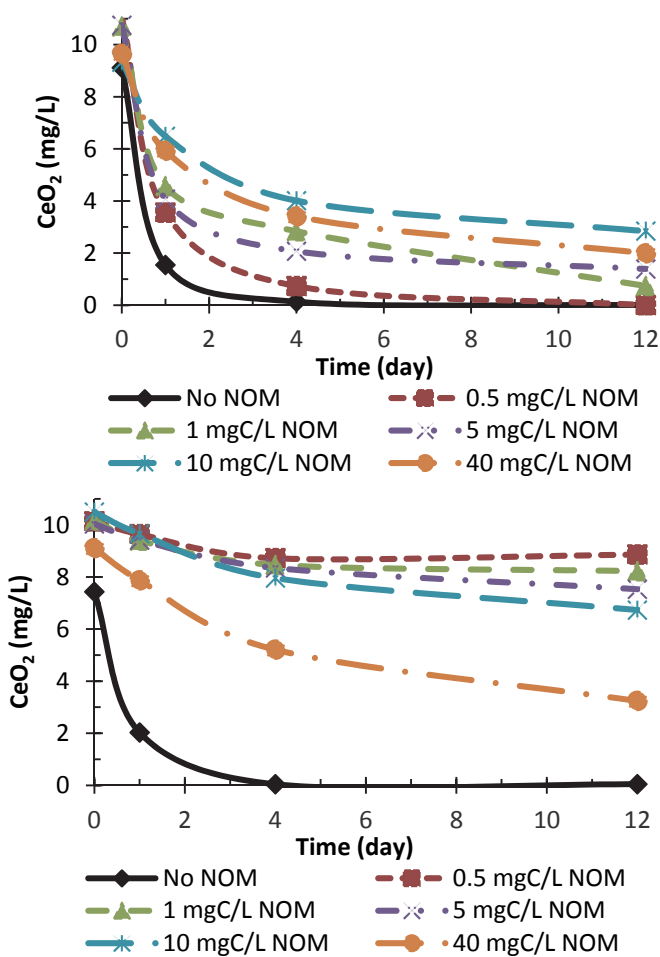


Figure B.4. The concentration of cerium dioxide remaining in the supernatant after settling for 0, 1, 4 and 12 days for suspensions prepared in the algae medium (top) and pure water (bottom) with various concentrations of Biobain dissolved organic matter (0 – 40 mg C/L DOM).

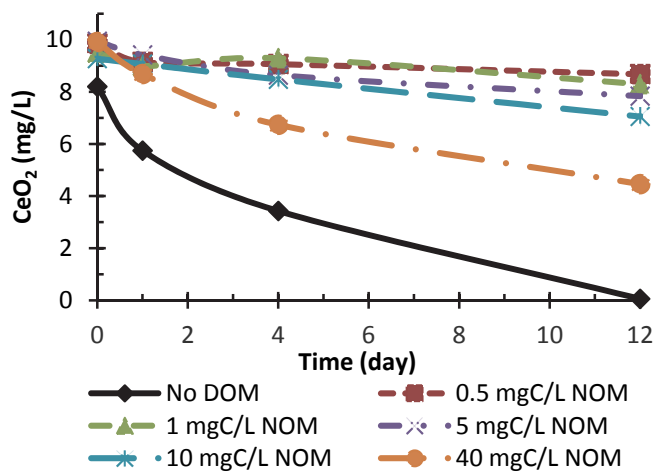


Figure B.5. The concentration of cerium dioxide remaining in the supernatant after settling for 0, 1, 4 and 12 days for suspensions prepared in deionized water with various concentrations of Suwannee river dissolved organic matter (0 – 40 mg C/L DOM).

Appendix C

C: Supporting information to chapter 4: Natural colloids are the dominant factor in the sedimentation of nanoparticles

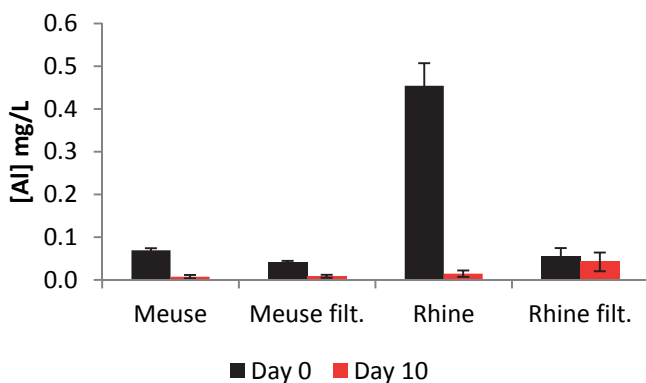


Figure C.1. Concentration Aluminum in the supernatant of Meuse and Rhine water at start of experiment and after 10 days settling in filtered and unfiltered water. Error bars represent standard deviation between 4 separate flasks.

Table C.1. Water quality parameters for Meuse and Rhine river water as sampled on 22 and 23 september 2009.

Measured in actual CeO ₂ suspensions		Meuse		Rhine	
		Unfiltered	Filtered	Unfiltered	Filtered
pH [†]	(-)	7.60 ± 0.02	7.57 ± 0.04	7.87 ± 0.03	7.97 ± 0.01
Electric conductivity [†]	(mS m ⁻¹)	72.1 ± 0.5	72.0 ± 0.9	78.4 ± 0.6	78.3 ± 0.5
Total organic carbon [†]	(mg L ⁻¹)	4.41 ± 0.17	4.99 ± 0.19	5.08 ± 0.09	3.99 ± 0.11
Measured in river water at the time of sample collection or on the same day					
pH	(-)	7.7	nd	7.9	nd
Electric conductivity	(mS m ⁻¹)	68	nd	69	nd
Total organic carbon	(mg L ⁻¹)	3	3	3	2
Oxygen	(mg L ⁻¹)	7.6	nd	8.9	nd
Chloride	(mg L ⁻¹)	nd	70.1	nd	102
Iron	(mg L ⁻¹)	0.07	<0.01	0.53	<0.01
Potassium	(mg L ⁻¹)	5.5	nd	5.4	nd
Copper	(mg L ⁻¹)	2.56	2.39	4.41	2.26
Sodium	(mg L ⁻¹)	56	nd	62	nd
Nitrate	(mg L ⁻¹)	nd	2.93	nd	1.98
Nitrite	(mg L ⁻¹)	nd	0.12	nd	<0.01
Silicate	(mg L ⁻¹)	nd	2.99	nd	2.25
Phosphate	(mg L ⁻¹)	0.23	nd	0.45	nd
Suspended solids (dry weight) [#]	(mg L ⁻¹)	5		12	
Total organic carbon in suspended solids [#]	%	32		18	
Suspended solids (dry weight) [*]	(mg L ⁻¹)	1.74		15.8	
Total organic carbon in suspended solids [*]	%	18.6		nd	
Iron in suspended solids [*]	(g kg ⁻¹)	26		31	
Potassium in suspended solids [*]	(Bq kg ⁻¹)	310		460	
Copper in suspended solids [*]	(mg kg ⁻¹)	92		97	
Phosphate in suspended solids [*]	(mg g ⁻¹)	6.11		1.7	
Size fraction suspended solids smaller than 2 µm [*]	%	23		25	
Size fraction suspended solids smaller than 10 µm [*]	%	36		43	
Size fraction suspended solids smaller than 16 µm [*]	%	44		48	
Size fraction suspended solids smaller than 20 µm [*]	%	44		50	
Size fraction suspended solids smaller than 50 µm [*]	%	46		59	
Size fraction suspended solids smaller than 63 µm [*]	%	49		61	

[†] Measured in actual CeO₂ suspensions, average of the 0, 1, 10, 100 mg L⁻¹ CeO₂ suspension with standard error (N=4).

[#] Collection of suspended solids by filtration with 1.2 µm Whatman GF/C filters.

^{*} Collection of suspended solids by water centrifuge.

nd: no data

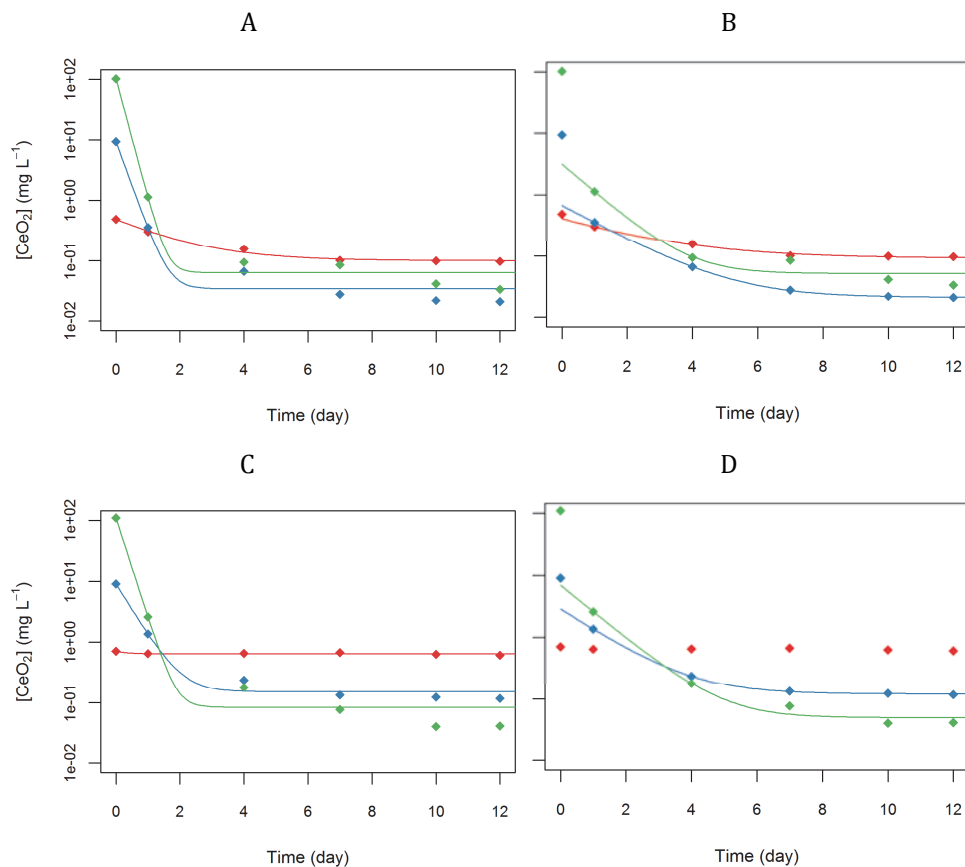


Figure C.2. Sedimentation of CeO_2 nanoparticles in Meuse water during 12 days in unfractionated (A, B) and filtered (C, D) water. Three different initial CeO_2 concentrations were used, 1, 10 and 100 mg L^{-1} . The model $C_t = (C_0 - C_{\text{res}})e^{-kt} + C_{\text{res}}$ is fitted to the observed sedimentation behavior for all data points, $N=6$, (A, C) and, without taking the first measurement into account, $N=5$ (B, D). Y-axis in log scale.

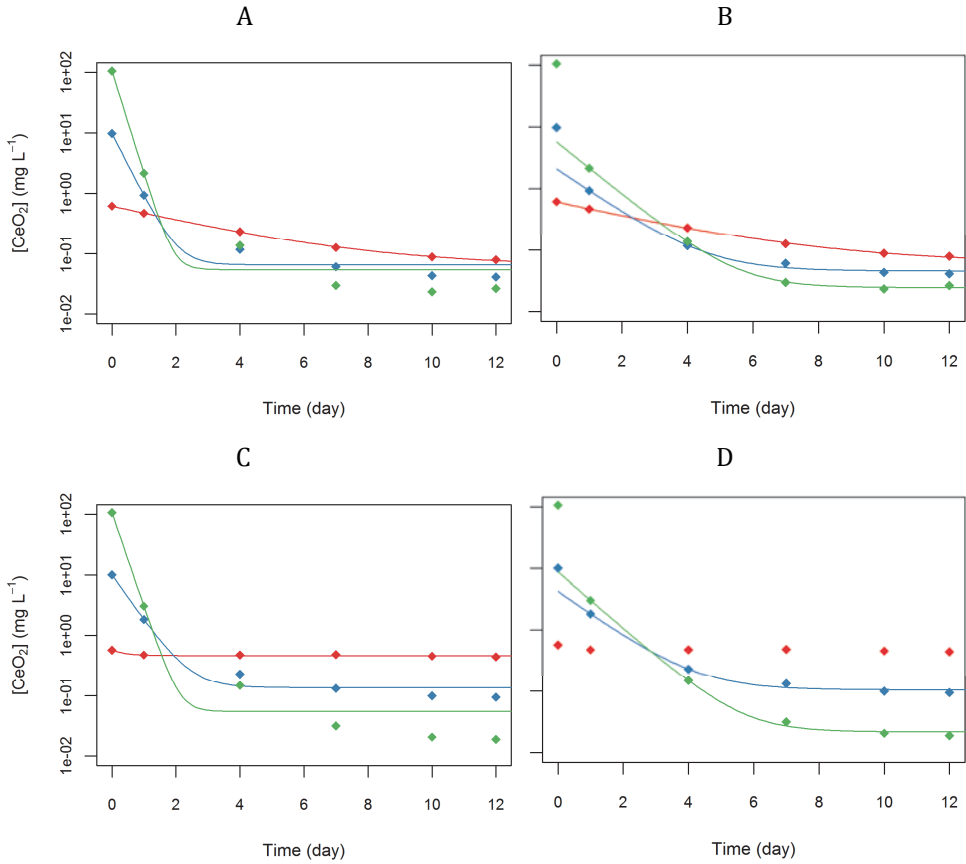


Figure C.3. Sedimentation of CeO_2 nanoparticles in Rhine water during 12 days in unfractionated (A, B) and filtered (C, D) water. Three different initial CeO_2 concentrations were used, 1, 10 and 100 mg L^{-1} . The model $C_t = (C_0 - C_{\text{res}})e^{-kt} + C_{\text{res}}$ is fitted to the observed sedimentation behavior for all data points, $N=6$ (A, C) and , without taking the first measurement into account, $N=5$ (B, D). Y-axis in log scale.

Appendix D

D: Supporting information to chapter 5: Nanomaterials in natural waters: Sedimentation rates and attachment efficiencies for heteroaggregation

Table D.1. Characteristics of the stock nanoparticle suspensions.

Particle	Diameter (nm)	Hydrodynamic diameter (nm)	ZP (mV)	pHa (-)	Mass conc. (g L ⁻¹)
PVP-Ag	51 ± 22.1	101.6	-12.4	6.5	10.23
SiO2-Ag	Core: 40.5 ± 20.5 Shell: 24.6	147.7	25.4	6.2	4.66
CeO2	20	147	38.7	4	100
C60	na	217	-13.7	5.6	1

a: pH of stock suspensions

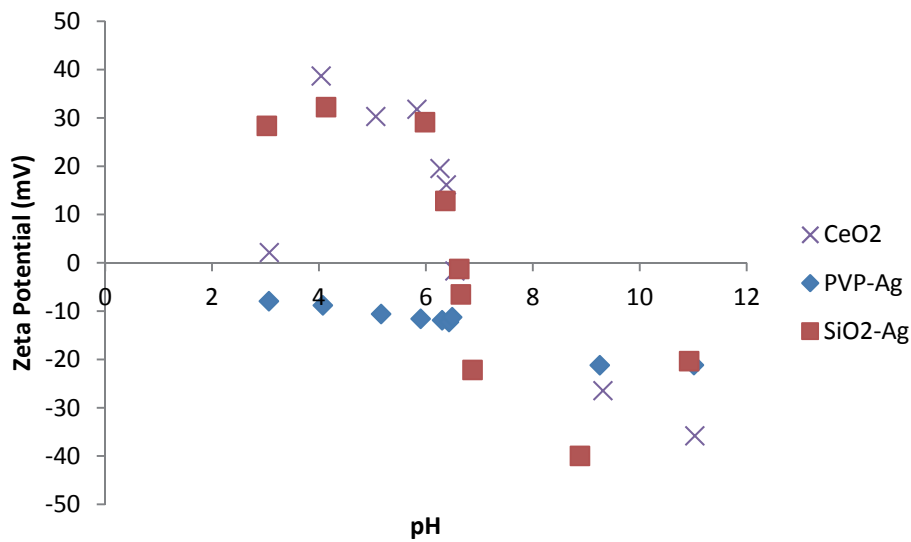


Figure D.1. Zeta potential of 10 mg L⁻¹ dilution of nanoparticle stocks in deionized water as a function of pH.

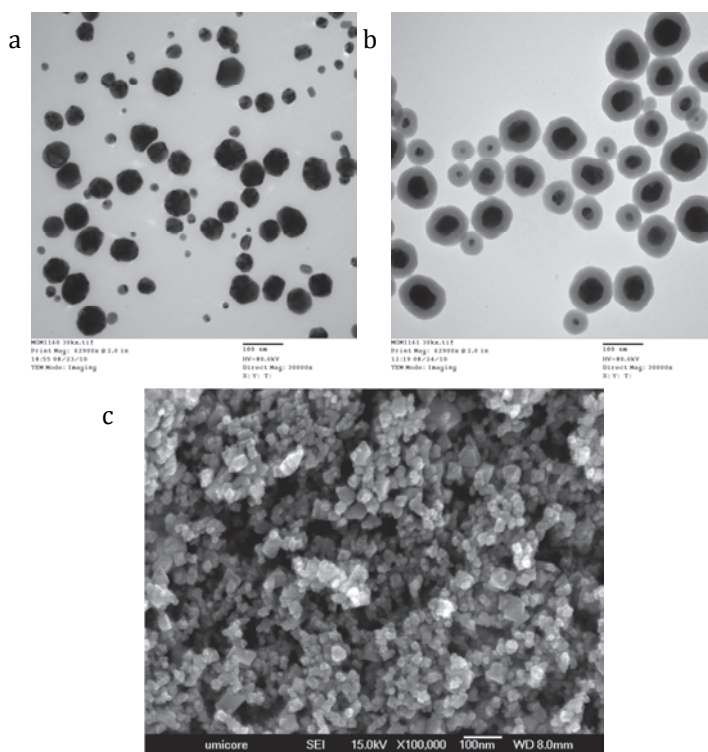


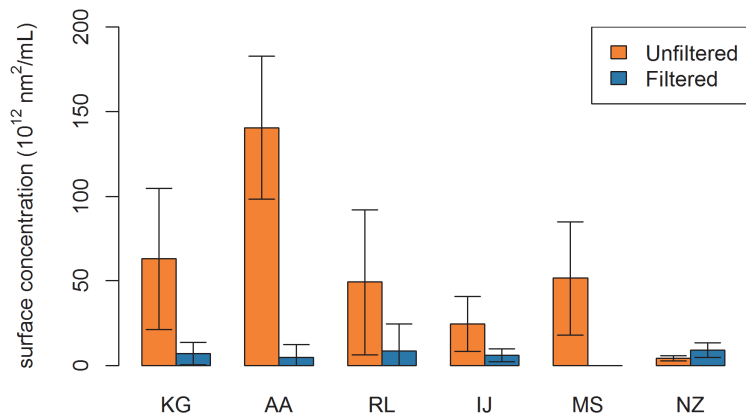
Figure D.2. Transmission Electron Microscopy (JEOL 1010 Transmission Electron Microscope, kindly provided by NanoComposix) images of PVP-Ag (a) and SiO₂-Ag nanoparticles (b) and scanning electron microscopy image (kindly provided by Umicore as part of NanoInteract project) of CeO₂ nanoparticles (c).

Table D.2. Water sampling locations and methods.

Water body	Sampling	Longitude	Latitude
Brabantse Aa (AA)	Bucket	51.391350°	5.741789°
Rhine (RL)	Pump	51.853845°	6.091116°
Nieuwe Waterweg (MS)	Bucket	51.914349°	4.249928°
Karregat (KG)	Beaker on a pole	51.730449°	5.418963°
IJsselmeer (IJ)	Bucket	52.575146°	5.530710°
North Sea (NZ)	Ship	n.a.	n.a.

n.a.: no data available

A



B

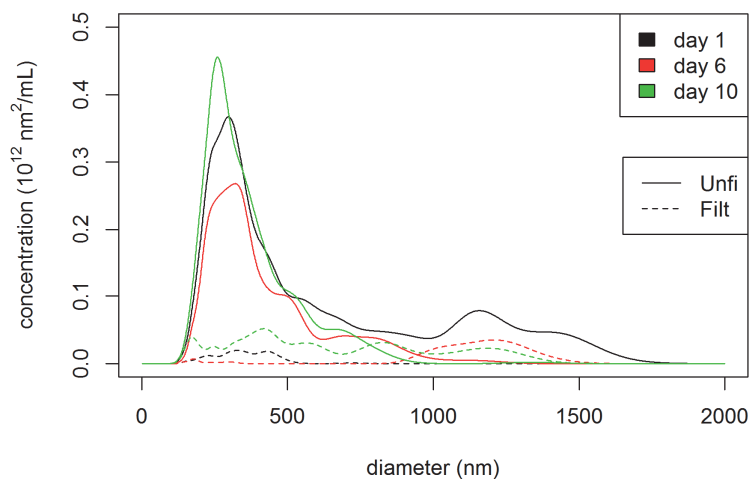


Figure D.3. A: Total surface area concentration present in filtered and unfiltered natural waters. B: Surface area distribution of filtered and unfiltered AA water.

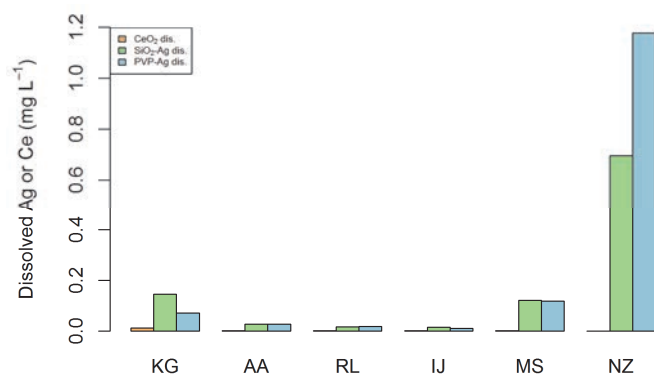


Figure D.4. Concentration of dissolved metal (Me) Ag and Ce in MilliQ water after 15 days at pH ranging from 3 to 11. Initial particle suspensions contained 10 mg L⁻¹ CeO₂, SiO₂-Ag or PVP-Ag nanoparticles.

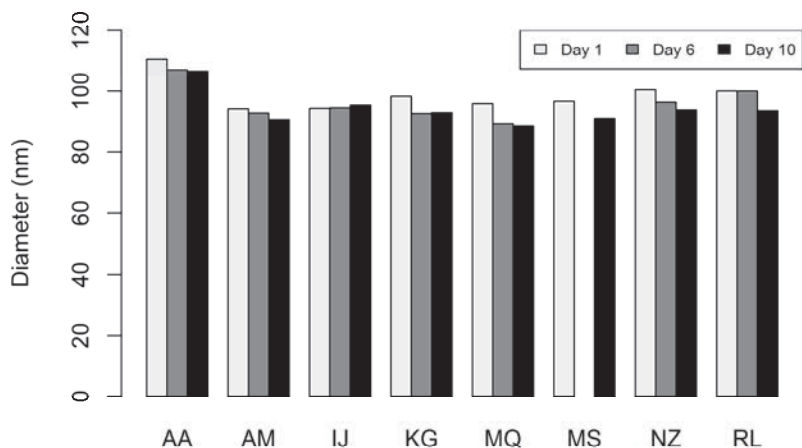


Figure D.5. Average PVP-Ag particle diameter after 1, 6 and 10 days in different water types.

Table D.3. CHEAQs speciation calculations

Output from CHEAQs pro version P2012.1 for Ag in RL, MS and NZ water covering a range in ionic strength and chloride content.

	Concentration (M)	% of dissolved concentration	% of total concentration	Activity (M)	Intrinsic equilibrium constant	Conditional equilibrium constant
Rhine (RL)						
Free Ag ⁺	1.066E-05	11.49	11.49	9.787E-06		
AgCl (aq)	6.308E-05	68.04	68.04	6.308E-05	3.310	3.236
AgCl ₂ ⁻	1.880E-05	20.37	20.37	1.734E-05	5.250	5.176
AgCl ₃ ²⁻	6.858E-08	0.07	0.07	4.879E-08	5.200	5.200
AgCl ₄ ³⁻	1.922E-08	0.02	0.02	8.936E-09	6.964	7.111
Total concentration	9.271E-05		100.00			
Nieuwe Waterweg (MS)						
Free Ag ⁺	1.835E-08	0.02	0.02	1.434E-08		
AgCl (aq)	2.482E-06	2.68	2.68	2.482E-06	3.310	3.095
AgCl ₂ ⁻	2.347E-05	25.32	25.32	1.833E-05	5.250	5.035
AgCl ₃ ²⁻	3.723E-06	4.02	4.02	1.386E-06	5.200	5.200
AgCl ₄ ³⁻	6.301E-05	67.97	67.97	6.817E-06	6.964	7.393
Total concentration	9.271E-05		100.00			
North Sea (NZ)						
Free Ag ⁺	1.246E-11	0.00	0.00	9.265E-12		
AgCl (aq)	6.884E-09	0.01	0.01	9.884E-09	3.310	3.053
AgCl ₂ ⁻	6.049E-07	0.65	0.65	4.498E-07	5.250	4.993
AgCl ₃ ²⁻	6.852E-07	0.74	0.74	2.095E-07	5.200	5.200
AgCl ₄ ³⁻	9.140E-05	98.60	98.60	6.350E-06	6.964	7.478
Total concentration	9.271E-05		100.00			

Table D.4.

Source:

Chinnapongse et
al.¹⁵⁸:

Explanation of data:

The sedimentation rates were obtained from the figures in their paper. The sedimentation rate was calculated by multiplying the observed rates with the sedimentation length (10.6 mm). The water surface reached 23 mm above the base of the cuvette. And the measurement

	height was between 9.2 mm and 15.6 mm above the base of the cuvette, this gives an average sedimentation length of 10.6 mm. It should also be noted that the k_{obs} was the rate of disappearance of absorbance from singly dispersed metallic silver nanoparticles. Potential mechanisms for their disappearance could range from agglomeration and sedimentation, to surface reactions that would quench the surface plasmon resonance absorbance of the silver metal nanoparticles, to dissolution of the particles.
Kennedy et al. ⁹² :	The raw sedimentation data were obtained from the author and Eq. 5.1 was fitted. The calculated sedimentation rates were obtained using a 16.75 mm sedimentation length. The water surface was 28-29 mm above the bottom of the cuvette. The exact measurement point was not clear, but most photo spectrometers measure between 8.5 and 15 mm above the bottom of the cuvette. In this case an average height of 11.75 mm is used resulting in a 16.75 mm sedimentation length.
Keller et al. ⁶⁷ :	Sedimentation rates were obtained from the figures in their paper. The sedimentation length was 1 cm.

Table D.5 Sedimentation rates and C_{15}/C_0

This table can be found at:

<http://goo.gl/2iDOF> or <http://iquik.nl/thesis/tableD5.pdf>



Table D.5 Sedimentation rates and C_{15}/C_0

			V _s (m d ⁻¹)		Std.Error V _s (m d ⁻¹)	C ₀ (mg L ⁻¹)		Std.Error C ₀ (mg L ⁻¹)	C ₁₅ /C ₀	
Aa	Filt	0.5	5.42E-03	±	7.13E-04	3.43E-01	±	5.54E-03	6.95E-01	
		2.5	6.19E-03	±	1.32E-03	1.79E+00	±	3.34E-02	7.64E-01	
		10	9.94E-03	±	5.49E-03	7.77E+00	±	1.03E-01	9.38E-01	
	C ₆₀	5	1.42E-01	±	1.13E-01	1.01E+00	±	3.17E-02	6.27E-02	
		25	1.12E-01	±	6.92E-03	8.39E+00	±	4.58E-02	7.52E-03	
		100	1.07E-01	±	7.74E-03	2.83E+01	±	2.08E-01	2.47E-03	
	CeO ₂	0.5	3.82E-03	±	7.81E-04	3.96E-01	±	8.34E-03	7.34E-01	
		2.5	6.07E-03	±	3.37E-03	2.09E+00	±	5.81E-02	8.92E-01	
		10	1.12E-02	±	6.45E-03	8.30E+00	±	1.39E-01	9.22E-01	
	SiO ₂ Ag	0.5	4.81E-03	±	3.28E-03	2.58E-01	±	1.41E-02	7.32E-01	
		2.5	6.33E-03	±	3.47E-03	1.41E+00	±	7.01E-02	7.21E-01	
		10	3.14E-02	±	5.99E-03	5.98E+00	±	7.49E-02	8.43E-01	
	Unfilt	Ag	0.5	5.44E-03	±	1.44E-03	3.70E-01	±	5.42E-03	8.53E-01
			2.5	4.90E-03	±	6.42E-04	1.93E+00	±	9.98E-03	9.03E-01
			10	8.14E-03	±	2.31E-03	8.20E+00	±	1.52E-01	8.29E-01
		C ₆₀	5	1.14E-01	±	1.23E-02	1.27E+00	±	1.11E-02	5.63E-02
			25	1.54E-01	±	1.08E-02	1.38E+01	±	2.96E-02	5.67E-03
			100	1.11E-01	±	7.46E-03	3.59E+01	±	2.17E-01	2.73E-03
		CeO ₂	0.5	4.46E-03	±	1.26E-03	3.94E-01	±	9.14E-03	8.10E-01
			2.5	3.59E-03	±	1.21E-03	2.03E+00	±	4.55E-02	8.56E-01
			10	4.70E-03	±	1.05E-03	8.29E+00	±	1.15E-01	8.56E-01
		SiO ₂ Ag	0.5	4.13E-03	±	6.01E-04	2.86E-01	±	5.92E-03	6.38E-01
			2.5	3.69E-03	±	9.20E-04	1.54E+00	±	2.50E-02	8.27E-01
			10	1.14E-02	±	1.38E-02	5.56E+00	±	1.09E-01	9.72E-01

			Vs (m d-1)	Std.Error Vs (m d-1)	C0 (mg L- 1)	Std.Error C0 (mg L- 1)	C ₁₅ /C ₀
IJ	Filt	Ag	0.5	-2.16E-03 ± 1.27E-02	1.85E-01 ± 1.77E-02		
			2.5	7.60E-04 ± 2.43E-03	1.31E+00 ± 7.61E-02		
			10	7.60E-05 ^a ± 1.34E-04	7.01E+00 ± 2.40E-01		9.44E-01
		C60	5	1.35E-01 ± 1.83E-02	2.61E+00 ± 1.73E-02		9.47E-03
			25	1.05E-01 ± 8.79E-03	5.58E+00 ± 4.97E-02		1.16E-02
			100	1.18E-01 ± 7.91E-03	3.92E+01 ± 1.99E-01		5.83E-03
		CeO2	0.5	2.75E-03 ± 1.52E-03	2.41E-01 ± 1.83E-02		5.88E-01
			2.5	3.33E-03 ± 8.54E-04	1.81E+00 ± 1.27E-01		2.60E-01
			10	1.29E-02 ± 2.58E-03	8.63E+00 ± 6.85E-01		1.21E-04
	Unfilt	SiO2Ag	0.5	5.54E-02 ± 2.00E-02	2.31E-01 ± 4.61E-03		8.17E-01
			2.5	2.71E-03 ± 2.74E-03	9.25E-01 ± 7.22E-02		
			10	5.15E-02 ± 1.35E-02	6.13E+00 ± 1.49E-01		7.12E-01
		Ag	0.5	2.84E-03 ± 2.98E-03	1.89E-01 ± 2.74E-02		5.24E-01
			2.5	8.66E-04 ^a ± 1.41E-04	1.30E+00 ± 4.34E-02		6.26E-01
			10	1.08E-04 ^a ± 8.77E-05	7.23E+00 ± 1.77E-01		9.14E-01
		C60	5	8.34E-02 ± 5.87E-03	9.38E-01 ± 1.12E-02		1.90E-02
			25	7.56E-02 ± 7.76E-03	2.94E+00 ± 6.13E-02		8.28E-03
			100	8.75E-02 ± 4.38E-03	3.05E+01 ± 2.41E-01		1.88E-03
		CeO2	0.5	7.18E-03 ± 2.06E-03	4.17E-01 ± 3.50E-02		2.54E-01
			2.5	6.49E-03 ± 1.31E-03	1.83E+00 ± 1.23E-01		1.35E-01
			10	1.15E-02 ± 2.07E-03	8.72E+00 ± 6.08E-01		7.14E-03
		SiO2Ag	0.5	4.32E-03 ± 6.97E-04	2.63E-01 ± 6.85E-03		5.73E-01
			2.5	1.58E-02 ± 4.59E-03	1.37E+00 ± 5.14E-02		7.00E-01
			10	8.78E-03 ± 1.59E-03	6.13E+00 ± 1.70E-01		5.81E-01

		V_s (m d ⁻¹)		Std.Error V_s (m d ⁻¹)	C_0 (mg L ⁻¹)		Std.Error C_0 (mg L ⁻¹)	C_{15}/C_0
KG	Filt	Ag	0.5	4.08E-03	± 9.71E-04	3.10E-01	± 7.18E-03	7.52E-01
			2.5	1.13E-02	± 5.37E-03	1.83E+00	± 4.00E-02	8.88E-01
			10	1.37E-04 ^a	± 6.99E-05	7.72E+00	± 1.41E-01	9.22E-01
		C ₆₀	5	1.80E-01	± 3.37E-02	3.20E+00	± 8.87E-03	1.20E-02
			25	1.13E-01	± 8.62E-03	1.01E+01	± 6.75E-02	4.46E-03
			100	1.13E-01	± 7.78E-03	3.34E+01	± 2.01E-01	4.70E-03
	CeO ₂	0.5	4.04E-03	± 2.45E-03	3.67E-01	± 7.87E-03	8.95E-01	
		2.5	7.30E-05 ^a	± 1.00E-04	1.85E+00	± 4.75E-02	9.22E-01	
		10	9.04E-03	± 5.44E-03	7.85E+00	± 1.82E-01	9.00E-01	
	SiO ₂ Ag	0.5	1.03E-02	± 9.31E-03	3.09E-01	± 7.64E-03	9.22E-01	
		2.5	5.66E-05 ^a	± 7.86E-05	1.52E+00	± 3.08E-02	9.65E-01	
		10	7.52E-05 ^a	± 9.42E-05	5.85E+00	± 1.41E-01	9.37E-01	
	Unfilt	Ag	0.5	5.87E-03	± 1.86E-03	3.37E-01	± 2.37E-02	4.62E-01
			2.5	6.38E-03	± 2.60E-03	1.67E+00	± 5.65E-02	8.09E-01
			10	1.61E-04 ^a	± 9.12E-05	7.45E+00	± 1.77E-01	9.10E-01
		C ₆₀	5	1.08E-01	± 9.42E-03	8.47E-01	± 7.00E-03	4.79E-02
			25	7.49E-02	± 4.12E-03	3.47E+00	± 3.90E-02	1.36E-02
			100	1.08E-01	± 8.65E-03	3.66E+01	± 2.84E-01	1.82E-03
		CeO ₂	0.5	3.06E-03	± 1.12E-03	3.79E-01	± 1.45E-02	7.44E-01
			2.5	3.05E-03	± 9.11E-04	1.99E+00	± 5.79E-02	7.44E-01
			10	4.66E-03	± 9.86E-04	7.81E+00	± 8.95E-02	8.69E-01
		SiO ₂ Ag	0.5	2.98E-03	± 1.44E-03	3.01E-01	± 2.86E-03	9.52E-01
			2.5	2.20E-03	± 1.69E-03	1.54E+00	± 2.38E-02	9.45E-01
			10	1.18E-02	± 4.76E-03	6.12E+00	± 5.78E-02	9.41E-01

		V_s (m d ⁻¹)	Std.Error V_s (m d ⁻¹)	C_0 (mg L ⁻¹)	Std.Error C_0 (mg L ⁻¹)	C_{15}/C_0
MS	Filt	Ag	0.5	2.31E-02 ± 2.83E-02	9.74E-02 ± 2.37E-02	5.50E-01
			2.5	7.63E-03 ± 3.60E-03	1.11E+00 ± 1.37E-01	3.27E-01
			10	1.01E-02 ± 8.06E-03	6.59E+00 ± 4.08E-01	7.92E-01
		C ₆₀	5	6.61E-02 ± 8.34E-03	3.62E-01 ± 1.06E-02	6.22E-02
			25	1.01E-01 ± 9.05E-03	4.38E+00 ± 4.52E-02	9.61E-03
			100	1.26E-01 ± 7.74E-03	4.38E+01 ± 1.72E-01	1.10E-03
		CeO ₂	0.5	1.18E-02 ± 7.07E-03	3.41E-01 ± 6.00E-02	2.83E-01
			2.5	9.72E-03 ± 2.99E-03	1.89E+00 ± 2.19E-01	1.30E-02
			10	3.94E-02 ± 8.28E-05	7.94E+00 ± 6.43E-03	6.80E-04
	SiO ₂ Ag	0.5	3.33E-03 ± 1.64E-03	1.26E-01 ± 2.30E-02	5.11E-01	
		2.5	1.01E-02 ± 3.01E-03	6.87E-01 ± 5.99E-02	2.57E-01	
		10	1.04E-02 ± 2.85E-03	4.58E+00 ± 4.56E-01	5.62E-02	
	Unfilt	Ag	0.5	NA	NA	NA
			2.5	5.63E-03 ± 3.64E-03	1.05E+00 ± 1.52E-01	4.20E-01
			10	1.01E-02 ± 7.97E-03	6.55E+00 ± 2.89E-01	8.29E-01
		C ₆₀	5	1.30E-01 ± 9.19E-03	2.63E+00 ± 1.07E-02	6.88E-03
			25	1.36E-01 ± 4.38E-03	1.28E+01 ± 2.02E-02	2.29E-03
			100	7.39E-02 ± 5.39E-04	4.08E+01 ± 6.30E-02	9.31E-04
		CeO ₂	0.5	9.43E-03 ± 4.11E-03	2.72E-01 ± 4.24E-02	6.09E-02
			2.5	1.85E-02 ± 1.83E-03	1.87E+00 ± 7.77E-02	6.75E-03
			10	5.52E-02 ± 2.71E-03	7.98E+00 ± 1.19E-01	4.97E-04
		SiO ₂ Ag	0.5	1.31E-02 ± 6.82E-03	2.02E-01 ± 2.54E-02	4.07E-01
			2.5	1.04E-02 ± 4.37E-03	8.53E-01 ± 9.84E-02	3.11E-01
			10	9.22E-03 ± 1.69E-03	3.56E+00 ± 2.29E-01	8.14E-02

		V_s (m d ⁻¹)		Std.Error V_s (m d ⁻¹)	C_0 (mg L ⁻¹)		Std.Error C_0 (mg L ⁻¹)	C_{15}/C_0		
NZ	Filt	Ag	0.5	3.53E-03	±	1.39E-03	3.64E-01	±	9.98E-03	7.90E-01
			2.5	1.19E-02	±	1.49E-02	1.79E+00	±	1.03E-01	8.97E-01
			10	-1.71E-03	±	4.51E-03	5.52E+00	±	5.62E-01	
		C_{60}	5	1.22E-01	±	9.45E-03	5.84E-01	±	2.90E-03	7.33E-02
			25	1.28E-01	±	2.06E-03	2.25E+01	±	2.17E-02	2.75E-03
			100	1.33E-01	±	4.59E-03	6.08E+01	±	1.12E-01	1.75E-03
		CeO_2	0.5	1.88E-02	±	1.50E-03	2.90E-01	±	9.22E-03	6.38E-02
			2.5	1.58E-02	±	1.50E-03	1.93E+00	±	7.53E-02	3.36E-03
			10	4.01E-02	±	1.50E-04	8.70E+00	±	1.25E-02	9.04E-04
	SiO_2Ag	0.5	5.70E-03	±	8.37E-04	2.97E-01	±	3.88E-03	7.65E-01	
		2.5	7.70E-03	±	1.83E-03	1.50E+00	±	9.78E-02	2.75E-01	
		10	1.53E-02	±	5.01E-03	6.18E+00	±	7.46E-01	1.06E-01	
	Unfilt	Ag	0.5	4.32E-03	±	6.67E-04	3.57E-01	±	8.24E-03	6.17E-01
			2.5	6.08E-03	±	1.24E-03	1.52E+00	±	7.75E-02	3.24E-01
			10	8.93E-05	±	2.13E-03	6.56E+00	±	3.51E-01	9.26E-01
		C_{60}	5	4.20E-02	±	3.21E-03	2.61E+00	±	7.38E-02	8.78E-03
			25	3.98E-02	±	3.66E-03	1.05E+01	±	3.69E-01	2.80E-03
			100	1.26E-01	±	4.17E-03	6.16E+01	±	1.30E-01	9.85E-04
		CeO_2	0.5	7.92E-03	±	1.45E-03	2.21E-01	±	1.47E-02	4.27E-02
			2.5	1.51E-02	±	2.27E-03	1.57E+00	±	9.60E-02	4.83E-03
			10	4.63E-02	±	8.32E-03	8.03E+00	±	5.06E-01	7.48E-04
	SiO_2Ag	0.5	6.44E-03	±	5.94E-04	2.33E-01	±	2.44E-03	7.02E-01	
		2.5	6.52E-03	±	1.11E-03	1.37E+00	±	5.35E-02	3.98E-01	
		10	1.11E-02	±	1.86E-03	5.69E+00	±	3.29E-01	1.12E-01	

		V_s (m d ⁻¹)		Std.Error V_s (m d ⁻¹)	C_0 (mg L ⁻¹)		Std.Error C_0 (mg L ⁻¹)	C_{15}/C_0
RL	Filt	Ag	0.5	2.64E-03	± 1.60E-03	1.27E-01	± 1.88E-02	4.14E-01
			2.5	3.31E-03	± 9.51E-04	1.03E+00	± 6.79E-02	4.06E-01
			10	3.04E-03	± 1.44E-03	7.10E+00	± 3.66E-01	6.57E-01
		C_{60}	5	1.54E-01	± 4.91E-02	8.66E-01	± 7.94E-03	3.52E-02
			25	1.35E-01	± 1.13E-02	8.41E+00	± 3.51E-02	5.24E-03
			100	1.23E-01	± 7.00E-03	3.18E+01	± 1.23E-01	3.10E-03
		CeO_2	0.5	2.40E-03	± 1.21E-03	2.71E-01	± 2.25E-02	5.86E-01
			2.5	3.25E-03	± 1.75E-03	1.28E+00	± 2.39E-01	8.78E-02
			10	3.72E-02	± 9.76E-04	7.23E+00	± 7.51E-02	4.24E-04
	SiO_2Ag	0.5	4.12E-03	± 7.30E-04	1.96E-01	± 9.85E-03	2.53E-01	
		2.5	5.35E-03	± 5.37E-04	1.25E+00	± 2.96E-02	3.93E-01	
		10	5.66E-03	± 4.45E-04	5.92E+00	± 1.22E-01	3.19E-01	
	Unfilt	Ag	0.5	1.08E-02	± 1.85E-03	1.64E-01	± 7.81E-03	2.88E-01
			2.5	4.85E-03	± 5.62E-04	1.20E+00	± 3.52E-02	3.39E-01
			10	1.99E-03	± 1.68E-03	6.79E+00	± 3.35E-01	7.68E-01
		C_{60}	5	9.69E-02 ^a	± 2.21E-02	1.34E+00	± 3.92E-02	4.54E-02
			25	1.09E-01	± 8.06E-03	5.51E+00	± 3.93E-02	3.66E-03
			100	1.26E-01	± 7.76E-03	3.94E+01	± 1.54E-01	1.03E-03
		CeO_2	0.5	2.23E-02	± 7.48E-03	3.32E-01	± 4.46E-02	7.41E-02
			2.5	7.79E-03	± 8.83E-04	1.74E+00	± 7.34E-02	2.07E-02
			10	4.39E-02	± 1.63E-03	6.11E+00	± 8.21E-02	8.35E-04
	SiO_2Ag	0.5	6.39E-03	± 4.23E-04	2.45E-01	± 4.87E-03	2.09E-01	
		2.5	7.41E-03	± 7.35E-04	1.34E+00	± 3.62E-02	2.75E-01	
		10	6.25E-03	± 4.24E-04	6.01E+00	± 1.19E-01	2.36E-01	

a: C_{n5} assumed 0 in order to estimate V_s .

Appendix E

E: Estimating the attachment efficiency for heteroaggregation of nanoparticles and natural colloids from sedimentation experiments

This Appendix describes the method to estimate attachment efficiencies for heteroaggregation (α_{het}) from sedimentation experiments. First, an introductory outline of the approach is given. Then, the different steps in the calculation of α_{het} are described in terms of fundamental as well as simplified equations for aggregation-sedimentation. Finally, it is shown how the model equations can be used to fit values for α_{het} from the data. This final section also presents a validation of the simplified model approach by comparing its results against predictions of an aggregation-sedimentation model without simplifications.

E.1.1 Principle

ENM sedimentation experiments were performed for filtered (no NCs) and unfiltered natural water samples. In the unfiltered experimental systems, removal of the engineered nanomaterials (ENMs) from the water column can be assumed to be driven by (ENM-ENM) homoaggregation, (ENM-NC) heteroaggregation and/or settling of ENM aggregates.^{46, 135, 153} To determine the attachment efficiency for heteroaggregation, the process parameters for heteroaggregation need to be isolated from those for homoaggregation and sedimentation. This is done as follows. First, it is assumed that aggregation is the rate limiting process for the observed removal of ENMs from the water phase. This is based on the reasonable assumption that aggregates first need to be large enough for sedimentation to occur.³⁵ If aggregation is the rate determining process, the observed removal rates will depend on the parameters describing homo- and heteroaggregation and not on parameters describing sedimentation. Second, the process parameters for homoaggregation are estimated by fitting a homoaggregation-only process equation to the data for the sedimentation experiments with filtered water samples. This assumes that heteroaggregation does not occur in water samples where NCs are removed by filtration. Finally, a process equation accounting for homo- and heteroaggregation is

fitted to the data for the sedimentation experiments in unfiltered water samples, using the parameters for homoaggregation from the previous step. This leaves the process parameters for heteroaggregation as the only unknowns, from which relative attachment efficiencies for heteroaggregation can be calculated. The process equations and assumptions required in the different steps are discussed in the next section.

E.1.2 Model equations

The basics for the calculation of the contributions of homoaggregation and heteroaggregation to the removal of ENMs from the water phase are condensed in the combined Von Smoluchowski –Stokes equation:²⁴

$$\frac{dN_C}{dt} = \frac{1}{2} \sum_{i=1}^{j-1} \alpha_{i,j-i} K_{i,j-i} N_i N_{j-i} - N_j \sum_{i=1}^{j-1} \alpha_{i,j} K_{i,j} N_i - \alpha_{NC,j} K_{NC,j} N_{NC} N_j - \frac{v_{s,j}}{d_s} N_j \quad (\text{Eq. E.1})$$

With:

$\alpha_{i,j}$: attachment efficiency between ENM aggregates i and j

$\alpha_{NC,j}$: attachment efficiency between ENM and NCs

j: number of primary nPs in ENM aggregate

$K_{i,j}$: Collision frequency between ENM aggregates i and j [$\text{m}^3 \text{s}^{-1}$]

$K_{NC,j}$: Collision frequency between ENM particle aggregates j and NCs [$\text{m}^3 \text{s}^{-1}$]

N_j : Number concentration of the ENM aggregate j [m^{-3}]

N_{NC} : Number concentration of NCs [m^{-3}]

$v_{s,j}$: Sedimentation rate of ENM aggregate j [m s^{-1}]

d_s : Sedimentation length [m]

and where the first two terms accounts for homoaggregation, the third term for heteroaggregation, and the last term for sedimentation of ENM aggregates.

The concentration of natural colloids N_{NC} is assumed to decrease due to Stokes settling;^{40, 153}

$$\frac{dN_{NC}}{dt} = - \frac{v_{s,NC}}{d_s} N_{NC} \quad (\text{Eq. E.2})$$

Below, Eq E.1 is simplified based on a series of informed assumptions, which subsequently are validated against simulations using the full deterministic Eq E.1. First it is assumed that aggregation is the rate limiting process for the observed removal of ENMs from the water phase. This is based on the concept that aggregates first need to be large enough for sedimentation to occur.³⁵ This means that the aggregation terms in Eq E.1 are considered to be rate determining and that the last term in Eq E.1 can be omitted. Second, it is assumed that the summations in Eq E.1 can

be replaced by single terms accounting for the *apparent critical* collision behavior for sedimentation. This is motivated as follows. The summation in Eq. 1 accounts for numerous collisions that will not (yet) lead to homo- or heteroaggregates large enough to settle. However, a certain fraction of all possible collisions will at some point reach a critical limit after which rapid settling occurs. The measured removal in the sedimentation experiments relate to this apparent removal of settleable ENMs only ($C_{ENM,crit}$). Because size distributions of these settling ENM aggregates will probably not be monodisperse, the single terms are governed by apparent parameters reflecting average properties of the particles at the onset of settling. Third, it is assumed that the ENM concentration change in the overlying water is determined by aggregation to settling particles only i.e. is not affected by progressive aggregation to larger particles. Progressive aggregation cannot affect $C_{ENM,crit}$ concentrations beyond the critical size for sedimentation because they would have settled already. This implies that the first two terms for aggregation in Eq. E.1 can be combined. Consequently, Eq. E.1 can be simplified to:

$$\frac{dC_{ENM,crit}}{dt} = -\alpha_{hom,crit}K_{hom,crit}C_{ENM,crit}^q - \alpha_{het,crit}K_{het,crit}C_{NC}C_{ENM,crit} \quad (\text{Eq. E.3})$$

where

$C_{ENM,crit}$ is the concentration of settleable ENMs

$K_{hom,crit}$ is the apparent collision rate constant for the formation of settleable ENM homoaggregates

$\alpha_{hom,crit}$ is the apparent attachment efficiency for settleable ENM homoaggregates

$\alpha_{het,crit}$ is the apparent attachment efficiency for settleable ENM-NC heteroaggregates

$K_{het,crit}$ is the apparent collision rate constant for the formation of settleable ENM heteroaggregates

The exponent q defines the kinetics for homoaggregation and may take a value between 1 and 2. For instance, the formation of doublets would follow second order kinetics ($q = 2$), whereas the kinetics of collisions between large aggregates and primary particles would approach pseudo first order kinetics ($q=1$).

The best value for q was obtained by fitting the analytical solution to Eq. E.3 for q is 1, 1.5 and 2 respectively, against simulations based on Eq. E.1. The simulations used a numerical model which takes into account all size classes up to 350 nm CeO_2 ENM aggregates and all processes as condensed in equation E.1. The largest aggregate consists of 2629 primary particles with a fractal dimension of 2.5. The fit for removal due to homoaggregation only is given in Figure E.1. The simulation shows a time lag of

about 1 day needed for the formation of aggregates large enough for settling. From day 2 onwards the removal of ENMs from the water phase is best described by apparent first order removal kinetics, i.e. $q=1$. Simulations with $q=1.5$ and $q=2$ showed a worse overall quality of fit (Figure E.1). With $q=1$ and combination of Eq. E.2, Eq. E.3 can be further simplified to:

$$\frac{dC_{ENM}}{dt} = -\alpha_{hom,crit} K_{hom,crit} C_{ENM} - \alpha_{het,crit} K_{het,crit} C_{0,NC} e^{-\frac{v_{s,NC} t}{d}} C_{ENM} \quad \text{Eq. E.4}$$

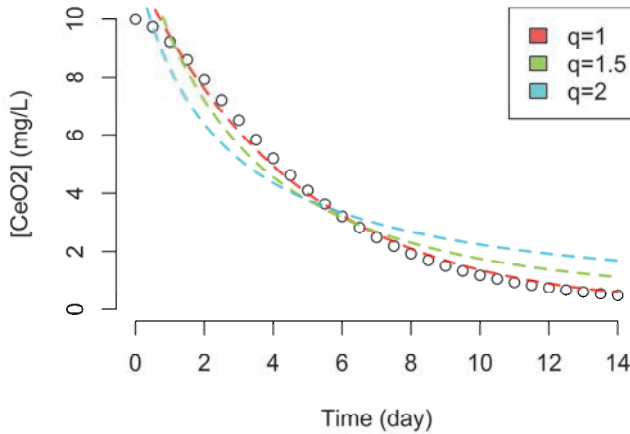


Figure E.1. Fit of the homoaggregation term in equation 3 for q is 1, 1.5 and 2, to model simulation data calculated from a mechanistic numerical model based on equation E.1 and E.2. Mechanistic model for 10 mg L^{-1} 15 nm CeO_2 ENMs.

In summary, Eq. E.4 describes how the concentration of the (operationally defined) settling ENM fraction changes over time, as a function of the processes that drive the production of aggregates. Aggregates that do not settle substantially in the time interval over which settling is monitored (15 days in the present experiments) are also formed. Furthermore, primary particles may be stabilised and not settle at all. The latter two categories of processes lead to a residual fraction, which is also operationally defined (Table 5.2).

E.1.3 Calculating the attachment efficiency

Eq E.4 can be fitted to ENM sedimentation data in order to estimate $\alpha_{het,crit}$. However, not only $\alpha_{het,crit}$ is unknown, also $\alpha_{hom,crit}K_{hom,crit}$ in Eq. E.4 is unknown. Therefore the contribution of homoaggregation to the removal of ENMs from the water phase is separately assessed by fitting the solution of the first term in equation 4 to the ENM concentration in time for filtered water (Eq. E.5).

$$C(t) = C_0 e^{-\alpha_{hom,crit} K_{hom,crit} t} \quad (\text{Eq. E.5})$$

This assumes that heteroaggregation in filtered water is negligible due to the absence of natural colloids. The estimated values for $\alpha_{hom,crit}K_{hom,crit}$ then are substituted in the solution of Eq. E.4, with $\alpha_{het,crit}K_{het,crit}$ as the only unknown. $V_{s,NC}$ is calculated according to Stokes from the density and radius of the NCs (Table 5.1). The analytical solution to Eq. E.4 is:

$$C(t) = \frac{C_0 e^{-\frac{\alpha_{hom,crit} K_{hom,crit} t V_{s,NC} + \alpha_{het,crit} K_{het,crit} d_s C_0 NC e^{-\frac{V_{s,NC} t}{d_s}}}}{e^{\frac{\alpha_{het,crit} K_{het,crit} C_0 NC d_s}{V_{s,NC}}}} \quad (\text{Eq. E.6})$$

which then can be fitted to the sedimentation data in unfiltered water to obtain $\alpha_{het,crit}K_{het,crit}$. $K_{het,crit}$ can be estimated using the known description of the three main processes affecting the collision frequency: brownian motion, shear rate and differential settling.^{24, 35} The sum of the quantitative description of these three processes result in the collision frequency given by Eq. E.7.

$$K_{het} = \frac{\frac{2k_b T (a_{NC} + a_j)^2}{3\mu} + \frac{4}{3}G (a_{NC} + a_j)^3 + \pi(a_{NC} + a_j)^2 |V_{s,NC} - V_{s,j}|}{\rho_{NC} V_{NC}} \quad (\text{Eq. E.7})$$

Where

k_b : Boltzman constant [$m^2 \text{ kg s}^{-2} \text{ K}^{-1}$]

T: Temperature [K]

μ : Viscosity [Pa s]

a_{NC} : NC radius [m]

a_j : ENM j radius [m]

G: Shear rate [s^{-1}]

v_s : Sedimentation rate [$m \text{ s}^{-1}$]

with v_s given by:

$$v_s = \frac{2a^2 (\rho_p - \rho_w)g}{9\mu} \quad (\text{Eq. E.8})$$

in which

ρ_p : Density of the ENM or NC [kg m^{-3}]

ρ_w : Density of suspending medium [kg m^{-3}]

g : Gravitational acceleration [m s^{-2}]

The density of the NCs is calculated based on the dry weight (DW) and ash free dry weight (AFDW), by assuming that AFDW consists of an organic NC fraction with low density (1250 kg m^{-3}) and a mineral fraction with relatively high density (2700 kg m^{-3}).¹⁵⁵

With $K_{\text{het,crit}}$ known (Eq E.7), absolute $\alpha_{\text{het,crit}}$ values can be calculated. To increase the realism of these $\alpha_{\text{het,crit}}$ values, we scale the absolute $\alpha_{\text{het,crit}}$ values to the values where aggregation is diffusion limited, e.g. 100% attachment efficiency ($\alpha_{\text{het,crit}}=1$). We assume this is the case in the water type showing the fastest aggregation/sedimentation. The resulting relative $\alpha_{\text{het,crit}}$ is scaled to the water type with the highest absolute $\alpha_{\text{het,crit}}$. Similar methods for calculating attachment efficiencies have been published by e.g. Chen and Elimelech¹⁸⁶ and Keller et al.⁶⁷.

The fitting of Eq. E.6 on sedimentation data can be done in two ways. One method is to use all data, which is to be preferred if the data for filtered and unfiltered systems differ sufficiently (i.e. difference is substantial and statistically significant). These differences will increase in time. Consequently, more accurate results may be obtained by giving higher weight to later time points, or by using the last time point only. An equation that calculates $\alpha_{\text{het,crit}}K_{\text{het,crit}}$ directly from C_0 and any known concentration in time ($C(t)$) is obtained by rearrangement of Eq. E.6:

$$\alpha_{\text{het,crit}}K_{\text{het,crit}} = \frac{v_{s,\text{NC}}(\alpha_{\text{hom,crit}}K_{\text{hom,crit}}t + \ln \frac{C_t}{C_0})}{d_s C_{0,\text{NC}} \left(e^{\frac{v_{s,t}}{d_s}} - 1 \right)} \quad (\text{Eq. E.9})$$

E.2. Validation

Table E.1. Results from fitting $\alpha_{hom}K'_{hom}$ and $\alpha_{het}K'_{het}$ to simulated sedimentation data and subsequent calculation of α_{het} .

C0 (mg L ⁻¹)	α_{het}	Method A (Fit)		Method B (calc C0, C14)	
		$\alpha_{het,crit}$	Deviation ^a (%)	$\alpha_{het,crit}$	Deviation _a (%)
0.01	0.01	0.010	4.61	0.010	0.15
	0.1	0.11	6.21	0.10	0.63
	0.5	0.52	3.99	0.51	1.58
	1	1	0	1	0
0.5	0.01	b	b	0.0078	21.71
	0.1	0.06	39.16	0.08	19.57
	0.5	0.46	8.71	0.45	10.22
	1	1	0	1	0
2.5	0.01	b	b	0.0072	27.70
	0.1	b	b	0.08	25.26
	0.5	0.39	22.89	0.43	14.14
	1	1	0	1	0
10	0.01	b	b	0.0054	45.56
	0.1	b	b	0.06	41.40
	0.5	0.08	83.15	0.39	22.97
	1	1	0	1	0

a: % deviation of the estimated $\alpha_{het,crit}$ value (Eqs. 5, 6) from Smoluchowski-Stokes simulation (Eq.1)

B: No estimate of $\alpha_{het,crit}$ possible, addition of $K_{het,crit}$ did not decrease relative residuals of fit with $K_{het,crit}$ greater than 0.

To validate the method for estimating α_{het} from sedimentation data, the method is applied to simulation results calculated with Eq. E.1 and E.2, thus taking homo- and heteroaggregation into account. The simulations used a numerical model which takes into account all size classes up to 350 nm CeO₂ ENM aggregates and processes as given by equation 1. The largest aggregate consisted of 2629 primary particles with a fractal dimension of 2.5. The primary CeO₂ particle size was 15 nm. The NCs had an average radius of 0.5 μ m, density of 1250 kg m⁻³, and 100 mg L⁻¹ initial concentration. Two series were simulated with 10 μ g L⁻¹, 0.5 mg L⁻¹, 2.5 mg L⁻¹ and 10 mg L⁻¹ monodisperse CeO₂ suspension with α_{het} set to 0, 0.01, 0.1, 0.5 and 1. The case where α_{het} is 0 was used to estimate $\alpha_{hom,crit}K_{hom,crit}$. Subsequently, $\alpha_{hom,crit}K_{hom,crit}$ and $\alpha_{het,crit}K_{het,crit}$ were back-calculated from the Eq.1 simulation results using the

simplified equations E.5 and E.6. . Alternatively, $\alpha_{\text{hom,crit}}K_{\text{hom,crit}}$ and $\alpha_{\text{het,crit}}K_{\text{het,crit}}$ were also calculated using data from the last time point and C0, using Eq. E.9.

Results of estimating $\alpha_{\text{het,crit}}$ are presented in Table E.1, for method A that used a fit of equation E.6 to all data, and method B that used the concentration at day 14 (C14) and the initial ENM concentration (C0) only. Both methods work best when the difference between settled ENMs is largest between cases where only homoaggregates are formed compared to homo- and heteroaggregates (Figure E.2). With increasing initial ENM concentration, the deviation from the α_{het} used in the simulation increases. The deviation in estimated $\alpha_{\text{het,crit}}$ is lower when based on using eq. E.9 and C14 and C0 only. This shows that although the information on $\alpha_{\text{het,crit}}$ can be derived from sedimentation data, the fit is not always precise enough to discern the small differences in the change of the concentration over time, between systems with and without heteroaggregation.

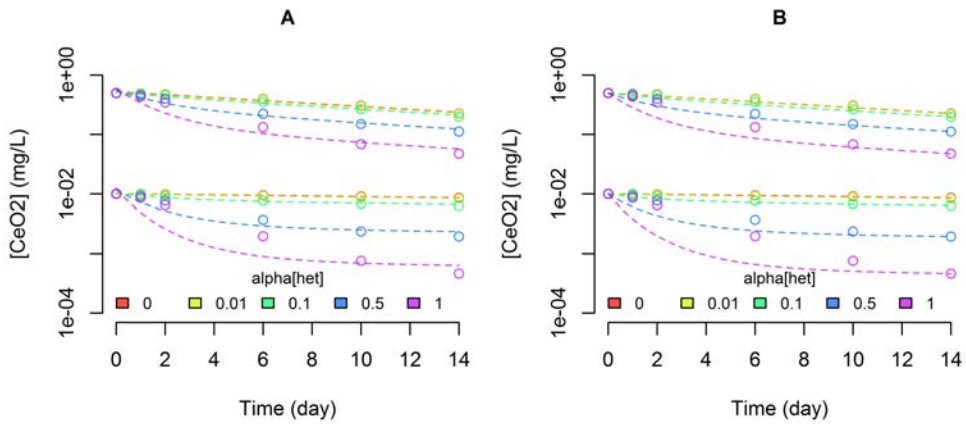


Figure E.2. Plot of fit of Eq. E.6 to simulated data (A) and direct calculation of $\alpha_{\text{hom,crit}}K_{\text{hom,crit}}$ and $\alpha_{\text{het,crit}}K_{\text{het,crit}}$ from C14 and C0 of simulated data (B). With simulated data of sedimentation of CeO2 ENMs by homo- and heteroaggregation with α_{het} ranging between 0 and 1.

Even though the proposed method gives an error for $\alpha_{\text{hetero,crit}}$ of up to 50% in some cases, the simulation uses an α_{hom} of 1 resulting in the small differences between removal due homo and heteroaggregation. In most surface waters α_{hom} will be lower than 1, e.g. due to presence of DOM, meaning heteroaggregation will play a greater role in removal of ENMs from the water phase compared to homoaggregation as shown here (Table E.1), and the resulting errors of estimating $\alpha_{\text{hetero,crit}}$ will be smaller.

Table E.2. Homo and heteroaggregation rates ($\alpha_{crit}K_{crit}$) obtained using equations E.5 and E.9 in 6 natural waters with 4 ENM types at the lowest initial particle concentration. Estimate of K_{het} using equation E.7 and the absolute and relative attachment efficiencies (α_{crit}).

		KG	AA	RL	IJ	MS	NZ
C_{60}	$\alpha_{hom,crit}K_{hom,crit}$	9.09E-01	7.99E-01	8.37E-01	9.25E-01	7.99E-01	7.88E-01
	$\alpha_{het,crit}K_{het,crit}$	-1.98E+01	6.82E-01	-1.78E+00	-4.23E+00	1.49E+01	6.00E+01
	K_{het}	5720	6717	5150	15236	4293	3991
	$\alpha_{het,crit}K_{het,crit}/K_{het}$	-3.45E-03	1.02E-04	-3.46E-04	-2.77E-04	3.48E-03	1.50E-02
	$\alpha_{het,crit}$	-2.30E-01	6.75E-03	-2.30E-02	-1.84E-02	2.31E-01	1.00E+00
CeO_2	$\alpha_{hom,crit}K_{hom,crit}$	6.21E-01	6.35E-01	6.50E-01	6.49E-01	6.98E-01	7.98E-01
	$\alpha_{het,crit}K_{het,crit}$	2.63E+00	-6.28E-01	1.45E+01	5.12E+00	1.04E+01	1.14E+01
	K_{het}	6332	7353	5640	16417	4725	4410
	$\alpha_{het,crit}K_{het,crit}/K_{het}$	4.16E-04	-8.54E-05	2.57E-03	3.12E-04	2.20E-03	2.58E-03
	$\alpha_{het,crit}$	1.61E-01	-3.31E-02	9.96E-01	1.21E-01	8.54E-01	1.00E+00
SiO_2	$\alpha_{hom,crit}K_{hom,crit}$	6.19E-01	6.35E-01	7.06E-01	6.28E-01	6.59E-01	6.32E-01
	$\alpha_{het,crit}K_{het,crit}$	-4.61E-01	8.74E-01	1.34E+00	2.16E+00	1.54E+00	2.40E+00
	K_{het}	7758	8865	6805	19336	5742	5392
	$\alpha_{het,crit}K_{het,crit}/K_{het}$	-5.94E-05	9.86E-05	1.97E-04	1.12E-04	2.68E-04	4.44E-04
	$\alpha_{het,crit}$	-1.34E-01	2.22E-01	4.44E-01	2.52E-01	6.03E-01	1.00E+00
PVP-Ag	$\alpha_{hom,crit}K_{hom,crit}$	6.33E-01	6.38E-01	6.73E-01	6.30E-01	6.54E-01	6.30E-01
	$\alpha_{het,crit}K_{het,crit}$	6.96E+00	-1.31E+00	2.54E+00	2.47E+00	5.01E+00	6.98E+00
	K_{het}	9667	10910	8379	23369	7110	6708
	$\alpha_{het,crit}K_{het,crit}/K_{het}$	7.20E-04	-1.20E-04	3.04E-04	1.06E-04	7.05E-04	1.04E-03
	$\alpha_{het,crit}$	6.92E-01	-1.16E-01	2.92E-01	1.02E-01	6.78E-01	1.00E+00

$\alpha_{hom,crit}K_{hom,crit}$ in [day^{-1}] $\alpha_{het,crit}K_{het,crit}$ in [$m^3 kg^{-1} day^{-1}$] $K_{het,crit}$ [$m^3 kg^{-1} day^{-1}$]

Appendix F

F: Supporting information to Chapter 6: Rapid settling of nanoparticles due to heteroaggregation with suspended sediment

Table F.1. Characteristics of the natural waters and sediment used in this study

	RL	MS	NZ
pH	7.9	7.9	7.8
EC ($\mu\text{S cm}^{-1}$)	584	7200	47000
particulate matter (mg L^{-1})	10.3	11.9	2.7
O ₂ (mg L^{-1})	9.3	7.9	8.4
T (Celsius)	16.9	16.4	17.3
Salinity (‰)	n.m. ^a	4.4	34
Cl (mg L^{-1}) ^b	126	3970	28600
NO ₃ +NO ₂ (mg N L^{-1}) ^c	2.75	2.44	0.19
PO ₄ ($\mu\text{g P L}^{-1}$) ^c	36	103	344
NH ₃ (mg N L^{-1}) ^c	0.03	0.07	0.11
Total P (mg P L^{-1}) ^c	0.04	0.12	0.12
Total N (mg N L^{-1}) ^c	1.68	1.72	0.06
Ca (mg L^{-1}) ^d	56	104	401
K (mg L^{-1}) ^d	4.4	50	371
Mg (mg L^{-1}) ^d	10.6	160	1233
Na (mg L^{-1}) ^d	46	1370	10630
DIC (mg C L^{-1}) ^e	24.6	31.2	40.9
DOC (mg C L^{-1}) ^e	2.45	2.85	0.17
DW (mg L^{-1}) ^f	10.3	11.9	2.7
AFDW (mg L^{-1}) ^g	2.4	3.6	1.3
Sediment (mg L^{-1})	3409.6 \pm 29.4	3317.5 \pm 138.1	3451.4 \pm 97.0

^a not measured

^b determined with ion selective electrode (Orion 94-17, Thermo Electron Corporation)

^c determined with continuous flow analyser (CFA, Skalar Analytical BV)

^d determined with radial ICP-AES (Vista PRO, Varian Inc)

^e determined with total organic carbon (TOC) analyser (Model 700, O.I.C. International BV)

^f determined using a 0.3 μm quartz filter (Sartorius Quartz-Microfibre Discs T293) and dried in a stove (Heraeus, type T6060) at 105°C for 2 h

^g DW filters determined in a muffle furnace (Heraeus electronic, type MR 170E) at 520°C for 3 h

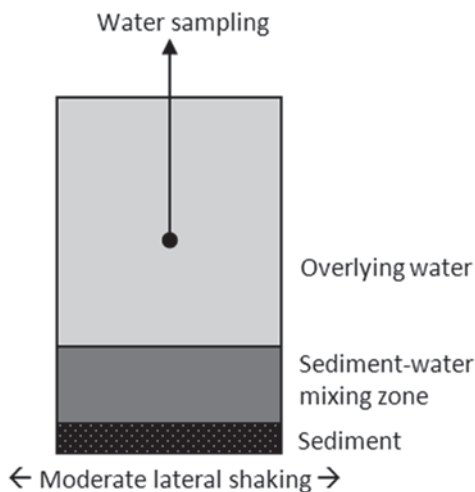


Figure F.1. Schematic representation of the experimental set-up

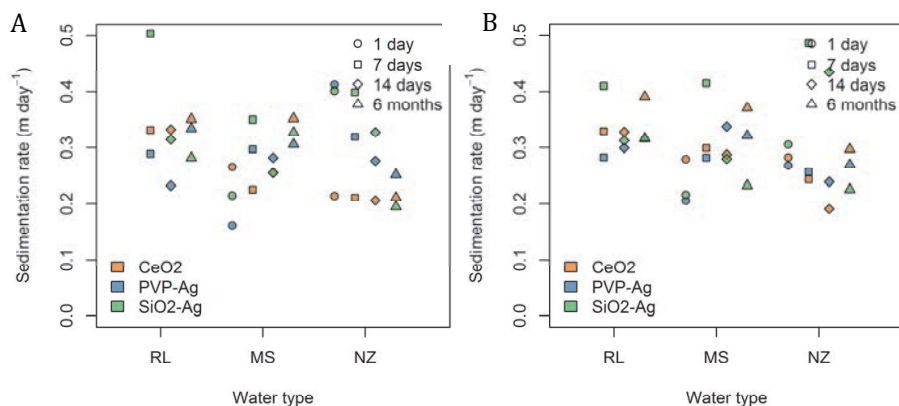


Figure F.2. Sedimentation rates for 3 ENMs at A: 2.5 mg L^{-1} and B: 10 mg L^{-1} suspension concentration in 3 water types in presence of suspended sediment observed after 1, 7, 14, and 6 months of incubation.

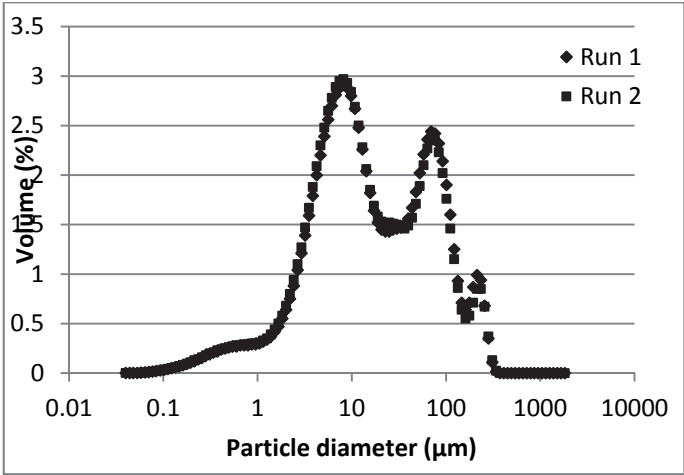


Figure F.3. Particle size distribution of Ketelmeer sediment, measured by laser diffraction.

F.1 Method for measuring sediment particle size

Wet sediment from lake Ketelmeer was characterized for particle size distribution (PSD) with Beckman Coulter LS 230 laser diffraction particle size analyser with Polarization Intensity Differential of Scattered Light (PIDS). The Fraunhofer theory of light scattering was used to determine the PSD. Sediment samples were brought into suspension in demineralized water and well homogenized prior to particle size analysis. The injected suspension volume was controlled to obtain a total obscuration level of $10 \pm 3\%$ and a PIDS obscuration of $50 \pm 10\%$.

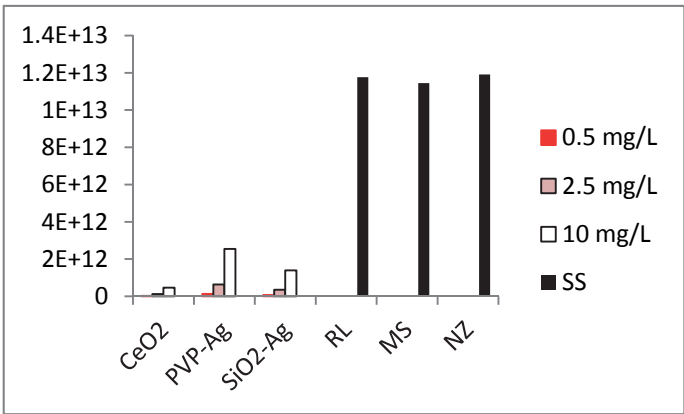


Figure F.4. Particle number concentration of the ENMs and the SS in the systems

Table F.2. Zetapotential measured after 1, 7 and 14 days of incubation.

ENM	water	C _{added} (mg L ⁻¹)	Zetapotential (mV)		
			day 1	day 7	day 14
CeO ₂	RL	0.5	n.m. ^a	-18.8	-16.7
		2.5	n.m.	-18.8	-17.2
		10	n.m.	-19.6	-17.0
	MS	0.5	n.m.	-11.0	-13.9
		2.5	n.m.	-11.7	-13.5
		10	n.m.	-13.2	-14.1
	NZ	0.5	-10.6	-8.3	-7.7
		2.5	-5.9	-7.1	-8.7
		10	-10.3	-8.0	-9.0
PVP-Ag	RL	0.5	n.m.	-20.0	-17.3
		2.5	n.m.	-18.7	-16.5
		10	n.m.	-18.7	-17.7
	MS	0.5	n.m.	-11.9	-13.9
		2.5	n.m.	-11.9	-12.7
		10	n.m.	-12.0	-14.1
	NZ	0.5	-8.7	-7.8	-8.1
		2.5	-5.1	-7.9	-8.6
		10	-8.2	-5.6	-7.7
SiO ₂ -Ag	RL	0.5	n.m.	-19.5	-16.2
		2.5	n.m.	-18.5	-17.5
		10	n.m.	-18.2	-17.4
	MS	0.5	n.m.	-12.8	-13.9
		2.5	n.m.	-12.0	-13.2
		10	n.m.	-12.5	-13.9
	NZ	0.5	-9.3	-6.2	-9.7
		2.5	-6.6	-10.7	-8.4
		10	-8.8	-15.0	-7.4

^a not measured

Table F.3. Average particles size measured in overlying water with NTA.

ENM	Average particles size (nm)								
	RL			MS			NZ		
blank	405	±	31	429	±	42	423	±	94
CeO ₂	437	±	71	453	±	116	508	±	115
PVP-Ag	391	±	58	432	±	33	504	±	98
SiO ₂ -Ag	426	±	60	453	±	68	551	±	197
average	418			446			521		

F.2 Model validation of method for estimating the heteroaggregation attachment efficiency

To validate the method for estimating α_{het} from sedimentation data, the method is applied to simulation results calculated with Eq. E.1 and E.2, thus taking homo- and heteroaggregation into account. The simulations used a numerical model which takes into account all size classes up to 350 nm CeO₂ ENM aggregates and processes as given by Eq. E.1. The largest aggregate consisted of 2629 primary particles with a fractal dimension of 2.5. The primary CeO₂ particle size was 15 nm. The suspended sediment (SS) had an average radius of 1 μm , density of 2000 kg m⁻³, and 3500 mg L⁻¹ initial concentration. Two series with $\alpha_{\text{hom}}=1$ (A) and $\alpha_{\text{hom}}=0$ (B) were simulated with 2.5 mg L⁻¹ monodisperse CeO₂ suspension with α_{het} set to 0, 0.01, 0.05, 0.1, 0.5, 0.9 and 1. The case where α_{het} is 0 was used to estimate $\alpha_{\text{hom,crit}}K_{\text{hom,crit}}$. Subsequently, $\alpha_{\text{hom,crit}}K_{\text{hom,crit}}$ and $\alpha_{\text{het,crit}}K_{\text{het,crit}}$ were back-calculated from the Eq. E.1 simulation results using data from the last time point and C0, in Eq. E.9.

Table F.4. Results from fitting $\alpha_{\text{hom}}K'_{\text{hom}}$ and $\alpha_{\text{het}}K'_{\text{het}}$ to simulated sedimentation data and subsequent calculation of α_{het} .

C0 (mg L ⁻¹)	α_{het}	$\alpha_{\text{hom}} = 1$		$\alpha_{\text{hom}} = 0$	
		$\alpha_{\text{het,crit}}$	Deviation ^{a)} (%)	$\alpha_{\text{het,crit}}$	Deviation ^{a)} (%)
0.01	0.01	0.006772	32.28273	0.01	2.14E-06
	0.05	0.034474	31.05203	0.05	2.11E-06
	0.1	0.070497	29.5031	0.1	2.11E-06
	0.5	0.416368	16.72634	0.5	1.70E-06
	0.9	0.869445	3.395031	0.9	5.29E-07
	1	1	0	1	0

a: % deviation of the estimated $\alpha_{\text{het,crit}}$ value (Eqs. E.5, E.6) from Smoluchowski-Stokes simulation (Eq. E.1)

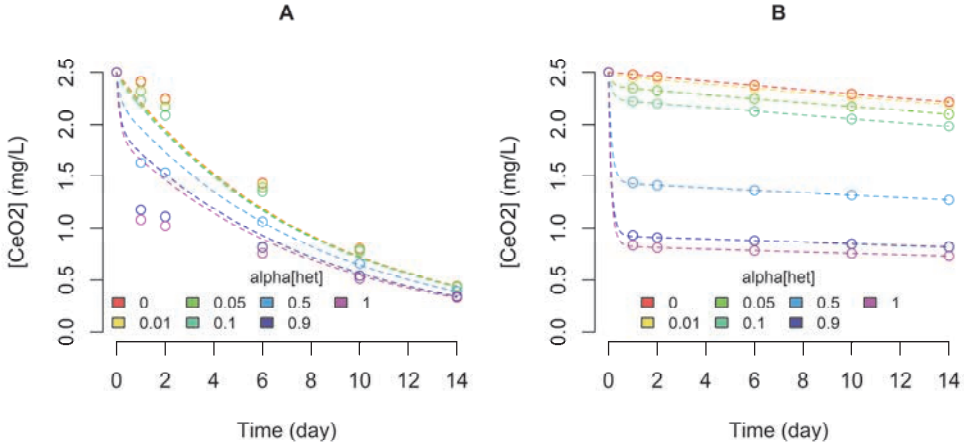


Figure F.5. Plot of direct calculation of $\alpha_{hom,crit}K_{hom,crit}$ and $\alpha_{het,crit}K_{het,crit}$ from C_{14} and C_0 of simulated data with $\alpha_{hom} = 1$ (A) and $\alpha_{hom} = 0$ (B). With simulated data of sedimentation of CeO₂ ENMs by homo (A) – and/or heteroaggregation with α_{het} ranging between 0 and 1.

Results of estimating $\alpha_{het,crit}$ are presented in Table F4 and Figure F5. Table F4 showed much smaller deviations when $\alpha_{hom} = 0$ and also Figure E.2 showed the best fit when $\alpha_{hom} = 0$. With this validation can be concluded that the model is more accurate when α_{hom} is low.

Literature cited

1. Feynman, R., There's plenty of room at the bottom. *Engineering and Science magazine* **1960**, 23, (5), 22-36.
2. Toumey, C., Plenty of room, plenty of history. *Nat Nano* **2009**, 4, (12), 783-784.
3. Woodrow Wilson International Centre for Scholars, The project on Emerging Nanotechnologies. Consumer Products Inventory of Nanotechnology Products. <http://www.nanotechproject.org/inventories/consumer> (5-12-2012)
4. Wijnhoven, S. W. P.; Dekkers, S.; Kooi, M.; Jongeneel, W. P.; Jong, W. H. d., *Nanomaterials in consumer products. Update of products on the European market in 2010*; National Institute for Public Health and the Environment: 2010.
5. Reed, M. A., Quantum Dots. *Sci. Am.* **1993**, 268, (1), 118-123.
6. Pal, T.; Sau, T. K.; Jana, N. R., Reversible Formation and Dissolution of Silver Nanoparticles in Aqueous Surfactant Media. *Langmuir* **1997**, 13, (6), 1481-1485.
7. Ebbesen, T. W.; Lezec, H. J.; Hiura, H.; Bennett, J. W.; Ghaemi, H. F.; Thio, T., Electrical conductivity of individual carbon nanotubes. *Nature* **1996**, 382, (6586), 54-56.
8. Powell, B. R.; Bloink, R. L.; Eickel, C. C., Preparation of Cerium Dioxide Powders for Catalyst Supports. *J. Am. Ceram. Soc.* **1988**, 71, (2), C-104-C-106.
9. Hendren, C. O.; Mesnard, X.; Dröge, J.; Wiesner, M. R., Estimating Production Data for Five Engineered Nanomaterials As a Basis for Exposure Assessment. *Environ. Sci. Technol.* **2011**, 45, (7), 2562-2569.
10. Blossey, R., Self-cleaning surfaces - virtual realities. *Nat Mater* **2003**, 2, (5), 301-306.
11. Buffle, J., The key role of environmental colloids/nanoparticles for the sustainability of life. *Environmental Chemistry* **2006**, 3, (3), 155-158.
12. Moore, M. N., Do nanoparticles present ecotoxicological risks for the health of the aquatic environment? *Environ. Int.* **2006**, 32, (8), 967-976.
13. Boxall, A. B.; Tiede, K.; Chaudhry, Q., Engineered nanomaterials in soils and water: How do they behave and could they pose a risk to human health? *Nanomedicine* **2007**, 2, (6), 919-927.
14. Owen, R.; Handy, R., Viewpoint: Formulating the Problems for Environmental Risk Assessment of Nanomaterials. *Environ. Sci. Technol.* **2007**, 41, (16), 5582-5588.
15. Nowack, B.; Bucheli, T. D., Occurrence, behavior and effects of nanoparticles in the environment. *Environ. Pollut.* **2007**, 150, (1), 5-22.
16. Klaine, S. J.; Alvarez, P. J. J.; Batley, G. E.; Fernandes, T. F.; Handy, R. D.; Lyon, D. Y.; Mahendra, S.; McLaughlin, M. J.; Lead, J. R., Nanomaterials in the environment: Behavior, Fate, Bioavailability, and Effects. *Environ. Toxicol. Chem.* **2008**, 27, (9), 1825-1851.
17. ECHA, *Guidance on information requirements and chemical safety assessment. Version 1.1*; European Chemicals Agency: 2011.
18. Leeuwen, C. J. v.; Vermeire, T. G., *Risk Assessment of Chemicals, An Introduction*. Springer: Dordrecht, 2007.
19. Vonk, J. A.; Struijs, J.; Meent, D. v. d.; Peijnenburg, W. J. G. M., *Nanomaterials in the aquatic environment: toxicity, exposure and risk assessment*; RIVM: 2009.

20. Bleeker, E. A. J.; de Jong, W. H.; Geertsma, R. E.; Groenewold, M.; Heugens, E. H. W.; Koers-Jacquemijns, M.; van de Meent, D.; Popma, J. R.; Rietveld, A. G.; Wijnhoven, S. W. P.; Cassee, F. R.; Oomen, A. G., Considerations on the EU definition of a nanomaterial: Science to support policy making. *Regul. Toxicol. Pharmacol.* **2013**, *65*, (1), 119-125.
21. European Commission, Commission recommendation of 18 October 2011 on the definition of nanomaterial (2011/696/EU). *Official Journal of the European Union* **2011**, *54*, 38-40.
22. Hassinger, C.; Sellers, K., *What Defines Nanomaterials?*; ARCADIS: 2012.
23. Lyklema, J., Pair Interactions. In *Fundamentals of Interface and Colloid Science, Volume IV, Particulate Colloids*, Lyklema, J., Ed. Elsevier Academic Press: Amsterdam, 2005.
24. Friedlander, S. K., *Smoke, dust, and haze: fundamentals of aerosol behavior*. Second ed.; Oxford University Press: New York, 2000.
25. Stokes, G. G., On the effect of the internal friction of fluids on the motion of pendulums. *Transactions of the Cambridge Philosophical Society* **1850**, *IX*, 8.
26. Einstein, A., *Investigations on the Theory of the Brownian Movement*. Dover Publications Inc.: 1956 (translation from the 1905 original).
27. Von Smoluchowski, M., Versuch einer mathematischen Theorie der Koagulationskinetik kolloider Lösungen. *Zeitschrift fuer physikalische Chemie* **1917**, *92*, 129 - 168.
28. Derjaguin, B.; Landau, L., Theory of the stability of strongly charged lyophobic sols and of the adhesion of strongly charged particles in solutions of electrolytes. *Acta Physicochim* **1941**, *14*, 633-662.
29. Verwey, E.; Overbeek, J., *Theory of the stability of lyophobic colloids*. Amsterdam, 1948.
30. Grasso, D.; Subramaniam, K.; Butkus, M.; Strevett, K.; Bergendahl, J., A review of non-DLVO interactions in environmental colloidal systems. *Reviews in Environmental Science and Biotechnology* **2002**, *1*, (1), 17-38.
31. Petosa, A. R.; Jaisi, D. P.; Quevedo, I. R.; Elimelech, M.; Tufenkji, N., Aggregation and Deposition of Engineered Nanomaterials in Aquatic Environments: Role of Physicochemical Interactions. *Environ. Sci. Technol.* **2010**, *44*, (17), 6532-6549.
32. Zhang, W.; Crittenden, J.; Li, K.; Chen, Y., Attachment Efficiency of Nanoparticle Aggregation in Aqueous Dispersions: Modeling and Experimental Validation. *Environ. Sci. Technol.* **2012**, *46*, (13), 7054-7062.
33. Phenrat, T.; Song, J. E.; Cisneros, C. M.; Schoenfelder, D. P.; Tilton, R. D.; Lowry, G. V., Estimating Attachment of Nano- and Submicrometer-particles Coated with Organic Macromolecules in Porous Media: Development of an Empirical Model. *Environ. Sci. Technol.* **2010**, *44*, (12), 4531-4538.
34. Elimelech, M.; Gregory, J.; Jia, X.; Williams, R. A., Particle Deposition and Aggregation - Measurement, Modelling and Simulation. In Elsevier: 1998.
35. Farley, K. J.; Morel, F. M. M., Role of coagulation in the kinetics of sedimentation. *Environ. Sci. Technol.* **1986**, *20*, (2), 187-195.

36. Praetorius, A.; Scheringer, M.; Hungerbühler, K., Development of environmental fate models for engineered nanoparticles - a case study of TiO₂ nanoparticles in the Rhine River. *Environ. Sci. Technol.* **2012**, *46*, (12), 6705-6713.
37. Gottschalk, F.; Sonderer, T.; Scholz, R. W.; Nowack, B., Possibilities and limitations of modeling environmental exposure to engineered nanomaterials by probabilistic material flow analysis. *Environ. Toxicol. Chem.* **2010**, *29*, (5), 1036-1048.
38. Arvidsson, R.; Molander, S.; Sandén, B. A.; Hasselöv, M., Challenges in Exposure Modeling of Nanoparticles in Aquatic Environments. *Hum. Ecol. Risk Assess.* **2011**, *17*, (1), 245-262.
39. Buffle, J.; Leppard, G. G., Characterization of Aquatic Colloids and Macromolecules. 1. Structure and Behavior of Colloidal Material. *Environ. Sci. Technol.* **1995**, *29*, (9), 2169-2175.
40. Filella, M., Chapter 2. Colloidal Properties of Submicron Particles in Natural Waters. In *Environmental Colloids and Particles: behaviour, separation, and characterisation*, Wilkinson, K. J.; Lead, J. R., Eds. Wiley: 2007.
41. Buffle, J.; Wilkinson, K. J.; Stoll, S.; Filella, M.; Zhang, J. W., A generalized description of aquatic colloidal interactions: The three-colloidal component approach. *Environ. Sci. Technol.* **1998**, *32*, (19), 2887-2899.
42. Wilkinson, K. J.; Joz-Roland, A.; Buffle, J., Different Roles of Pedogenic Fulvic Acids and Aquagenic Biopolymers on Colloid Aggregation and Stability in Freshwaters. *Limnol. Oceanogr.* **1997**, *42*, (8), 1714-1724.
43. Pizarro, J.; Belzile, N.; Filella, M.; Leppard, G. G.; Negre, J. C.; Perret, D.; Buffle, J., Coagulation/sedimentation of submicron iron particles in a eutrophic lake. *Water Res.* **1995**, *29*, (2), 617-632.
44. Filella, M.; Buffle, J.; Leppard, G. G., Characterization of submicrometre colloids in freshwaters: Evidence for their bridging by organic structures. *Water Sci. Technol.* **1993**, *27*, (11), 91-102.
45. Doucet, F. J.; Lead, J. R.; Santschi, P. H., Chapter 3. Colloid - Trace Element Interactions in Aquatic Systems. In *Environmental Colloids and Particles: behaviour, separation, and characterisation*, Wilkinson, K. J.; Lead, J. R., Eds. Wiley: 2007.
46. Hotze, E. M.; Phenrat, T.; Lowry, G. V., Nanoparticle Aggregation: Challenges to Understanding Transport and Reactivity in the Environment. *J. Environ. Qual.* **2010**, *39*, (6), 1909-1924.
47. Tipping, E., The Adsorption of Aquatic Humic Substances by Iron-Oxides. *Geochim. Cosmochim. Acta* **1981**, *45*, (2), 191-199.
48. Tipping, E.; Higgins, D. C., The effect of adsorbed humic substances on the colloid stability of haematite particles. *Colloids and Surfaces* **1982**, *5*, 35-92.
49. Kretzschmar, R.; Holthoff, H.; Sticher, H., Influence of pH and Humic Acid on Coagulation Kinetics of Kaolinite: A Dynamic Light Scattering Study. *J. Colloid Interface Sci.* **1998**, *202*, (1), 95-103.

50. Bob, M. M.; Walker, H. W., Effect of natural organic coatings on the polymer-induced coagulation of colloidal particles. *Colloids Surf. Physicochem. Eng. Aspects* **2000**, 177, (2–3), 215–222.
51. Tombácz, E.; Dobos, Á.; Szekeres, M.; Narres, H. D.; Klumpp, E.; Dékány, I., Effect of pH and ionic strength on the interaction of humic acid with aluminium oxide. *Colloid & Polymer Science* **2000**, 278, (4), 337–345.
52. Walker, H. W.; Bob, M. M., Stability of particle flocs upon addition of natural organic matter under quiescent conditions. *Water Res.* **2001**, 35, (4), 875–882.
53. Mosley, L. M.; Hunter, K. A.; Ducker, W. A., Forces between Colloid Particles in Natural Waters. *Environ. Sci. Technol.* **2003**, 37, (15), 3303–3308.
54. Wilkinson, K. J.; Reinhardt, A., Contrasting roles of natural organic matter on colloidal stabilization and flocculation in freshwaters. In *Flocculation in Natural and Engineered Environmental Systems*, Droppo, I. G.; Leppard, G. G.; Liss, S. N.; Milligan, T. G., Eds. CRC Press: Boca Raton, 2005; pp 143–170.
55. Harbour, P. J.; Dixon, D. R.; Scales, P. J., The role of natural organic matter in suspension stability - 1. Electrokinetic-rheology relationships. *Colloids and Surfaces A-Physicochemical and Engineering Aspects* **2007**, 295, (1–3), 38–48.
56. Harbour, P. J.; Dixon, D. R.; Scales, P. J., The role of natural organic matter in suspension stability - 2. Modelling of particle-particle interaction. *Colloids and Surfaces A-Physicochemical and Engineering Aspects* **2007**, 295, (1–3), 67–74.
57. Chen, K. L.; Elimelech, M., Influence of humic acid on the aggregation kinetics of fullerene (C-60) nanoparticles in monovalent and divalent electrolyte solutions. *J. Colloid Interface Sci.* **2007**, 309, (1), 126–134.
58. Hyung, H.; Fortner, J. D.; Hughes, J. B.; Kim, J. H., Natural organic matter stabilizes carbon nanotubes in the aqueous phase. *Environ. Sci. Technol.* **2007**, 41, (1), 179–184.
59. Hyung, H.; Kim, J.-H., Natural Organic Matter (NOM) Adsorption to Multi-Walled Carbon Nanotubes: Effect of NOM Characteristics and Water Quality Parameters. *Environ. Sci. Technol.* **2008**, 42, (12), 4416–4421.
60. Diegoli, S.; Manciulea, A. L.; Begum, S.; Jones, I. P.; Lead, J. R.; Preece, J. A., Interaction between manufactured gold nanoparticles and naturally occurring organic macromolecules. *Sci. Total Environ.* **2008**, 402, (1), 51–61.
61. Ghosh, S.; Mashayekhi, H.; Pan, B.; Bhowmik, P.; Xing, B., Colloidal Behavior of Aluminum Oxide Nanoparticles As Affected by pH and Natural Organic Matter. *Langmuir* **2008**, 24, (21), 12385–12391.
62. Domingos, R. F.; Tufenkji, N.; Wilkinson, K. J., Aggregation of Titanium Dioxide Nanoparticles: Role of a Fulvic Acid. *Environ. Sci. Technol.* **2009**, 43, (5), 1282–1286.
63. Handy, R. D.; von der Kammer, F.; Lead, J. R.; Hasselov, M.; Owen, R.; Crane, M., The ecotoxicology and chemistry of manufactured nanoparticles. *Ecotoxicology* **2008**, 17, (4), 287–314.
64. EU, European Union System for the Evaluation of Substances (EUSES). Version 2.1. In Institute for Health and Consumer Protection, E. C. B., Ed. 2008.

65. SCENIHR, *Risk assessment of products of nanotechnologies*; Scientific Committee on Emerging and Newly Identified Health Risks: 2009.
66. SCENIHR, *Opinion on the appropriateness of the risk assessment methodology in accordance with the technical guidance documents for new and existing substances for assessing the risk of nanomaterials*; Scientific Committee on Emerging and Newly Identified Health Risks: 2007.
67. Keller, A. A.; Wang, H.; Zhou, D.; Lenihan, H. S.; Cherr, G.; Cardinale, B. J.; Miller, R.; Ji, Z., Stability and Aggregation of Metal Oxide Nanoparticles in Natural Aqueous Matrices. *Environ. Sci. Technol.* **2010**, *44*, (6), 1962-1967.
68. Kiser, M. A.; Ryu, H.; Jang, H.; Hristovski, K.; Westerhoff, P., Biosorption of nanoparticles to heterotrophic wastewater biomass. *Water Res.* **2010**, *44*, (14), 4105-4114.
69. Limbach, L. K.; Bereiter, R.; Mueller, E.; Krebs, R.; Gaelli, R.; Stark, W. J., Removal of oxide nanoparticles in a model wastewater treatment plant: Influence of agglomeration and surfactants on clearing efficiency. *Environ. Sci. Technol.* **2008**, *42*, (15), 5828-5833.
70. Quik, J. T. K.; Lynch, I.; Van Hoecke, K.; Miermans, C. J. H.; De Schamphelaere, K. A. C.; Janssen, C. R.; Dawson, K. A.; Cohen Stuart, M. A.; Van De Meent, D., Effect of natural organic matter on cerium dioxide nanoparticles settling in model fresh water. *Chemosphere* **2010**, *81*, (6), 711-715.
71. von der Kammer, F.; Ottofuelling, S.; Hofmann, T., Assessment of the physico-chemical behavior of titanium dioxide nanoparticles in aquatic environments using multi-dimensional parameter testing. *Environ. Pollut.* **2010**, *158*, (12), 3472-3481.
72. Schmidt, J.; Vogelsberger, W., Aqueous Long-Term Solubility of Titania Nanoparticles and Titanium(IV) Hydrolysis in a Sodium Chloride System Studied by Adsorptive Stripping Voltammetry. *J. Solution Chem.* **2009**, *38*, (10), 1267-1282.
73. Vogelsberger, W.; Schmidt, J.; Roelofs, F., Dissolution kinetics of oxidic nanoparticles: The observation of an unusual behaviour. *Colloids Surf. Physicochem. Eng. Aspects* **2008**, *324*, (1-3), 51-57.
74. Roelofs, F.; Vogelsberger, W., Dissolution kinetics of nanodispersed [gamma]-alumina in aqueous solution at different pH: Unusual kinetic size effect and formation of a new phase. *J. Colloid Interface Sci.* **2006**, *303*, (2), 450-459.
75. Jakab, S.; Picart, S. b.; Tribollet, B.; Rousseau, P.; Perrot, H.; Gabrielli, C., Study of the Dissolution of Thin Films of Cerium Oxide by Using a GaPO₄ Crystal Microbalance. *Anal. Chem.* **2009**, *81*, (13), 5139-5145.
76. Gerischer, H.; Sorg, N., Chemical dissolution of zinc oxide crystals in aqueous electrolytes--An analysis of the kinetics. *Electrochim. Acta* **1992**, *37*, (5), 827-835.
77. Elzey, S.; Grassian, V., Agglomeration, isolation and dissolution of commercially manufactured silver nanoparticles in aqueous environments. *J. Nanopart. Res.* **2010**, *12*, (5), 1945-1958.

78. Lundborg, M.; Eklund, A.; Lind, B.; Camner, P., Dissolution of metals by human and rabbit alveolar macrophages. *British Journal of Industrial Medicine* **1985**, *42*, (9), 642-645.
79. Zhou, Y.; Cheng, Y. S.; Wang, Y., Dissolution rate and biokinetic model of zirconium tritide particles in rat lungs. *Health Phys.* **2010**, *98*, (5), 672-682.
80. Guldberg, M.; Christensen, V. R.; Perander, M.; Zito, B.; Koenig, A. R.; Sebastian, K., Measurement of in-vitro fibre dissolution rate at acidic pH. *Ann. Occup. Hyg.* **1998**, *42*, (4), 233-243.
81. Lerman, A.; Mackenzie, F. T.; Bricker, O. P., Rates of dissolution of aluminosilicates in seawater. *Earth. Planet. Sci. Lett.* **1975**, *25*, (1), 82-88.
82. Johnson, S. B.; Yoon, T. H.; Brown, G. E., Adsorption of Organic Matter at Mineral/Water Interfaces: 5. Effects of Adsorbed Natural Organic Matter Analogues on Mineral Dissolution. *Langmuir* **2005**, *21*, (7), 2811-2821.
83. Xia, T.; Kovochich, M.; Liong, M.; Mädler, L.; Gilbert, B.; Shi, H.; Yeh, J. I.; Zink, J. I.; Nel, A. E., Comparison of the Mechanism of Toxicity of Zinc Oxide and Cerium Oxide Nanoparticles Based on Dissolution and Oxidative Stress Properties. *ACS Nano* **2008**, *2*, (10), 2121-2134.
84. Franklin, N. M.; Rogers, N. J.; Apte, S. C.; Batley, G. E.; Gadd, G. E.; Casey, P. S., Comparative toxicity of nanoparticulate ZnO, bulk ZnO, and ZnCl₂ to a freshwater microalga (*Pseudokirchneriella subcapitata*): The importance of particle solubility. *Environ. Sci. Technol.* **2007**, *41*, (24), 8484-8490.
85. Wong, S.; Leung, P.; Djurišić, A.; Leung, K., Toxicities of nano zinc oxide to five marine organisms: influences of aggregate size and ion solubility. *Anal. Bioanal. Chem.* **2010**, *396*, (2), 609-618.
86. Fabrega, J.; Fawcett, S. R.; Renshaw, J. C.; Lead, J. R., Silver Nanoparticle Impact on Bacterial Growth: Effect of pH, Concentration, and Organic Matter. *Environ. Sci. Technol.* **2009**, *43*, (19), 7285-7290.
87. Blinova, I.; Ivask, A.; Heinlaan, M.; Mortimer, M.; Kahru, A., Ecotoxicity of nanoparticles of CuO and ZnO in natural water. *Environ. Pollut.* **2010**, *158*, (1), 41-47.
88. Liu, J.; Aruguete, D. M.; Murayama, M.; Hochella Jr, M. F., Influence of Size and Aggregation on the Reactivity of an Environmentally and Industrially Relevant Nanomaterial (PbS). *Environ. Sci. Technol.* **2009**, *43*, (21), 8178-8183.
89. Stebounova, L.; Guio, E.; Grassian, V., Silver nanoparticles in simulated biological media: a study of aggregation, sedimentation, and dissolution. *J. Nanopart. Res.* **2011**, *13*, (1), 233-244.
90. Ho, C. M.; Yau, S. K. W.; Lok, C. N.; So, M. H.; Che, C. M., Oxidative Dissolution of Silver Nanoparticles by Biologically Relevant Oxidants: A Kinetic and Mechanistic Study. *Chemistry – An Asian Journal* **2010**, *5*, (2), 285-293.
91. Liu, J.; Hurt, R. H., Ion Release Kinetics and Particle Persistence in Aqueous Nano-Silver Colloids. *Environ. Sci. Technol.* **2010**, *44*, (6), 2169-2175.
92. Kennedy, A. J.; Hull, M. S.; Steevens, J. A.; Dontsova, K. M.; Chappell, M. A.; Gunter, J. C.; Weiss, C. A., Factors influencing the partitioning and toxicity of

- nanotubes in the aquatic environment. *Environ. Toxicol. Chem.* **2008**, *27*, (9), 1932-1941.
93. Phenrat, T.; Long, T. C.; Lowry, G. V.; Veronesi, B., Partial Oxidation ("Aging") and Surface Modification Decrease the Toxicity of Nanosized Zerovalent Iron. *Environ. Sci. Technol.* **2009**, *43*, (1), 195-200.
94. Lin, D.; Liu, N.; Yang, K.; Xing, B.; Wu, F., Different stabilities of multiwalled carbon nanotubes in fresh surface water samples. *Environ. Pollut.* **2010**, *158*, (5), 1270-1274.
95. Phenrat, T.; Saleh, N.; Sirk, K.; Tilton, R. D.; Lowry, G. V., Aggregation and Sedimentation of Aqueous Nanoscale Zerovalent Iron Dispersions. *Environ. Sci. Technol.* **2007**, *41*, (1), 284-290.
96. Battin, T. J.; Kammer, F. v. d.; Weilhartner, A.; Ottofuelling, S.; Hofmann, T., Nanostructured TiO₂: Transport Behavior and Effects on Aquatic Microbial Communities under Environmental Conditions. *Environ. Sci. Technol.* **2009**, *43*, (21), 8098-8104.
97. Ferry, J. L.; Craig, P.; Hexel, C.; Sisco, P.; Frey, R.; Pennington, P. L.; Fulton, M. H.; Scott, I. G.; Decho, A. W.; Kashiwada, S.; Murphy, C. J.; Shaw, T. J., Transfer of gold nanoparticles from the water column to the estuarine food web. *Nat Nano* **2009**, *4*, (7), 441-444.
98. Van Hoecke, K.; Quik, J. T. K.; Mankiewicz-Boczek, J.; De Schamphelaere, K. A. C.; Elsaesser, A.; Van der Meeren, P.; Barnes, C.; McKerr, G.; Howard, C. V.; Van De Meent, D.; Rydzyninski, K.; Dawson, K. A.; Salvati, A.; Lesniak, A.; Lynch, I.; Silversmit, G.; De Samber, B.; Vincze, L.; Janssen, C. R., Fate and Effects of CeO₂ Nanoparticles in Aquatic Ecotoxicity Tests. *Environ. Sci. Technol.* **2009**, *43*, (12), 4537-4546.
99. Filella, M.; Rellstab, C.; Chanudet, V.; Spaak, P., Effect of the filter feeder *Daphnia* on the particle size distribution of inorganic colloids in freshwaters. *Water Res.* **2008**, *42*, (8-9), 1919-1924.
100. Baun, A.; Sørensen, S. N.; Rasmussen, R. F.; Hartmann, N. B.; Koch, C. B., Toxicity and bioaccumulation of xenobiotic organic compounds in the presence of aqueous suspensions of aggregates of nano-C₆₀. *Aquat. Toxicol.* **2008**, *86*, (3), 379-387.
101. Roberts, A. P.; Mount, A. S.; Seda, B.; Souther, J.; Qiao, R.; Lin, S. J.; Ke, P. C.; Rao, A. M.; Klaine, S. J., In vivo biomodification of lipid-coated carbon nanotubes by *Daphnia magna*. *Environ. Sci. Technol.* **2007**, *41*, (8), 3025-3029.
102. Zhang, Y.; Chen, Y.; Westerhoff, P.; Hristovski, K.; Crittenden, J. C., Stability of commercial metal oxide nanoparticles in water. *Water Res.* **2008**, *42*, (8-9), 2204-2212.
103. Fang, J.; Shan, X.-q.; Wen, B.; Lin, J.-m.; Owens, G., Stability of titania nanoparticles in soil suspensions and transport in saturated homogeneous soil columns. *Environ. Pollut.* **2009**, *157*, (4), 1101-1109.
104. Simon-Deckers, A. I.; Loo, S.; Mayne-L'Hermitte, M.; Herlin-Boime, N.; Menguy, N.; Reynaud, C. c.; Gouget, B.; Carri  re, M., Size-, Composition- and Shape-

- Dependent Toxicological Impact of Metal Oxide Nanoparticles and Carbon Nanotubes toward Bacteria. *Environ. Sci. Technol.* **2009**, *43*, (21), 8423-8429.
105. Gao, J.; Youn, S.; Hovsepyan, A.; Llana, V. n. L.; Wang, Y.; Bitton, G.; Bonzongo, J.-C. J., Dispersion and Toxicity of Selected Manufactured Nanomaterials in Natural River Water Samples: Effects of Water Chemical Composition. *Environ. Sci. Technol.* **2009**, *43*, (9), 3322-3328.
106. Baalousha, M.; Manciu, A.; Cumberland, S.; Kendall, K.; Lead, J. R., Aggregation and Surface Properties Of Iron Oxide Nanoparticles: influence of pH and natural organic matter. *Environ. Toxicol. Chem.* **2008**, *27*, (9), 1875-1882.
107. Taboada-Serrano, P.; Chin, C. J.; Yiacoumi, S.; Tsouris, C., Modeling aggregation of colloidal particles. *Current Opinion in Colloid & Interface Science* **2005**, *10*, (3-4), 123-132.
108. Burguera, E. F.; Love, B. J.; Sahul, R.; Ngatu, G.; Wereley, N. M., A Physical Basis for Stability in Bimodal Dispersions Including Micrometer-sized Particles and Nanoparticles using Both Linear and Non-linear Models to Describe Yield. *J. Intell. Mater. Syst. Struct.* **2008**, *19*, (11), 1361-1367.
109. Seijo, M.; Ulrich, S.; Filella, M.; Buffle, J.; Stoll, S., Modeling the Adsorption and Coagulation of Fulvic Acids on Colloids by Brownian Dynamics Simulations. *Environ. Sci. Technol.* **2009**, *43*, (19), 7265-7269.
110. Kim, C.; Liu, Y.; Kühnle, A.; Hess, S.; Viereck, S.; Danner, T.; Mahadevan, L.; Weitz, D. A., Gravitational Stability of Suspensions of Attractive Colloidal Particles. *Phys. Rev. Lett.* **2007**, *99*, (2), 028303.
111. Gottschalk, F.; Scholz, R. W.; Nowack, B., Probabilistic material flow modeling for assessing the environmental exposure to compounds: Methodology and an application to engineered nano-TiO₂ particles. *Environ. Model. Software* **2010**, *25*, (3), 320-332.
112. Koelmans, A. A.; Nowack, B.; Wiesner, M. R., Comparison of manufactured and black carbon nanoparticle concentrations in aquatic sediments. *Environ. Pollut.* **2009**, *157*, (4), 1110-1116.
113. Mueller, N. C.; Nowack, B., Exposure Modeling of Engineered Nanoparticles in the Environment. *Environ. Sci. Technol.* **2008**, *42*, (12), 4447-4453.
114. Blaser, S. A.; Scheringer, M.; MacLeod, M.; Hungerbühler, K., Estimation of cumulative aquatic exposure and risk due to silver: Contribution of nano-functionalized plastics and textiles. *Sci. Total Environ.* **2008**, *390*, (2-3), 396-409.
115. Ferguson, P. L.; Chandler, G. T.; Templeton, R. C.; Demarco, A.; Scrivens, W. A.; Englehart, B. A., Influence of sediment-amendment with single-walled carbon nanotubes and diesel soot on bioaccumulation of hydrophobic organic contaminants by benthic invertebrates. *Environ. Sci. Technol.* **2008**, *42*, (10), 3879-3885.
116. Cornelis, G.; Kirby, J. K.; Beak, D.; Chittleborough, D.; McLaughlin, M. J., A method for determination of retention of silver and cerium oxide manufactured nanoparticles in soils. *Environmental Chemistry* **2010**, *7*, (3), 298-308.

117. Hollander, d., H.A.; Eijkeren, v., J.C.H. ; Meent, v. d., D., *SimpleBox 3.0: multimedia mass balance model for evaluating the fate of chemical in the environment*; National Institute of Public Health and the Environment: Bilthoven, 2004.
118. Rosenbaum, R.; Bachmann, T.; Gold, L.; Huijbregts, M.; Jolliet, O.; Juraske, R.; Koehler, A.; Larsen, H.; MacLeod, M.; Margni, M.; McKone, T.; Payet, J.; Schuhmacher, M.; van de Meent, D.; Hauschild, M., USEtox—the UNEP-SETAC toxicity model: recommended characterisation factors for human toxicity and freshwater ecotoxicity in life cycle impact assessment. *The International Journal of Life Cycle Assessment* **2008**, *13*, (7), 532-546.
119. Hauschild, M. Z.; Huijbregts, M.; Jolliet, O.; Macleod, M.; Margni, M.; van de Meent, D.; Rosenbaum, R. K.; McKone, T. E., Building a Model Based on Scientific Consensus for Life Cycle Impact Assessment of Chemicals: The Search for Harmony and Parsimony. *Environ. Sci. Technol.* **2008**, *42*, (19), 7032-7037.
120. Klaine, S. J., Considerations for research on the environmental fate and effects of nanoparticles. *Environ. Toxicol. Chem.* **2009**, *28*, (9), 1787-1788.
121. OECD, *List of manufactured nanomaterials and list of endpoints for phase one of the OECD testing programme*; ENV/JM/MONO(2008)13/REV; Organisation for Economic Co-operation and Development: Paris, 07-07-2008, 2008.
122. Fall, M.; Guerbet, M.; Park, B.; Gouriou, F.; Dionnet, F.; Morin, J. P., Evaluation of cerium oxide and cerium oxide based fuel additive safety on organotypic cultures of lung slices. *Nanotoxicology* **2007**, *1*, (3), 227-234.
123. Masui, T.; Yamamoto, M.; Sakata, T.; Mori, H.; Adachi, G. Y., Synthesis of BN-coated CeO₂ fine powder as a new UV blocking material. *J. Mater. Chem.* **2000**, *10*, (2), 353-357.
124. Dawson, J. J. C.; Malcolm, I. A.; Middlemas, S. J.; Tetzlaff, D.; Soulsby, C., Is the Composition of Dissolved Organic Carbon Changing in Upland Acidic Streams? *Environ. Sci. Technol.* **2009**, *43*, (20), 7748-7753.
125. Frimmel, F. H., Characterization of natural organic matter as major constituents in aquatic systems. *J. Contam. Hydrol.* **1998**, *35*, (1-3), 201-216.
126. Au, K. K.; Penisson, A. C.; Yang, S.; O'Melia, C. R., Natural organic matter at oxide/water interfaces: Complexation and conformation. *Geochim. Cosmochim. Acta* **1999**, *63*, (19-20), 2903-2917.
127. Cumberland, S. A.; Lead, J. R., Particle size distributions of silver nanoparticles at environmentally relevant conditions. *J. Chromatogr.* **2009**, *1216*, (52), 9099-9105.
128. Yang, K.; Lin, D.; Xing, B., Interactions of Humic Acid with Nanosized Inorganic Oxides. *Langmuir* **2009**, *25*, (6), 3571-3576.
129. Zhang, Y.; Chen, Y.; Westerhoff, P.; Crittenden, J., Impact of natural organic matter and divalent cations on the stability of aqueous nanoparticles. *Water Res.* **2009**, *43*, (17), 4249-4257.
130. OECD, *Freshwater Alga and Cyanobacteria, Growth Inhibition Test*; 201; Organisation for economic co-operation and development: Paris, 2006.

131. De Faria, L. A.; Trasatti, S., The Point of Zero Charge of CeO₂. *J. Colloid Interface Sci.* **1994**, *167*, (2), 352-357.
132. van Zomeren, A.; Comans, R. N. J., Measurement of Humic and Fulvic Acid Concentrations and Dissolution Properties by a Rapid Batch Procedure. *Environ. Sci. Technol.* **2007**, *41*, (19), 6755-6761.
133. Beaudrie, C. E. H.; Kandlikar, M., Horses for courses: risk information and decision making in the regulation of nanomaterials. *J. Nanopart. Res.* **2011**, *13*, (4), 1477-1488.
134. Lin, D.; Tian, X.; Wu, F.; Xing, B., Fate and Transport of Engineered Nanomaterials in the Environment. *J. Environ. Qual.* **2010**, *39*, (6), 1896-1908.
135. Quik, J. T. K.; Vonk, J. A.; Hansen, S. F.; Baun, A.; Van De Meent, D., How to assess exposure of aquatic organisms to manufactured nanoparticles? *Environ. Int.* **2011**, *37*, 1068-1077.
136. Abbott, L. C.; Maynard, A. D., Exposure Assessment Approaches for Engineered Nanomaterials. *Risk Anal.* **2010**, *30*, (11), 1634-1644.
137. Lowry, G. V.; Hotze, E. M.; Bernhardt, E. S.; Dionysiou, D. D.; Pedersen, J. A.; Wiesner, M. R.; Xing, B., Environmental occurrences, behavior, fate, and ecological effects of nanomaterials: An introduction to the special series. *J Environ Qual* **2010**, *39*, (6), 1867-1874.
138. Thio, B. J. R.; Zhou, D.; Keller, A. A., Influence of natural organic matter on the aggregation and deposition of titanium dioxide nanoparticles. *J. Hazard. Mater.* **2011**, *189*, (1-2), 556-563.
139. Waterbase, Monitoring Programme of the National Water Systems. www.waterbase.nl (28-11-2008)
140. R Development Core Team, *R: A language and environment for statistical computing.*; 3-900051-07-0; URL <http://www.R-project.org/>; Vienna, Austria, 2012.
141. Saleh, N. B.; Pfefferle, L. D.; Elimelech, M., Influence of Biomacromolecules and Humic Acid on the Aggregation Kinetics of Single-Walled Carbon Nanotubes. *Environ. Sci. Technol.* **2010**, *44*, (7), 2412-2418.
142. Abe, T.; Kobayashi, S.; Kobayashi, M., Aggregation of colloidal silica particles in the presence of fulvic acid, humic acid, or alginate: Effects of ionic composition. *Colloids Surf. Physicochem. Eng. Aspects* **2011**, *379*, (1-3), 21-26.
143. Liu, X.; Wazne, M.; Han, Y.; Christodoulatos, C.; Jasinkiewicz, K. L., Effects of natural organic matter on aggregation kinetics of boron nanoparticles in monovalent and divalent electrolytes. *J. Colloid Interface Sci.* **2010**, *348*, (1), 101-107.
144. Kretzschmar, R.; Barmettler, K.; Grolimund, D.; Yan, Y.-d.; Borkovec, M.; Sticher, H., Experimental determination of colloid deposition rates and collision efficiencies in natural porous media. *Water Resour. Res.* **1997**, *33*, (5), 1129 - 1137.

145. Klaine, S. J.; Koelmans, A. A.; Horne, N.; Handy, R. D.; Kapustka, L.; Nowack, B.; von der Kammer, F., Paradigms to assess the Environmental Impact of Manufactured Nanomaterials. *Environ. Toxicol. Chem.* **2012**, *31*, 3-14.
146. Wiesner, M. R.; Lowry, G. V.; Alvarez, P.; Dionysiou, D.; Biswas, P., Assessing the Risks of Manufactured Nanomaterials. *Environ. Sci. Technol.* **2006**, *40*, (14), 4336-4345.
147. Batley, G. E.; Kirby, J. K.; McLaughlin, M. J., Fate and Risks of Nanomaterials in Aquatic and Terrestrial Environments. *Acc. Chem. Res.* **2013**, *46*, (3), 854-862.
148. Morris, J.; Willis, J.; De Martinis, D.; Hansen, B.; Laursen, H.; Sintes, J. R.; Kearns, P.; Gonzalez, M., Science policy considerations for responsible nanotechnology decisions. *Nat Nano* **2011**, *6*, (2), 73-77.
149. Petersen, E. J.; Zhang, L.; Mattison, N. T.; O'Carroll, D. M.; Whelton, A. J.; Uddin, N.; Nguyen, T.; Huang, Q.; Henry, T. B.; Holbrook, R. D.; Chen, K. L., Potential Release Pathways, Environmental Fate, And Ecological Risks of Carbon Nanotubes. *Environ. Sci. Technol.* **2011**, *45*, (23), 9837-9856.
150. Westerhoff, P.; Nowack, B., Searching for Global Descriptors of Engineered Nanomaterial Fate and Transport in the Environment. *Acc. Chem. Res.* **2013**, *46*, (3), 844-853.
151. Huynh, K. A.; McCaffery, J. M.; Chen, K. L., Heteroaggregation of Multiwalled Carbon Nanotubes and Hematite Nanoparticles: Rates and Mechanisms. *Environ. Sci. Technol.* **2012**, *46*, (11), 5912-5920.
152. Afroz, A. R. M. N.; Khan, I. A.; Hussain, S. M.; Saleh, N. B., Mechanistic Heteroaggregation of Gold Nanoparticles in a Wide Range of Solution Chemistry. *Environ. Sci. Technol.* **2013**, *47*, (4), 1853-1860.
153. Quik, J. T. K.; Stuart, M. C.; Wouterse, M.; Peijnenburg, W.; Hendriks, A. J.; van de Meent, D., Natural colloids are the dominant factor in the sedimentation of nanoparticles. *Environ. Toxicol. Chem.* **2012**, *31*, (5), 1019-1022.
154. Van Hoecke, K.; De Schampelaere, K. A. C.; Van der Meeren, P.; Smagghe, G.; Janssen, C. R., Aggregation and ecotoxicity of CeO₂ nanoparticles in synthetic and natural waters with variable pH, organic matter concentration and ionic strength. *Environ. Pollut.* **2011**, *159*, (4), 970-976.
155. Boyd, C. E., *Bottom Soils, Sediment, and Pond Aquaculture*. Chapman & Hall: New York, 1995.
156. Verweij, W. *CHEAQS, computer program for calculating CHEmical Equilibria in AQUatic Systems*, CHEAQS Pro 2011.1; 2011.
157. Newman, K. A.; Morel, F. M. M.; Stolzenbach, K. D., Settling and coagulation characteristics of fluorescent particles determined by flow cytometry and fluorometry. *Environ. Sci. Technol.* **1990**, *24*, (4), 506-513.
158. Chinnapongse, S. L.; MacCuspie, R. I.; Hackley, V. A., Persistence of singly dispersed silver nanoparticles in natural freshwaters, synthetic seawater, and simulated estuarine waters. *Sci. Total Environ.* **2011**, *409*, (12), 2443-2450.
159. Ottofuelling, S.; Von Der Kammer, F.; Hofmann, T., Commercial Titanium Dioxide Nanoparticles in Both Natural and Synthetic Water: Comprehensive

- Multidimensional Testing and Prediction of Aggregation Behavior. *Environ. Sci. Technol.* **2011**, *45*, (23), 10045-10052.
160. Li, K.; Chen, Y., Effect of natural organic matter on the aggregation kinetics of CeO₂ nanoparticles in KCl and CaCl₂ solutions: Measurements and modeling. *J. Hazard. Mater.* **2012**, 209-210, 264-270.
 161. Gottschalk, F.; Ort, C.; Scholz, R. W.; Nowack, B., Engineered nanomaterials in rivers – Exposure scenarios for Switzerland at high spatial and temporal resolution. *Environ. Pollut.* **2011**, *159*, (12), 3439-3445.
 162. Li, X.; Lenhart, J. J.; Walker, H. W., Aggregation kinetics and dissolution of coated silver nanoparticles. *Langmuir* **2012**, *28*, (2), 1095-1104.
 163. Levard, C.; Hotze, E. M.; Lowry, G. V.; Brown, G. E., Environmental Transformations of Silver Nanoparticles: Impact on Stability and Toxicity. *Environ. Sci. Technol.* **2012**.
 164. Nowack, B.; Ranville, J. F.; Diamond, S.; Gallego-Urrea, J. A.; Metcalfe, C.; Rose, J.; Horne, N.; Koelmans, A. A.; Klaine, S. J., Potential Scenarios for Nanomaterial Release and Subsequent Alteration in the Environment. *Environ. Toxicol. Chem.* **2012**, *31*, (1), 50-59.
 165. Petosa, A. R.; Brennan, S. J.; Rajput, F.; Tufenkji, N., Transport of two metal oxide nanoparticles in saturated granular porous media: Role of water chemistry and particle coating. *Water Res.* **2012**, *46*, (4), 1273-1285.
 166. Chen, K. L.; Elimelech, M., Interaction of Fullerene (C₆₀) Nanoparticles with Humic Acid and Alginate Coated Silica Surfaces: Measurements, Mechanisms, and Environmental Implications. *Environ. Sci. Technol.* **2008**, *42*, (20), 7607-7614.
 167. Von der Kammer, F.; Ferguson, P. L.; Holden, P.; Masion, A.; Rogers, K.; Klaine, S. J.; Koelmans, A. A.; Horne, N.; Unrine, J., Analysis of nanomaterials in complex matrices (environment and biota): general considerations and conceptual case studies. *Environ. Toxicol. Chem.* **2012**, *31*, 32-49.
 168. Quik, J. T. K.; Velzeboer, I.; Wouterse, M.; Koelmans, A. A.; Meent, D. v. d., Nanomaterials in natural waters: Sedimentation rates and attachment efficiencies for heteroaggregation. **2013**, *Submitted*.
 169. Velzeboer, I.; Hendriks, A. J.; Ragas, A. M. J.; Van De Meent, D., Aquatic ecotoxicity tests of some nanomaterials. *Environ. Toxicol. Chem.* **2008**, *27*, (9), 1942-1947.
 170. Zhang, H.; Smith, J. A.; Oyanedel-Craver, V., The effect of natural water conditions on the anti-bacterial performance and stability of silver nanoparticles capped with different polymers. *Water Res.* **2012**, *46*, (3), 691-699.
 171. McCave, I. N., Size spectra and aggregation of suspended particles in the deep ocean. *Deep Sea Research Part A. Oceanographic Research Papers* **1984**, *31*, (4), 329-352.
 172. Stolzenbach, K. D.; Newman, K. A.; Wong, C. S., Aggregation of Fine Particles at the Sediment-Water Interface. *J. Geophys. Res.* **1992**, *97*, (C11), 17889-17898.
 173. Bilotta, G. S.; Brazier, R. E., Understanding the influence of suspended solids on water quality and aquatic biota. *Water Res.* **2008**, *42*, (12), 2849-2861.

174. Handy, R. D.; Cornelis, G.; Fernandes, T.; Tsyusko, O.; Decho, A.; Sabo-Attwood, T.; Metcalfe, C.; Steevens, J. A.; Klaine, S. J.; Koelmans, A. A.; Horne, N., Ecotoxicity test methods for engineered nanomaterials: Practical experiences and recommendations from the bench. *Environ. Toxicol. Chem.* **2012**, *31*, (1), 15-31.
175. Peeters, E. T. H. M.; de Lange, H. J.; de la Haye, M. A. A.; Reeze, A. J. G., *KRW-maatlat macrofauna voor zoet getijdenwater (R8)*; Hoofdrapport. Grontmij. Rapportnummer: 228629-1: 2010.
176. Gustafsson, O.; Haghseta, F.; Chan, C.; MacFarlane, J.; Gschwend, P. M., Quantification of the dilute sedimentary soot phase: Implications for PAH speciation and bioavailability. *Environ. Sci. Technol.* **1997**, *31*, (1), 203-209.
177. Jonker, M. T. O.; Koelmans, A. A., Sorption of polycyclic aromatic hydrocarbons and polychlorinated biphenyls to soot and soot-like materials in the aqueous environment mechanistic considerations. *Environ. Sci. Technol.* **2002**, *36*, (17), 3725-3734.
178. Avnimelech, Y.; Ritvo, G.; Meijer, L. E.; Kochba, M., Water content, organic carbon and dry bulk density in flooded sediments. *Aquacult. Eng.* **2001**, *25*, 25-33.
179. Velde, B., *Clays and clay minerals in natural and synthetic systems*. Elsevier Scientific Publishing Company, Amsterdam, the Netherlands: 1977.
180. Zook, J. M.; Long, S. E.; Cleveland, D.; Geronimo, C. L. A.; MacCusprie, R. I., Measuring silver nanoparticle dissolution in complex biological and environmental matrices using UV-visible absorbance. *Anal. Bioanal. Chem.* **2011**, 1-10.
181. Poot, A.; Meerman, E.; Gillissen, F.; Koelmans, A. A., A kinetic approach to evaluate the association of acid volatile sulfide and simultaneously extracted metals in aquatic sediments. *Environ. Toxicol. Chem.* **2009**, *28*, (4), 711-717.
182. Thio, B. J. R.; Montes, M. O.; Mahmoud, M. A.; Lee, D.-W.; Zhou, D.; Keller, A. A., Mobility of Capped Silver Nanoparticles under Environmentally Relevant Conditions. *Environ. Sci. Technol.* **2012**, *46*, (13), 6985-6991.
183. Soetaert, K.; Petzoldt, T.; Setzer, R. W., Solving Differential Equations in R. *The R Journal* **2010**, *2*, (2), 5-15.
184. O'Brien, N.; Cummins, E., Ranking initial environmental and human health risk resulting from environmentally relevant nanomaterials. *Journal of Environmental Science and Health, Part A* **2010**, *45*, (8), 992-1007.
185. Kiser, M. A.; Westerhoff, P.; Benn, T.; Wang, Y.; Pérez-Rivera, J.; Hristovski, K., Titanium Nanomaterial Removal and Release from Wastewater Treatment Plants. *Environ. Sci. Technol.* **2009**.
186. Chen, K. L.; Elimelech, M., Aggregation and Deposition Kinetics of Fullerene (C60) Nanoparticles. *Langmuir* **2006**, *22*, (26), 10994-11001.

Summary

Ecological risk of chemicals is based on the concentration to which organisms are exposed and the effects this chemical has on them. This is measured by the quotient of predicted exposure concentrations and predicted no effect concentrations, which are hard to assess for engineered nanomaterials (ENMs). Understanding the processes that play a role in the assessment of exposure concentrations of ENMs is the topic of this thesis.

In the **chapter 2** modifications to currently used models are proposed, in order to make them suitable for estimating exposure concentrations of ENMs in the aquatic environment. In this chapter we have evaluated the adequacy of the current guidance documents for use with ENMs and conclude that nano-specific fate processes, such as sedimentation and dissolution need to be incorporated. We have reviewed the literature on sedimentation and dissolution of ENMs in environmentally relevant systems. We deduce that the overall kinetics of water-sediment transport of ENMs should be close to first-order. Based on limited data from literature, probable removal rates range from $0\text{--}10^{-4}\text{ s}^{-1}$ for sedimentation, and from $0\text{--}10^{-5}\text{ s}^{-1}$ for dissolution.

In **chapter 3** we measured the concentrations and particle size distributions of CeO_2 nanoparticles in algae growth medium and deionized water in the presence of various concentrations and two types of dissolved organic matter (DOM). The presence of DOM stabilizes the CeO_2 nanoparticles in suspension. In presence of DOM, up to 88% of the initially added CeO_2 nanoparticles remained suspended in deionized water and 41% in algae growth medium after 12 days of settling.

Because nanoparticles aggregate with each other (homoaggregation) and with other particles (heteroaggregation), the main route of the removal of most nanoparticles from water is aggregation followed by sedimentation. In **chapter 4** we used water samples from two rivers in Europe, the Rhine and Meuse. To distinguish between small (mainly DOM) and the remainder of the natural colloids present, both filtered and unfiltered river water was used to prepare the particle suspensions. The results show that the removal of nanoparticles from natural river water follows first-order kinetics towards a residual concentration. This was measured in river water with less than 1 mg L^{-1} CeO_2 nanoparticles. We inferred that the heteroaggregation with or deposition onto the solid fraction of natural colloids was the main mechanism causing sedimentation. In contrast, the DOM fraction in filtered river water stabilized the residual nanoparticles against further sedimentation. The proposed model could form the basis for the improved exposure assessment for nanomaterials.

The main aim of **chapter 5** is the estimation of input parameters for exposure modeling of ENMs. We investigated 4 different ENMs (C_{60} , CeO_2 , $\text{SiO}_2\text{-Ag}$ and PVP-Ag)

in 6 different water types ranging from a small stream to sea water. Sedimentation rates in the presence of natural colloids (NC) showed significant differences among particle and water types. The sedimentation rates ranged from 0.0001 m d^{-1} for $\text{SiO}_2\text{-Ag}$ to 0.14 m d^{-1} for C_{60} . NC-ENM apparent heteroaggregation rates and attachment efficiencies were estimated using a novel method that separates heteroaggregation from homoaggregation using a simplified Smoluchowski-based aggregation-settling equation applied to data from unfiltered and filtered waters. The attachment efficiencies for heteroaggregation ranged between 0.0067 and 1, with the highest values observed in seawater. We argue that such system specific parameters are key to the development of dedicated water quality models for ENMs.

Chapter 6 accompanies **chapter 5**, but investigates the effect of resuspending sediment on the removal of ENMs from the water phase due to heteroaggregation and subsequent sedimentation. This is an environmentally relevant scenario, e.g. in shallow lakes and streams or rivers with a sediment fluff layer. Approximately 10 to 100 fold higher sedimentation rates were observed in these systems with periodically suspended sediment and attachment efficiencies between 0.8 and 1.

In **chapter 7** a numeric model is used based on the Von Smoluchowski theory on aggregation coupled to Stokes sedimentation theory to better understand the effect of homoaggregation and heteroaggregation on the sedimentation out of the water phase. This shows that indeed in most cases first order kinetics adequately describe removal of ENMs from the water phase. This model can be used as a basis for further exposure modeling of ENMs in surface waters.

Samenvatting

De risico's van chemische stoffen voor het milieu worden beoordeeld op basis van de effecten die ze hebben op organismen en de mate waarin deze hieraan worden blootgesteld. Hiervoor wordt de risicoquotiënt tussen de voorspelde blootstellingsconcentraties en voorspelde concentraties zonder effect gebruikt. Het meten of schatten van de blootstelling aan synthetische nanomaterialen (ENMs) in het milieu is lastig. Het beter begrijpen van de processen die van belang zijn bij het vaststellen van de blootstelling aan ENMs is het onderwerp van dit proefschrift.

Het schatten van de blootstellingsconcentraties van chemische stoffen wordt door modellen gedaan. In **hoofdstuk 2** staan aanbevelingen hoe zulke modellen en de adviezen hieromtrent geschikt gemaakt kunnen worden voor het schatten van blootstellingsconcentraties van ENMs in het aquatisch milieu. Het blijkt dat nanospecifieke processen zoals oplossen en sedimenteren van ENMs hierin moeten worden opgenomen. In dit hoofdstuk wordt ook een overzicht gegeven van de beschikbare literatuur over het oplossen en sedimenteren van ENMs in milieu relevante omstandigheden. Hieruit concluderen wij dat de gehele kinetiek van het water-sediment transport van ENMs grotendeels door een eerste-orde proces beschreven kan worden. Gebaseerd op beperkte gegevens uit de literatuur, wordt geschat dat de snelheidsconstanten voor de verwijdering van ENMs variëren van $0\text{-}10^{-4}\text{ s}^{-1}$ voor sedimentatie en $0\text{-}10^{-5}\text{ s}^{-1}$ voor oplossen.

In **hoofdstuk 3** worden de aggregatie en sedimentatie van CeO_2 nanodeeltjes bestudeerd. De concentratie en deeltjes grootte verdeling van CeO_2 nanodeeltjes werden gevolgd gedurende 12 dagen. Dit werd gedaan in algen groeimedium of gedemineraliseerd water met verschillende hoeveelheden opgelost organisch materiaal (DOM). De aanwezigheid van DOM stabiliseert de CeO_2 nanodeeltjes in suspensie. In aanwezigheid hiervan bleef 88% van de CeO_2 nanodeeltjes in gedemineraliseerd water in suspensie en 41% in algen medium na 12 dagen sedimenteren.

Nanodeeltjes aggregeren met elkaar (homoaggregatie) en met andere deeltjes (heteroaggregatie). Hierdoor is aggregatie gevolgd door sedimentatie een belangrijke route voor verwijdering van nanodeeltjes uit water. In **hoofdstuk 4** wordt naar het effect van heteroaggregatie gekeken. Hiervoor is water gebruikt uit twee Europese rivieren, de Maas en de Rijn. Om onderscheid te kunnen maken tussen de kleine (vooral DOM) en grote natuurlijke colloïden, aanwezig in oppervlaktewater, is gefiltreerd en ongefiltreerd rivierwater gebruikt om CeO_2 nanodeeltjes suspensies te maken. In deze suspensies is de sedimentatie van CeO_2 nanodeeltjes gevolgd. De resultaten hiervan laten zien dat de sedimentatie uit natuurlijk water volgens eerste-

orde kinetiek plaatsvindt tot er een restconcentratie overblijft. Dit is gemeten in rivierwater met minder dan 1 mg L^{-1} CeO_2 nanodeeltjes. Uit deze resultaten konden we afleiden dat depositie van nanodeeltjes op de vaste fractie van natuurlijke colloïden het belangrijkste mechanisme is dat leidt tot sedimentatie. Daarentegen stabiliseerde de DOM fractie juist de suspensie van CeO_2 nanodeeltjes in rivierwater, waardoor verdere sedimentatie werd tegengegaan.

Het belangrijkste doel van **hoofdstuk 5** is het geven van een schatting van input parameters voor blootstellingsmodellen voor nanomaterialen. We onderzochten 4 verschillende nanodeeltjes (C_{60} , CeO_2 , $\text{SiO}_2\text{-Ag}$ en PVP-Ag) in 6 verschillende watertypen, variërend van een kleine beek tot zeewater. Bij aanwezigheid van natuurlijke colloïden (NC) werden significante verschillen in sedimentatiesnelheden gevonden tussen verscheidene ENMs en watertypen. De sedimentatiesnelheden varieerden van 0.0001 m d^{-1} voor $\text{SiO}_2\text{-Ag}$ tot 0.14 m d^{-1} voor C_{60} . Schijnbare heteroaggregatie snelheden en plakkansen tussen NC en ENMs werden geschat met behulp van een nieuwe methode die heteroaggregatie onderscheidt van homoaggregatie door middel van een vereenvoudigde Von Smoluchowski-gebaseerde aggregatie-sedimentatie vergelijking, toegepast op data van ongefiltreerd en gefiltreerd water. De schijnbare plakkans voor heteroaggregatie varieerde tussen 0.0067 en 1, waarbij de hoogste waarden werden aangetroffen in zeewater. We stellen dat zulke systeem-specifieke parameters noodzakelijk zijn voor de ontwikkeling van toegepaste waterkwaliteitsmodellen voor ENMs.

Hoofdstuk 6 sluit aan bij **hoofdstuk 5**, en beschrijft het effect van geresuspendeerd sediment op de verwijdering van nanodeeltjes uit het water door heteroaggregatie en de daaropvolgende sedimentatie. Dit is een zeer milieu relevant scenario, bijvoorbeeld in ondiepe meren en beken of rivieren met een losse sedimentlaag. Er werden sedimentatiesnelheden van circa 10 tot 100 keer hoger gevonden in deze systemen met periodiek geresuspendeerd sediment en schijnbare plakkansen tussen 0.8 en 1. Dit laat zien dat de aanwezigheid van geresuspendeerd sediment belangrijk kan zijn voor het transport van ENMs.

In **hoofdstuk 7** wordt door middel van een numeriek model gekeken naar het effect van homo- en heteroaggregatie op sedimentatie van ENMs uit de waterfase. Om dit beter te kunnen begrijpen, werd een numeriek model gebruikt gebaseerd op een combinatie van de Von Smoluchowski theorie van aggregatie en de sedimentatie theorie van Stokes. Dit laat zien dat in de meeste gevallen de verwijdering van nanodeeltjes uit de waterfase inderdaad adequaat beschreven kan worden door

eerste-orde kinetiek. Dit model kan gebruikt worden als basis voor verdere blootstellingsmodellen voor ENMs in oppervlaktewater.

Curriculum vitae and list of publications

Joris T.K. Quik was born on July 22, 1982 in Knokke-Heist, Belgium. He grew up in Paramaribo, Suriname, where he attended primary and secondary school. After graduating in 2000 from the “Vrije Atheneum” in Paramaribo he did a Bahá’í year of service as part of the Lights of the Caribbean project in Guyana and the interior of Suriname. In 2001 he chose to move to the Netherlands to start his studies Earth, Water and Atmosphere at the Wageningen University. His final research thesis as part of these studies was on comparing quantification methods of Black Carbon. A secondary research topic was conducted at the sub-department of Toxicology on the genotoxic effects of Rhine water on a small fish, the mudminnow, using two different assays. These two research theses resulted in the co-authoring of two peer-reviewed publications. Graduation took place in 2007 and in the same year his Doctoral research started at the Environmental Science group at the Radboud University Nijmegen. This research was conducted primarily at the Institute for Public Health and Environment (former Laboratory for Ecological Risk Assessment, RIVM) in Bilthoven which resulted in this thesis. At the moment Joris is continuing his research on the fate of nanomaterials as a postdoctoral researcher at the Wageningen University (Aquatic Ecology and Water Quality Management Group) as part of the NanoNextNL project.

Quik, J. T. K.; Velzeboer, I.; Wouterse, M.; Koelmans, A. A.; van de Meent, D., Heteroaggregation and sedimentation rates for nanomaterials in natural waters. **2013**, *Submitted*.

Quik, J. T. K.; Stuart, M. C.; Wouterse, M.; Peijnenburg, W.; Hendriks, A. J.; van de Meent, D., Natural colloids are the dominant factor in the sedimentation of nanoparticles. *Environ. Toxicol. Chem.* **2012**, *31*, (5), 1019-1022.

Quik, J. T. K.; Vonk, J. A.; Hansen, S. F.; Baun, A.; Van De Meent, D., How to assess exposure of aquatic organisms to manufactured nanoparticles? *Environ. Int.* **2011**, *37*, 1068-1077.

Quik, J. T. K.; Lynch, I.; Van Hoecke, K.; Miermans, C. J. H.; De Schamphelaere, K. A. C.; Janssen, C. R.; Dawson, K. A.; Cohen Stuart, M. A.; Van De Meent, D., Effect of natural organic matter on cerium dioxide nanoparticles settling in model fresh water. *Chemosphere* **2010**, *81*, (6), 711-715.

Van Hoecke, K.; **Quik, J. T. K.**; Mankiewicz-Boczek, J.; De Schamphelaere, K. A. C.; Elsaesser, A.; Van der Meeren, P.; Barnes, C.; McKerr, G.; Howard, C. V.; Van De Meent, D.; Rydzyninski, K.; Dawson, K. A.; Salvati, A.; Lesniak, A.; Lynch, I.; Silversmit, G.; De Samber, B.; Vincze, L.; Janssen, C. R., Fate and effects of CeO₂ nanoparticles in aquatic ecotoxicity tests. *Environ. Sci. Technol.* **2009**, *43*, (12), 4537-4546.

Poot, A.; **Quik, J. T. K.**; Veld, H.; Koelmans, A. A., Quantification methods of black carbon: Comparison of Rock-Eval analysis with traditional methods. *J. Chromatogr.* **2009**, *1216*, (3), 613-622.

Alink, G. M.; **Quik, J. T. K.**; Penders, E. J. M.; Spenkelink, A.; Rotteveel, S. G. P.; Maas, J. L.; Hoogenboezem, W., Genotoxic effects in the eastern mudminnow (*Umbra pygmaea* L.) after exposure to Rhine water, as assessed by use of the SCE and comet assays: A comparison between 1978 and 2005. *Mutation Research* **2007**, *631*, (2), 93-100.